

Laser-Induced Grating Spectroscopy in Non-Uniform Temperature Fields and Flames

Nilushi C. Wijeyasinghe

M.Sc. Thesis

Michaelmas 2013

Atomic & Laser Physics

Clarendon Laboratory, Department of Physics

University of Oxford

Laser-Induced Grating Spectroscopy in Non-Uniform Temperature Fields and Flames

Nilushi C. Wijeyasinghe - Worcester College - M.Sc. by Research - Michaelmas 2013

Abstract

The application of Laser-Induced Grating Spectroscopy (LIGS) to thermometry of temperature-controlled ethylene flows and an ethylene-air flame from a Gülder burner is studied. A model for simulating the effect of contributions from regions of different temperature within the LIGS probe volume is developed for comparison with experimental data. The model includes a weighted sum of contributions from regions at a single temperature to the total signal intensity. An appropriate experimental set-up is constructed for this study, with careful consideration given to the dimensions of the probe volume. Temperature measurements are made in a dual flow of ethylene, where the probe volume contains two distinct temperature regions: one from an unheated flow and the second from a temperature-controlled hot flow. The model is shown to correspond well with experimental data; the presence of two discrete contributions, 293 ± 2 K and 310 ± 2K (0.6 – 0.7% precision), is identified in the LIGS signal from the cooler region.

LIGS signals are recorded at several spatial positions in the lower region of a flame with fixed stoichiometry. Signals measured in the 0.0 – 5.0 mm height above burner (HAB) range and the 0.0 – 3.5 mm radial position range are analysed using MATLAB; temperature information is extracted with precisions of 0.9 – 4.4%. The OH* distribution in the flame is recorded during a chemiluminescence experiment to identify the location of the reaction zone. The model is used to demonstrate that derived temperatures are the spatial average of a continuous temperature gradient within the probe volume. The suitability of LIGS for thermometry in environments with unknown temperature gradients is thus verified. Comparisons are made between the flame measurements and ethylene flow data; simple changes to improve the model are proposed. Strong non-oscillatory decay features in the LIGS signal, indicative of the laser heating of soot, are reported at HAB 20.0 – 50.0 mm; relevant implications are discussed.

Acknowledgements

I want to use this opportunity to thank three people who made an immense contribution to my work over the past two years, and without whom the completion of this thesis would not have been possible. The first person I want to mention is my supervisor, Professor Paul Ewart, who gave me the opportunity to be a part of his research group and work on this exciting project. I am honoured to have received his excellent supervision and benefited from his extensive knowledge of the field.

Another person who particularly deserves a mention is my colleague, Dr Ben Williams, who has been a wonderful source of advice on all work-related matters and for which I am extremely grateful. The positive impact his presence had on my work environment was much appreciated; his kind and understanding nature made it easy for me to approach him whenever necessary. Thank you for taking time out of your busy schedule to help me whenever I needed it.

Finally, I would also like to thank my partner and friend, Richard Drury, for his encouragement over the course of this degree, and whose endless patience and emotional support made this experience a far more pleasant one.

Contents

1 Introduction **6**

1.1 Motivation 6

1.2 Literature Review 8

1.2.1 Early Advances in Wave Mixing Techniques 8

1.2.2 Development of LIGS for Thermometry and Combustion Diagnostics 9

1.2.3 Alternative Optical Techniques 13

1.2.4 Spatial Averaging of FWM Signals 15

2 LIGS as a Combustion Diagnostics Technique **16**

2.1 LIGS Signal Generation and Analysis 16

2.1.1 Signal Generation Process 16

2.1.2 Calculation of Temperature 20

2.1.3 Precision of Temperature Measurement 22

2.1.4 Derivation of Other Parameters 26

2.2 Signal Generation Model 26

2.3 Spatial Resolution and Spatial Averaging 28

3 Experimental Method **31**

3.1 Overview of Experimental Set-Up 31

3.2 Apparatus Set-Up at the Measurement Point 35

3.2.1 Toluene Test Cylinder 36

3.2.2 High Pressure Gas Cell 36

3.2.3 Ethylene Flow 37

3.2.4 Gülder Burner 39

3.3 Alignment Procedure 40

3.4 Design, Selection and Construction of Apparatus 42

3.5 Analysis of LIGS Signal Data 43

3.6 Preliminary Work 45

4 LIGS Thermometry in an Ethylene Flow 49

4.1 Calculation and Verification of Probe Volume 49

4.2 Uniform Temperature Field: Results and Discussion 54

4.2.1 Room Temperature Single Ethylene Flow 55

4.2.2 High Temperature Single Ethylene Flow 57

4.3 Non-Uniform Temperature Field: Results and Discussion 61

4.3.1 Dual Ethylene Flow LIGS Measurements 62

4.3.2 Overview of the Multiple Temperature Model 63

4.3.3 Two Temperature Model for the Dual Ethylene Flow 65

4.3.4 Three Temperature Model for the Dual Ethylene Flow 69

5 LIGS Thermometry in a Gülder Burner Flame 74

5.1 Gülder Burner 74

5.2 OH* Chemiluminescence Measurement 77

5.2.1 2D Flame Image 77

5.2.2 3D Tomographic Reconstruction of the Flame 79

5.3 LIGS Thermometry: Results and Discussion 81

5.3.1 Effects of Spatial Position 82

5.3.2 Comparison of Ethylene-Air Flame with Ethylene Flow 87

5.3.3 Advanced Multiple Temperature Model for the Flame 90

6 Conclusions and Future Work **94**

6.1 Conclusions 94

6.2 Future Work 96

6.2.1 Effects of Soot 97

6.2.2 One-Dimensional Measurement of LIGS Signals 100

7 Appendices **103**

7.1 Appendix 1 103

7.2 Appendix 2 109

7.3 Appendix 3 110

7.4 Appendix 4 111

Bibliography **113**

1 Introduction

Laser-Induced Grating Spectroscopy (LIGS) is a non-linear optical technique where a signal is generated through a Four-Wave Mixing (FWM) interaction. The LIGS technique has been used to study relaxation dynamics in solids, liquids and gases, and also has valuable applications in combustion diagnostics [1]. This thesis details the development of LIGS for the purpose of measuring non-uniform temperature fields in gaseous flows and flames. A MATLAB model has been developed to simulate the outcome of such measurements under a variety of conditions; subsequently comparisons are made between modelled and experimental results, with scope for future work discussed in the concluding chapter.

This chapter discusses the motivations for developing LIGS as a thermometry technique for application in combustion diagnostics, and provides a brief summary of the LIGS mechanism.

1.1 Motivation

Combustion of fossil fuels will continue to be the primary energy source for heat, transport and electricity generation until alternative sources are able to meet the growing demand of a world rapidly increasing in population. The limited availability of fossil fuels due to depleting natural reserves [2] means that we must improve the efficiency and flexibility of existing combustion systems, in order to sustain this supply. Furthermore, there is a need to reduce the harmful environmental impact caused by the emission of certain combustion products into the atmosphere. Amongst these compounds is carbon dioxide, which is a significant contributor to increases in climate change, while oxides of nitrogen and sulphur cause acid rain, smog and damage to human health. The generation of soot and polycyclic aromatic hydrocarbons (PAHs, which are precursors to soot formation [3] [4]) is of particular concern because these particles have a negative impact on both the environment and human health [5] [6]. These goals can be

achieved through an improved understanding of the physical processes that occur during combustion.

Since reaction rates are critically dependent on fundamental combustion parameters such as temperature [7], we must develop techniques to make accurate and precise measurements of these parameters, which can then be used to validate computer-based theoretical models. It is also desirable for these experimental measurements to be non-invasive in order to avoid perturbing the environment under study. Consequently, laser-based methods that do not require a physical sampling probe have gained popularity over the past two decades [1]. Once these models are validated by comparison with experimental data, they allow us to predict what will happen in situations that are difficult to investigate experimentally. LIGS is a highly precise and accurate temperature measurement technique, with the capability to simultaneously monitor additional combustion parameters such as pressure and gas composition. LIGS is also non-invasive due to its optical nature and thus the use of a physical probe is not required. Hence it is beneficial to investigate the suitability of LIGS as a thermometry tool in a range of combustion environments; an ethylene-air standard laboratory flame is the combustion system treated later in this thesis.

The temperature field of a flame is complex; there are unknown temperature gradients within the flame. The existence of temperature gradients within the LIGS probe volume can potentially modify the form of the signal since the detected signal will contain components at different temperatures, resulting in some type of averaging. A similar effect is referred to as *spatial averaging* in the context of Coherent anti-Stokes Raman Scattering (CARS), which is a competitive technique that is discussed later in this chapter [8]. Its effect on LIGS signals is as yet undetermined and requires further investigation prior to application of LIGS in the study of flames. A controlled system, where non-uniformities in temperature are known, can act as a test system. The objective is to identify how contributions from each temperature region alter the form of the LIGS signal, with the intention of developing a model to reconstruct the temperature

distribution of the measurement region. Once a procedure for multiple temperature LIGS signal analysis is established, its suitability for use in flame environments can be evaluated. Therefore the primary focus of this thesis is the study of controlled, multiple temperature ethylene flows, as a precursor to the ethylene-air flame measurements that follow.

1.2 Literature Review

1.2.1 Early Advances in Wave Mixing Techniques

In 1965, Kogelnik [9] developed a method of dynamically using holographic techniques, which involved 'writing' a grating into a solid material by generating an intensity pattern through the interference of two laser beams; a third beam then 'reads' it. LIGS is analogous to this dynamic hologram technique. In LIGS a grating is formed in a medium through a transfer of energy originating from interfering laser pulses, and a third laser beam acting as a probe is introduced to monitor the evolution of this induced grating. While the technology developed by Kogelnik at Bell Laboratories provided a significant stepping stone to the FWM research that followed, the focus of his research was on applications in solid state physics and not on gas phase experiments as reported in this thesis.

The first publication on laser induced acoustic wave research, which is directly relevant to this thesis, was in the 1970s. Auth [10] reports the generation of oppositely directed acoustic waves from the interference of two identical, high intensity optical pulses, which is also the basis of LIGS. However, this initial study was a demonstration of the physical processes, not an attempt at employing wave mixing as a measurement technique. Auth's work led to some of the earliest FWM experiments, as reported by authors such as Bloom and Bjorklund [11]. Studies of this type explored the use of FWM in a range of applications including devices for optical image reconstruction as detailed by Bloom and Bjorklund; however the suitability of FWM techniques for use in thermometry was yet to be determined.

1.2.2 Development of LIGS for Thermometry and Combustion Diagnostics

The coherent nature of FWM signals presented a significant advantage in situations where non-invasive, remote detection was desirable, because the signal intensity would be relatively high in comparison to any isotropic radiation that may originate from the environment under study. Rapid advancement of FWM in the 1990s established it as a powerful tool for gas phase measurements, where some of the landmark publications that provided the groundwork for this project are highlighted below. During this period, progress was made in the development and implementation of a variety of FWM techniques, LIGS being one such method. LIGS found favour with those who were interested in accurate and precise gas phase thermometry, initially proposed by Cummings [12] and Paul *et al.* [13].

Firstly, it is important to note that the LIGS gratings discussed in this thesis are *thermal gratings*. Thermal gratings are density perturbations generated from the localised heating of a bulk medium, which is the result of energy transfer processes that take place after resonant absorption of laser energy by a molecular species. Further details on thermal gratings can be found in Chapter 2. *Electrostrictive gratings* are created due to the movement of polarisable molecules towards regions of high electric field intensity; this phenomenon can produce a secondary grating at any frequency of incident laser radiation and generate a signal very similar to that observed in thermal LIGS by scattering the probe laser [13]. However, in the presence of an absorbing species, the signal from a thermal grating overwhelmingly dominates that from an electrostrictive grating [12]. Thus, in the current study, electrostrictive LIGS contributions are disregarded and expected to be insignificant due to the presence of absorbing species in the experiments.

Cummings successfully demonstrated that induced thermal gratings can be used to measure the speed of sound in a gas to an accuracy of 0.5%, from which the temperature of the probe region can be calculated if the composition of the gas is known. The author was also able

to determine the viscosity of the gas by measuring the thermal diffusivity and rate of acoustic damping, although this was to a significantly lower degree of accuracy. Furthermore, there was only a brief exploration of the effects of gas composition; the results showed that the LIGS signal was strongly dependent on this property and consequently it calls for further investigation into the subject. It was noted that the characteristics of experimentally measured signals were in excellent agreement with theoretical predictions made using the theory of light scattering and solutions to linearised hydrodynamic equations.

A publication by Paul *et al.* [13] in the same year as Cummings' article detailed above presented a comprehensive mathematical treatment of the LIGS mechanism. A dynamic model of how a thermal grating evolves with time was successfully developed, with predictions made using the model subsequently verified through comparison with results from laboratory experiments. However, the primary focus of this study was limited to uniform temperature fields below 300 K; hence this work provides a starting point for the multiple temperature LIGS signal model introduced in Chapter 4 of this thesis, and the high temperature LIGS studies detailed in Chapters 4 and 5.

FWM does not require physical probes, making it suitable for use in physically inaccessible combustion environments. This led to flame experiments, such as the high pressure LIGS thermometry work by Latzel *et al* [14]. However, most flame experiments that followed only focussed on investigating a range of absorbing species, with little emphasis on accuracy and precision. The precision of temperature measurements made using LIGS is determined by the uncertainty associated with a frequency measurement; it is not affected by intensity variations. Frequencies can typically be measured with greater precision than intensities. This is demonstrated by LIGS achieving precisions better than 0.2% on temperature measurements [15], while intensity dependent FWM techniques ordinarily achieve precisions of the order of 1% [16]. However, precision of LIGS is limited in situations where only a few oscillations are resolvable in the signal, which typically resembles an exponentially decaying sinusoid. This

poses a particular problem in very high temperature flame environments because predictions made using the models based on the work of Paul *et al.* [13] indicate that fewer oscillations are resolvable at higher temperatures; a detailed discussion of how the form of a LIGS signal is dependent on a variety of combustion parameters can be found in Chapter 2 of this thesis. LIGS temperature measurements can potentially achieve accuracies better than 0.5%, but this is only possible if gas composition and the spacing of grating planes are equally well known [14] [15].

Experiments examining the suitability of FWM for a range of applications relevant to combustion diagnostics, in addition to its use in thermometry, have also been widely documented. One such example is a velocimetry study, where velocity measurements have been made in gas flows [17]. Experiments on gas flows are also presented in Chapter 4 of this thesis, where the FWM measurements made are for the purpose of determining flow temperature as opposed to flow velocity. Studies on minor species detection and concentration measurement are also commonly seen in the literature; the species can be identified as the laser absorbing species when the frequency of the pump pulses is matched to a resonant transition in the molecule. For instance, Dreizler *et al.* [18] showed that FWM could be used to determine the concentration of hydrocarbon molecules such as ethylene and other combustion-related molecules in gas mixtures at a range of pressures, demonstrating the suitability of FWM as a measurement tool for technical combustion environments. Knowledge of gas composition is critical to the accurate determination of temperature using LIGS; this poses a limitation on the types of environments in which the technique could be applied and will be discussed in detail in Chapters 4 and 5 of this thesis. Moreover, LIGS has already been demonstrated in high pressure, sooting, turbulent environments [19] [20], providing evidence for its suitability for thermometry in engines [21], although the absence of optical access may provide a practical limitation.

The ethylene-air laboratory flame used in the experiments discussed in Chapters 5 and 6 originates from a Gülder burner. A Gülder burner is built to a standardised design which allows

comparative measurements to be made on nominally identical flames with state-of-the-art measurement techniques at research institutions across the globe [22]. A collaborating research group within the University of Oxford have recently mapped the three-dimensional temperature distribution of a Gülder burner flame using the imaging technique of three colour pyrometry [23]. Although these detailed temperature maps provide an important point of comparison for LIGS measurements made during this project, a disadvantage of the three colour pyrometry method is its inability to measure the lower region of the flame, as it relies on luminous soot particles that are only formed higher up in the flame. Validation of theoretical models requires knowledge of the temperature field throughout the flame, including the lower region containing colder unburned fuel and soot precursor molecules [3] [4]. Thus if LIGS is able to successfully make temperature measurements in the Gülder burner flame close to the fuel nozzle, this would provide a valuable contribution.

While the work presented in this thesis and most LIGS-related studies have focused on temperature measurement at a single point-like finite volume, simultaneous measurements along a line may be performed using a streak camera as a detector [24]. Flame measurements have yet to be made using this method; however this provides a possible way of simultaneously measuring the temperature of a flame at several points along a line segment. Such an imaging set-up could easily be incorporated into the laboratory flame set up described in Chapter 5 if it is considered desirable to explore this type of one-dimensional measurement.

The first set of results from the application of LIGS in a gasoline direct injection engine with optical access has recently been reported [21]; the high precision of the measurements (0.1% to 1%, depending on pressure) allowed for small changes in temperature caused by evaporative charge cooling to be measured, further demonstrating the potential for LIGS to be developed for commercial use in combustion research. This work, however, did not address the issue of spatial averaging in LIGS, which could be important in such environments where hot

and cold fluids are mixing. This provides further motive to perform highly controlled laboratory tests such as those described in Chapters 4 and 5.

1.2.3 Alternative Optical Techniques

This thesis employs LIGS, which is one of several optical thermometry techniques available for use in combustion research. The most widely used alternatives are Coherent Anti-Stokes Raman Scattering (CARS), Laser-Induced Fluorescence (LIF), Rayleigh scattering and absorption spectroscopy [1].

In Raman scattering, an incident photon is inelastically scattered following an interaction with a molecule; if the energy transfer increases the frequency of the photon, the process is described as 'anti-Stokes shifted'. CARS is a FWM technique that uses three interacting laser beams to generate a fourth signal beam. The difference in energy between two of the incident photons (the pump beam and the Stokes beam) matches a rotational or vibrational transition in the molecular species under investigation. The third beam scatters off the polarisation induced by the first two to generate the anti-Stokes beam. A theoretical spectrum is then fitted using temperature as a variable. LIGS has three key advantages over CARS: simpler experiment set-up, less complicated signal analysis procedure and in most instances, a more precise temperature measurement. LIGS measurements are typically an order of magnitude more precise than CARS [16], primarily due to the precision of CARS being strongly affected by fluctuations in signal intensity and spectral intensity variations in the incident Stokes beam.

LIF uses laser radiation to excite fluorescent molecules, after which a spectrometer is employed to measure the spectrum of the spontaneously emitted radiation. Both the integrated fluorescence intensity, and the relative line strengths that are dependent on the relative populations of excited energy states as governed by the Boltzmann distribution, convey

temperature information; thus the direct dependence of LIF on signal intensity puts it at a disadvantage relative to LIGS when used in precision thermometry [25]. A key advantage of LIF is that the use of laser sheets for illumination allows two-dimensional distribution maps of minor species in a flame environment to be obtained when the laser is tuned to resonances in each species [26]. However, quantitative interpretation of these maps is typically challenging, as non-radiative quenching effectively competes with spontaneous emission.

Rayleigh scattering is the elastic scattering of light by particles that are significantly smaller than the wavelength of the incident radiation. The wavelength of the scattered light is thus unchanged and the scattered signal intensity is proportional to the total number density of species present. Since the species number density is inversely proportional to the temperature of the measurement environment, this is another intensity dependent optical method that can be used in thermometry, which has the capability of being applied in two-dimensions. This thermometry technique has already been demonstrated in sooting flames and turbulent air flows [27] [28]. The simplicity of the technique and the lack of saturation effects in the signal due to its proportionality to the laser pulse energy are advantages. However, the indistinguishability of scattering species and the reduced accuracy of derived temperatures due to the difficulty in calculating the Rayleigh cross sections of individual species, prove to be limitations of the technique.

Furthermore, absorption spectroscopy can also be used for thermometry because the full-width at half-maximum (FWHM) of each Doppler-broadened spectral line is proportional to the square-root of temperature. However this technique has the disadvantage of poor spatial resolution due to its line-of-sight nature, unless complicated tomographic approaches are employed. Additional details of measurement techniques relevant to combustion research can be found in the recent review article by Kiefer and Ewart [1].

1.2.4 Spatial Averaging of FWM Signals

Both LIGS and CARS are affected by temperature non-uniformities in the measurement volume. A temperature derived from a signal containing contributions from a multiple temperature probe volume is described in the literature as being *spatially averaged*. In CARS, if a probe volume contains regions of cold gas and hot gas, the contribution to the signal from the colder region is likely to dominate as the CARS signal is proportional to the square of species density, and species density increases with decreasing temperature. The effect of multiple temperature contribution to a single CARS signal has been studied by Taran *et al.* [29], Parameswaran and Snelling [30], Thumann *et al*. [31] and Seeger *et al.* [8]. Efforts have been made to develop models to simulate theoretical spectra containing multiple temperature contributions, from which the volumetric fraction of gas at each temperature can be determined, with limited success.

However, no work has yet been published on the effect of spatial averaging in LIGS signals and thus it provides a starting point for the research presented in Chapters 4 and 5. Similarly to the CARS studies on this subject, this thesis will develop a spatial averaging model for LIGS and validate it with experimental data. Fitting the simulation to experimental results then offers a method of determining different temperature contributions in the probe volume and the volumetric fraction of gas at each temperature. The issues of spatial resolution and spatial averaging, and the challenges they pose for LIGS thermometry, will be discussed in greater detail in Chapter 2.

2 LIGS as a Combustion Diagnostics Technique

This chapter first provides a description of the processes involved in generating a LIGS signal for gas phase measurements, and the way in which information can be extracted from it. A signal generation model is then presented, along with examples of LIGS signals to demonstrate how different measurement conditions affect the form of the signal.

2.1 LIGS Signal Generation and Analysis

2.1.1 Signal Generation Process

To produce a thermal LIGS signal, an interference pattern must first be created by crossing two pump laser pulses of a wavelength corresponding to a resonance in the molecular species present in the measured gas. The two pump pulses originate from the same laser, which is a frequency-quadrupled Nd:YAG in this case. An appropriate arrangement of optical components (detailed in Chapter 3) is used to split each laser pulse into two, after which they are both directed towards the point where the measurement is to be made. Figure 2.1 summarises the key stages in LIGS signal generation. The intensity pattern generated at the intersection of the two coherent pulses forms a set of fringes as shown in Figure 2.1a.

At points of constructive interference where high intensity fringes are formed, energy from the pulses is absorbed by molecular species with an appropriate frequency response corresponding to the fourth harmonic of the Nd:YAG output radiation. Toluene, acetone and ethylene are the three species actively used in this study; a discussion of additional absorbing species present in a flame is provided in Chapter 5. The energy that is absorbed is temporarily stored in excited states. Molecules are able to decay back to the ground state through several different methods; some of these processes result in the emission of a photon, while others are non-radiative. A comprehensive discussion of the energy redistribution mechanisms and the

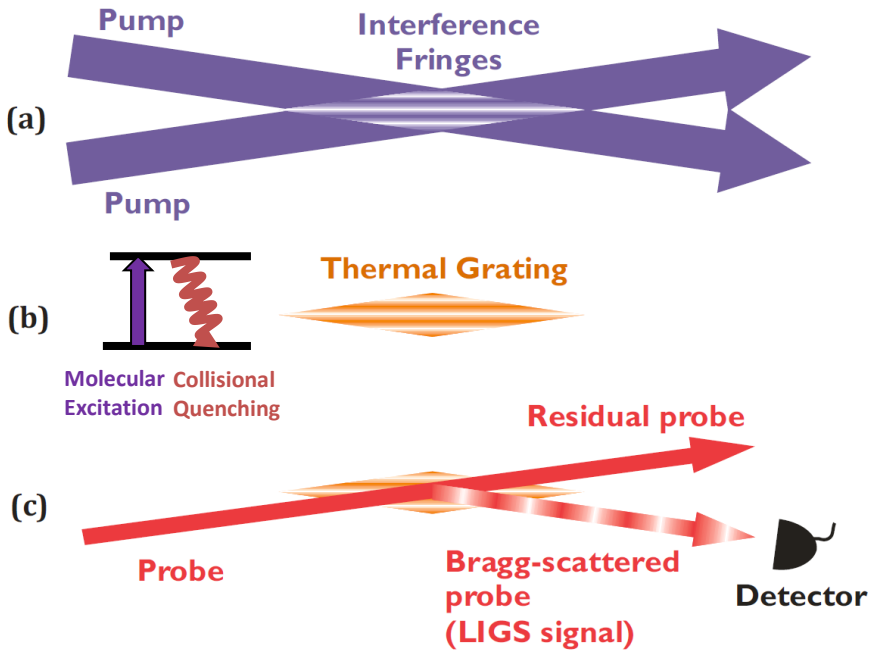


Figure 2.1: LIGS signal formation. a) Two coherent pump pulses interfere to form intensity fringes at the intersection. b) The collisional quenching that follows molecular excitation causes a grating to form in the bulk gas. c) Grating dynamics are monitored with the scattered component of the probe beam.

time scales over which they occur are beyond the scope of this thesis. Thus the primary focus of this chapter will be on the effects of collisional quenching, as this is the dominant molecular relaxation process at the temperatures and pressures relevant to the study reported in this thesis [32].

The Jablonski diagram in Figure 2.2 illustrates the energy transfer processes that can occur in the types of pump absorbing molecules used in LIGS experiments, with toluene used as the example. Collisional quenching is indicated in red. S_1, S_0 and T_1 are electronic energy manifolds, where the subscript number indicates the electronic energy state (0 and 1 denoting ground state and first excited state respectively), and the letter indicates the spin multiplicity (S and T denoting singlet and triplet respectively). It can be seen that collisions can cause the toluene molecule to lose energy by changing to a different spin state or decaying down the ladder of rotational and vibrational states within each electronic manifold. The energy from

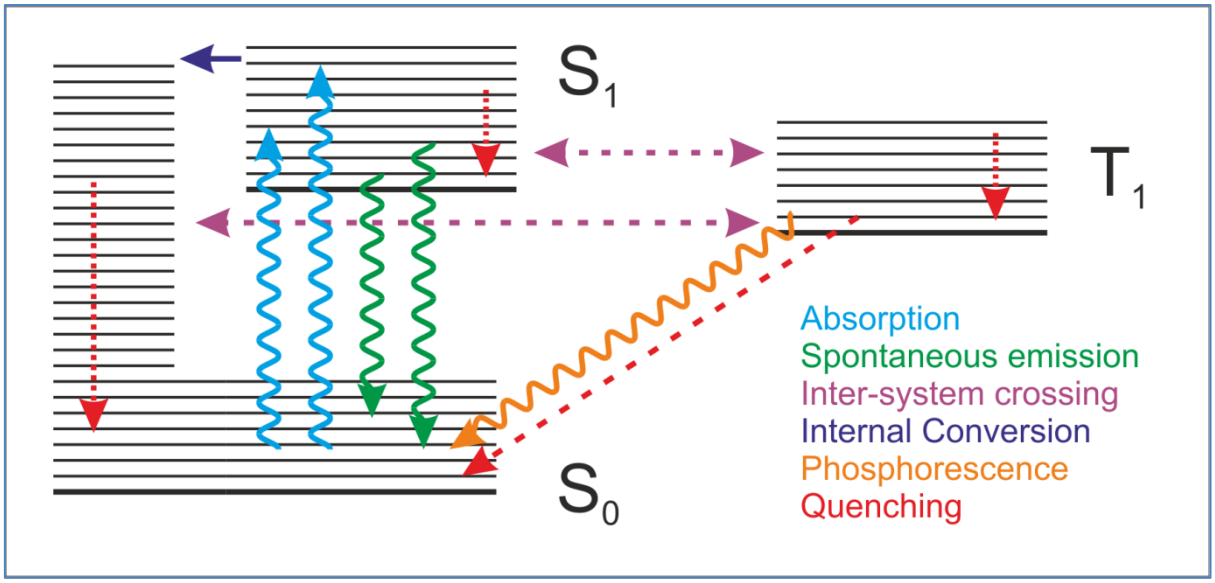


Figure 2.2: A Jablonski diagram of energy transfer processes in a toluene molecule. Wavy lines indicate the absorption or emission of a photon. Dotted lines within an electronic energy manifold indicate a change in rotational or vibrational state. The dashed lines indicate processes that are enhanced by the presence of oxygen [32].

the toluene molecules is transferred to the surrounding bulk gas as translational kinetic energy and consequently causes heating. The bulk gas present in a LIGS experiment could be air, a pure gas such as oxygen or some other mixture of gases; it is important to note that the quenching rate depends on the gas composition because the transition probability depends on the correspondence between energy levels of the colliding molecules.

Collisional energy transfers lead to localised heating of the bulk gas at the high intensity fringes. The resulting perturbation in temperature and pressure generates a periodic density modulation, with fringe spacing, Λ, given by

$$\Lambda = \frac{\lambda_p}{2\sin(\theta_p/2)} \tag{2.1}$$

where λ_p is pump wavelength and θ_p is the pump crossing angle.

This density modulation feature is called a *thermal grating* (illustrated in Figure 2.1b) and consists of two components: a stationary temperature grating and a standing wave acoustic grating. The temperature grating is a reduction in the local density due to a perturbation in temperature at the high intensity fringes. Over time, particle diffusion returns the system to equilibrium and hence this component decays exponentially with time. The decay rate is pressure dependent; this is because lower pressures facilitate higher diffusion rates, which consequently reduce the lifetime of the density modulation. Therefore the temperature grating decays more slowly in high pressure environments, when compared with systems at atmospheric pressure. Rapid heat deposition during the quenching process causes a sudden rise in local pressure; this generates two counter-propagating acoustic waves from each high intensity region which propagate outwards, perpendicular to the direction of the grating planes. These acoustic waves then interfere to form a standing wave, causing a sinusoidal modulation in the bulk gas density; this density modulation also decays exponentially with time, due to viscous damping effects.

A thermal grating is able to scatter an incoming laser beam in a manner that is analogous to the scattering of incident light from planes in a crystal. However, the reflectivity of the thermal grating is time-dependent, a further discussion of which can be found in Section 2.1.3. Grating dynamics are monitored by measuring the intensity variation of the Bragg-scattered part of a continuous-wave probe laser beam: this is the LIGS signal. The Bragg angle is defined by

$$\lambda_q = 2\Lambda \sin\theta_q \tag{2.2}$$

where λ_q is probe wavelength, θ_q is the probe's angle of incidence and Λ is the grating spacing, which is equivalent to the fringe spacing in the laser interference pattern. The scattered signal beam is monitored using a photomultiplier tube (PMT) module as was shown in Figure 2.1c. The portion of the probe that is transmitted through the grating without scattering is directed

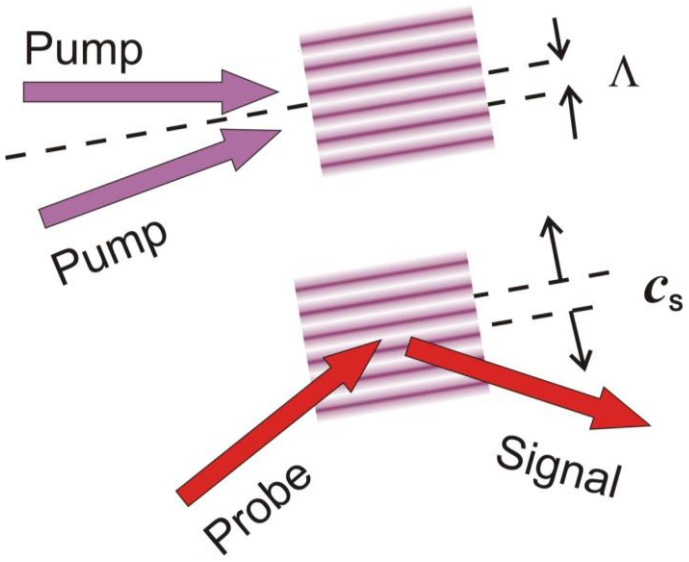


Figure 2.3: Acoustic waves generated in regions of high intensity of the thermal grating travel across the fringes at a speed c_s, which is the speed of sound in the medium. The waves travel a distance of Λ in time τ, where Λ is the spacing between grating planes and is identical to the spacing between intensity fringes in the laser interference pattern.

towards a beam dump. Note that the probe volume discussed in the previous chapter refers to the portion of the thermal grating that is illuminated by the probe. Efforts are made to ensure that the probe volume is of a similar size to the pump interaction region (see Section 4.1); this is done in order to maximise the intensity of the LIGS signal by making the most efficient possible use of the incident pump and probe energies.

2.1.2 Calculation of Temperature

Acoustic waves traverse one fringe spacing in time τ, which gives the temporal separation of adjacent maxima in the LIGS signal to be

$$\tau = \frac{\Lambda}{c_s} \tag{2.3}$$

where c_s is the speed of sound in the medium. Figure 2.3 illustrates this situation. Since τ is proportional to Λ, if Λ is too small, the oscillation frequency can become too high to measure

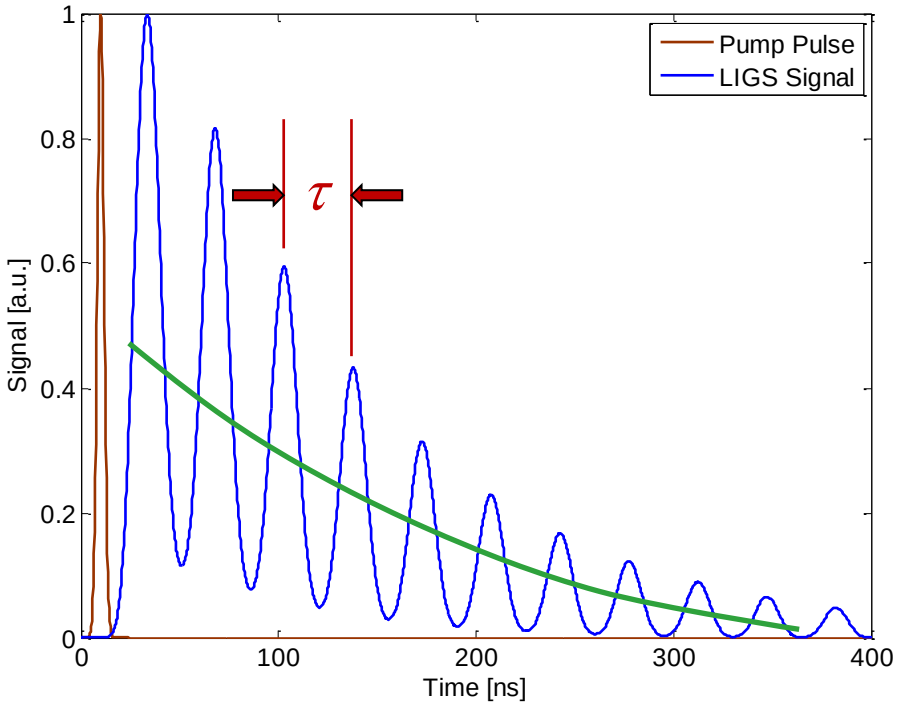


Figure 2.4: An example of a typical LIGS signal is indicated in blue, while the timing of the pump pulse is shown in brown. τ is the time taken for acoustic waves to travel one fringe spacing and gives the temporal separation of two consecutive maxima in the reflectivity of the thermal grating, which corresponds to two adjacent peaks in a LIGS signal. The green curve shows the exponential decay of the grating, which is dependent on pressure.

with a standard laboratory oscilloscope. If Λ is too large, there will be too few grating planes in the beam interaction region, meaning too few peaks in the LIGS signal to precisely measure τ.

Figure 2.4 shows an example LIGS signal, indicating the typical magnitude of τ. The oscillation frequency of the signal, f_{osc}, is given by:

$$\tau = \frac{1}{f_{osc}} \tag{2.4}$$

f_{osc} is found by examining the frequency spectrum found by a Fourier transform of a LIGS signal as a function of time. In the present work, a MATLAB program is used to analyse the LIGS signal data and calculate f_{osc} using its Fourier transform function. After τ has been calculated using

Equation 2.4, the temperature at the interaction region, *T*, is deduced from kinetic theory for an ideal gas:

$$c_s = \sqrt{\frac{\gamma k_B T}{m}} \tag{2.5}$$

where γ is the ratio of specific heats, k_B is Boltzmann constant and m is the molecular mass of the surrounding gas. By substitution of Equation 2.5 into Equation 2.3, we get

$$T = \frac{1}{k_B}\frac{\Lambda^2}{\tau^2}\frac{m}{\gamma} \tag{2.6}$$

Hence determining temperature by calculating Λ and measuring τ necessitates knowledge of gas composition to determine the value of $\frac{m}{\gamma}$. Accordingly, the accuracy of the temperature measurement relies on the accuracy to which the values of Λ and $\frac{m}{\gamma}$ are known. The measurement precision is discussed in Section 2.1.3.

A comprehensive mathematical treatment of LIGS is beyond the scope of this thesis. However, a full derivation of the physics underpinning the LIGS mechanism, including details of the hydrodynamic equations governing grating evolution, can be found in Paul *et al.* [13].

2.1.3 Precision of Temperature Measurement

It can be seen from Equations 2.4 and 2.6 that the temperature derived from a LIGS signal is dependent on its oscillation frequency and is independent of its intensity. Frequencies can typically be measured to a significantly greater precision than intensities, and this is the primary advantage of LIGS thermometry, as discussed in the first chapter.

However, the precision of a temperature measurement is dependent on the number of oscillatory peaks that are resolvable in the signal. For instance, a signal taking the form of a pure

sine wave of infinite length produces a delta function in the frequency domain when it is Fourier transformed. However, if a signal contains only a few resolvable oscillations, this produces a much broader frequency peak.

Several factors affect the number of peaks that are resolvable in a LIGS signal: pressure is a key factor. At higher pressures, the slower decay of the thermal grating gives a LIGS signal that oscillates for a longer time duration; given a fixed grating spacing, more cycles will be seen. Consequently, temperature readings can be made to a better precision in high pressure environments, since the uncertainty associated with determining the oscillation frequency decreases as the number of resolvable peaks increases. The effect of pressure on the form of a LIGS signal is illustrated in Figure 2.7 in Section 2.2.

The quenching rate, which in itself is a function of temperature and gas composition, also significantly affects the resolvability of peaks in a LIGS signal, as well as the delay between the timing of the pump pulse and the first observed LIGS peak. From the example LIGS signals presented in this chapter, it can be noted that there is a delay between the pump pulse, which in this study has a FWHM of 4 ns, and the first LIGS maximum. The local density decreases with increasing temperature, which means that the temperature and acoustic grating components are initially generated out of phase. The position of the first maximum is determined by the time taken for the dynamic acoustic grating to come into phase with the stationary temperature grating. If instantaneous relaxation is assumed, which implies that the absorbed laser energy is immediately converted into the heat that perturbs the temperature and density of the bulk gas, the relative amplitudes of the two grating components would be equal. In this case the total density modulation will be zero when the two components are out of phase; this is illustrated in Figure 2.5.

The amplitude of the stationary temperature grating component illustrated by the red line in Figure 2.5 decays to zero exponentially over time; however the amplitude of the dynamic acoustic component oscillates with time as it decays to zero exponentially. When the two

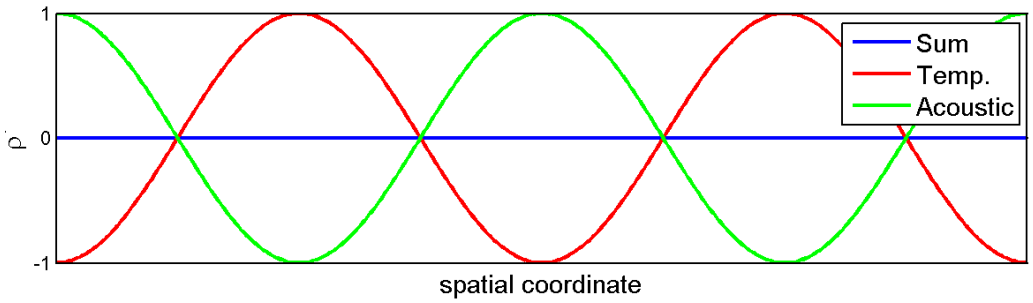


Figure 2.5: The x-axis of this plot shows spatial position within the pump interaction region, perpendicular to the grating planes. The y-axis shows ρ, the amplitude of the density perturbation. When the temperature grating (red line) and acoustic grating (green line) are out of phase, their resultant sum, the thermal grating (blue line), has an amplitude of zero as shown in this figure where the two grating components are of equal magnitude. The thermal grating will grow and decay over time as its two constituent components vary in amplitude and phase.

components first come into phase and reinforce the contribution to the density perturbation made by each other, the total density modulation reaches a peak and a principal maximum in the reflectivity of the thermal grating is created. Several other maxima are subsequently generated periodically when the two components move in and out of phase, at periods of τ as given by Equation 2.4, until the system reaches equilibrium again. However, quenching timescales are critical to the creation and evolution of a thermal grating, and also determine the relative amplitude of these density perturbations.

If the molecular relaxation that follows laser pulse absorption is not instantaneous, the density perturbation grows in time as heat is slowly deposited into the bulk gas over a long timescale through slow quenching. In this instance, *slow* refers to a quenching time of the order of 100 ns, which is much longer than the grating transit time, while *fast* refers to a quenching time of the order of 1 ns, which is less than the grating transit time. It can be seen from Figure 2.6 that if a slow quenching rate dominates, it strongly affects two features of a LIGS signal: the point of maximum intensity and the depth of oscillations.

The point of maximum intensity is determined by the temporal evolution of the stationary temperature grating. If the molecular relaxation rate is slow, the stationary grating

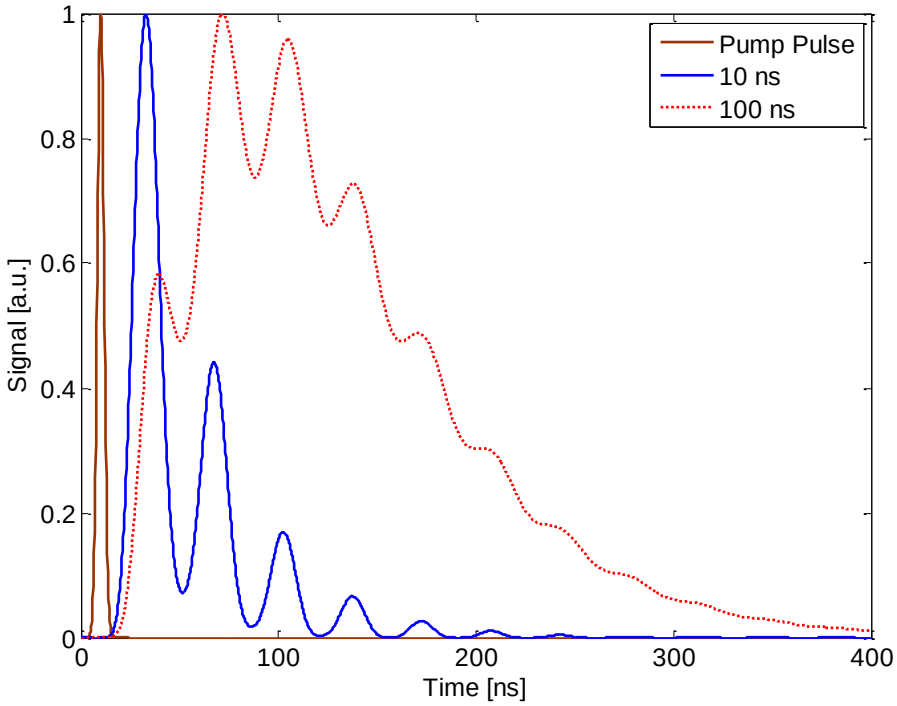


Figure 2.6: Modelled signals for 10 ns and 100 ns quenching times are shown in blue and red respectively, for measurements made in an air environment at atmospheric pressure and 293 K room temperature. The timing of the pump pulse is shown in brown. The form of a LIGS signal is strongly dependent on the timescale over which quenching occurs.

grows slowly and the density perturbation peaks at some later time determined by the decay rates, instead of coinciding with the first peak in the LIGS signal. The oscillation depth, sometimes referred to as signal contrast, indicates the relative amplitude of the acoustic and stationary gratings. If the energy transfer into the bulk gas happens at a slower rate, the acoustic wave generated will be of lower amplitude; if the molecular relaxation is instantaneous, the amplitude of the acoustic grating is equal to that of the stationary temperature grating yielding maximum contrast. In general, energy transfer which takes a time longer than the inter-fringe transit time, τ, will produce little to no modulation in the LIGS signal. Consequently, in order for high precision temperature measurements to be made, it is essential for the quenching to be fast enough to produce several resolvable peaks in the LIGS signal. The effects of slow quenching will be discussed further in Chapter 5 of this thesis.

2.1.4 Derivation of Other Parameters

While the temperature of the probe volume is the primary piece of information to be derived from a LIGS signal in this work, and also the simplest combustion-relevant parameter to extract from it, the form of the signal also allows for the simultaneous measurement of other properties of the environment in which the experiment is conducted. The exponential decay rate of the LIGS signal, which is indicated by the green curve in Figure 2.4, is dependent on the pressure of the bulk gas as discussed in Section 2.1.1. Thus the pressure of a gas can be derived by measuring this decay rate, provided the gas dynamic parameters are known. The pressure dependence of a LIGS signal is illustrated in Figure 2.7.

Furthermore, the contrast of the oscillations relative to the background in the signal is greater at higher pressures because high pressure generally induces faster quenching, which consequently creates stronger acoustic gratings. The oscillation depth may also provide information about the composition of the bulk gas. In particular, the presence of oxygen can accelerate quenching rates in many hydrocarbon molecular species. It is sometimes the case that an increase in species concentration leads to higher signal intensities because the rate of heat deposition can be proportional to species number density. Consequently, the integral of the LIGS signal in this situation provides information about the species number density.

2.2 Signal Generation Model

The modelling and data analysis in this study were performed using MATLAB, a numerical computing environment developed by MathWorks, Inc. A MATLAB based LIGS simulation program is available within the research group, entitled LIGS_signal_generator.m. The underlying model was originally developed by a past group member, R. E. Stevens [33]. The latest version of the program was developed by B. A. O. Williams at the University of Oxford in

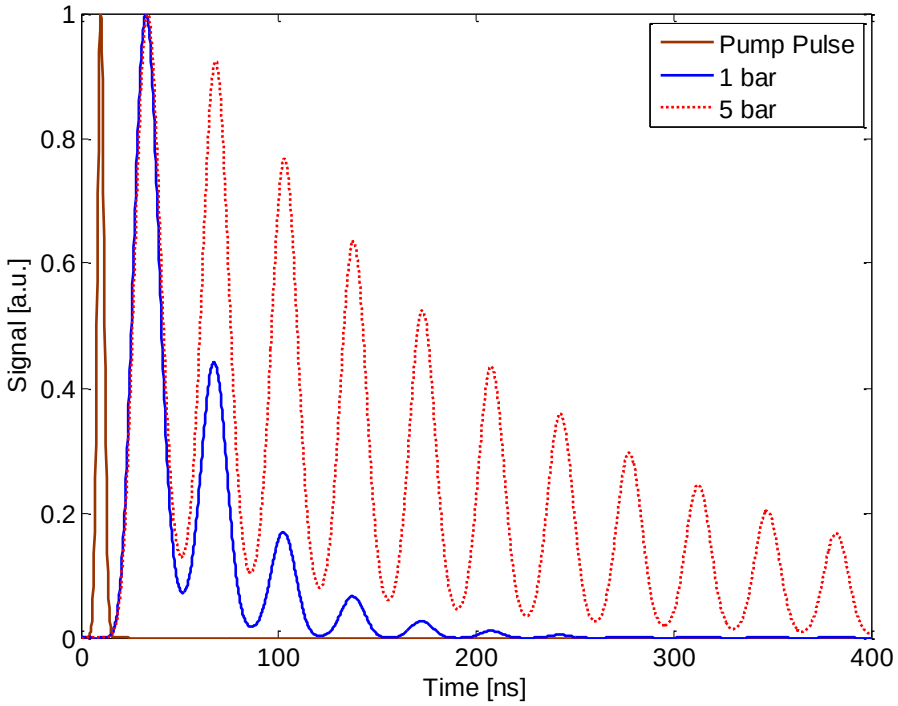


Figure 2.7: Modelled signals at 1 bar and 5 bar pressures are shown in blue and red respectively, for measurements made in an air environment at 293 K room temperature. The timing of the pump pulse is shown in brown. The decay rate of a LIGS signal is strongly dependent on pressure: the thermal grating decays faster at lower pressures because the rate of diffusion is faster when the pressure is lower.

2011 and has the capability of modelling a LIGS signal for a variety of experimental conditions; the modelled signals seen in Figures 2.6 and 2.7 were simulated using this version of the program. This code has been employed successfully on numerous occasions to simulate data for peer-reviewed publications, and thus its ability to generate accurate and precise LIGS signal data that agree well with experimental measurements has been verified.

The program allows the user to alter a set of input variables, some of which can be set up as parameters for a fit when making comparisons with experimental data. The variables that can be adjusted are temperature (T), pressure (p), ratio of specific heats (γ), mean molecular mass of the bulk gas (m), grating spacing (Λ), fast quenching time ($Q1$), slow quenching time ($Q2$) and the branching ratio between the two quenching times (Br) that indicates which rate

dominates. The pump laser's pulse width must also be specified. Using this input, the program generates a simulated pump pulse and LIGS signal, which are plotted in a MATLAB figure.

The pump laser pulse is modelled using a Gaussian function. Generating the LIGS signal by calculation of the time dependent grating diffraction efficiency is more complicated. The core of the simulation employs a set of coupled differential equations describing the hydrodynamic evolution of the induced density perturbation, based on the mathematical description of grating evolution presented by Paul *et al.* [13], which are prepared and solved. An option to perform a fitting routine on experimental data is also available.

A limitation of this model is that it assumes the probe volume to be of a uniform temperature; there is no scope to account for contributions from multiple temperature zones, which is the primary focus of the present work. Therefore it was necessary for the author to make significant modifications to the program prior to its use in this project. A detailed discussion of the achievements made in modelling LIGS signals from non-uniform temperature fields, and the challenges faced during the process, can be found in Chapters 4 and 5. The MATLAB scripts and functions that comprise the multiple temperature LIGS model are included in Appendices 1, 2, 3 and 4.

2.3 Spatial Resolution and Spatial Averaging

As noted above, the principal focus of this thesis is to examine the applicability of the LIGS technique in non-uniform temperature fields. In Chapter 1, it was explained that while temperature non-uniformities in the probe interaction region are expected to have a negative impact on the LIGS technique, this problem is yet to be experimentally investigated. This provides a starting point for the work detailed in this thesis.

The origin of the problem is the finite size of the probe volume. It is not possible to measure the temperature of a nanometre scale point using LIGS. The probe volume as defined by the region of the thermal grating illuminated by the probe beam is dependent on several parameters including the beam diameter and angle of incidence. The absolute minimum of this quantity is bounded by the diffraction limit. With the geometric configuration and apparatus arrangement required for LIGS measurement, it is typical for the probe volume to be a few hundred micrometres in diameter and of the order of ten millimetres in length. Consequently this determines the *spatial resolution* of a LIGS measurement. Analysis of LIGS signals typically assumes that the probe volume is of a single temperature; but it is apparent that in an environment where sharp temperature gradients exist, there may be multiple temperature contributions to the LIGS signal, potentially modifying the form of the signal and introducing unquantified uncertainties into the derived temperature.

To understand the impact of temperature gradients existing within the probe volume, Figure 2.8 provides a simple example of two simulated LIGS signals originating from probe volumes where each is of a single uniform temperature, and the two differ by approximately 300 K. The difference in oscillation frequency is significant and it is clear that their simultaneous presence would result in a signal sum of a different shape. It was the aim of this work to determine how this would modify a LIGS signal and its frequency spectrum.

It is of fundamental importance to gain a greater understanding of the effects of temperature non-uniformities in the probe volume prior to using LIGS in the study of flames because flames are environments containing unknown and significant temperature gradients. A dual ethylene flow system, where the temperature of each flow can be controlled individually, is the system under investigation in Chapter 4. The objective is to identify how contributions from each temperature region modify the LIGS signal and to develop a model to simulate the temperature zones present in the measurement region. A spatial averaging model for LIGS is

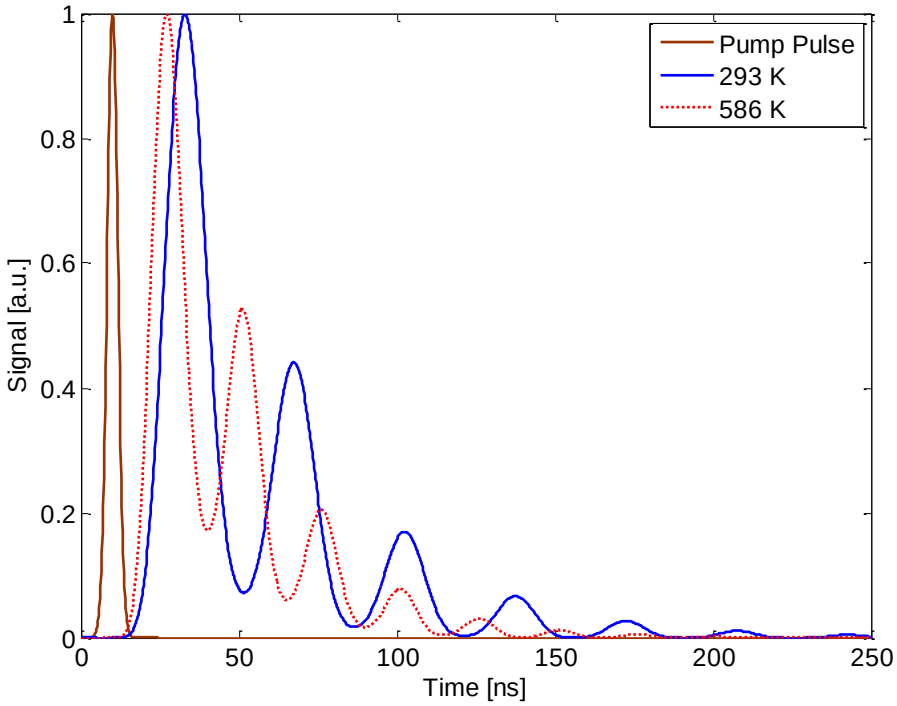


Figure 2.8: Modelled atmospheric pressure signals at 293 K room temperature and twice this value (586 K) are shown in blue and red respectively, for measurements made in an air environment at atmospheric pressure, where a fast quenching rate dominates. The timing of the pump pulse is shown in brown. The oscillation frequency of the signal is proportional to the square-root of temperature, as indicated by Equations 2.4 and 2.6, the effect of which is that LIGS signals from significantly higher temperature environments have a noticeably smaller oscillation period, τ.

thus developed based on the single temperature model described in Section 2.2 of this chapter and its validity is tested by comparison with experimental data. Chapter 5 then gives a description of LIGS measurements performed on ethylene-air flames, where the temperature field is more complex. Modelling flame environments would require further refinement of the model to account for continuous temperature gradients, as opposed to discrete temperature zones.

3 Experimental Method

This chapter describes the apparatus set-up used to conduct the experiments described in Chapters 4 and 5. Difficulties encountered during the process of designing and implementing the desired set-up is discussed where relevant. An explanation of how the LIGS data is collected and analysed is also provided. The first objective was to become familiar with the arrangement of optics, data collection and data processing. Consequently, some simple high pressure LIGS measurements were made during a preliminary experiment and a brief discussion of this work is provided in Sections 3.2 and 3.6.

3.1 Overview of Experimental Set-Up

Figure 3.1 shows a schematic diagram of the basic experiment layout used during this study for point measurement using LIGS. The term point in this case refers to a point-type probe volume defined by the interaction region of a cylindrical probe beam incident at the intersection of two cylindrical pump beams; in a point measurement set-up both pump beams and the probe beam are collimated or focussed using spherical lenses. This differs from a line-type probe volume defined by the interaction region formed by laser sheets generated using cylindrical lenses.

The pump pulses in this set of experiments originate from a Continuum Surelite I-10 flash lamp-pumped Nd:YAG laser. The output from the laser cavity gives infra-red radiation of 1064 nm wavelength, which is frequency-doubled within the laser housing to produce visible green radiation at 532 nm. The second harmonic is then frequency-doubled again to create the fourth harmonic of the fundamental frequency; this generates 266 nm ultraviolet (UV) pulses that coincide with suitable resonances in the molecular species investigated in this study, which will be detailed in the appropriate sections of this chapter. An intra-cavity adjustable aperture

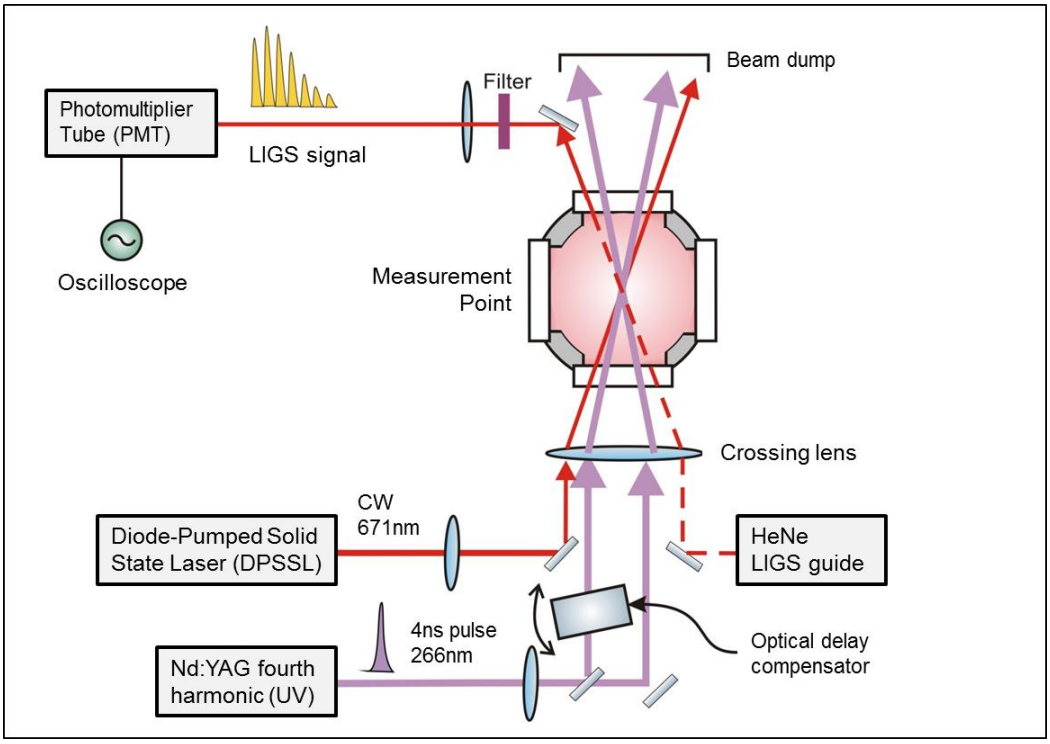


Figure 3.1: Schematic diagram of the LIGS experiment layout. The paths of the pump pulses are indicated in purple, while the continuous wave (CW) probe beam and the LIGS signal beam are illustrated in red. The dashed red line shows the path of the HeNe beam that acts as a dummy LIGS signal during the system alignment procedure. Spherical lenses, which are placed in the beam path to focus or collimate the beams as required, are indicated in blue. The white rectangles indicate the presence of high reflectivity mirrors that direct the laser beams towards the crossing lens. A detailed discussion of the apparatus at the location marked as the measurement point can be found in Section 3.2; a high pressure gas cell with optical access is shown as an example here.

confines the operation of this multi-mode laser to the TEM_{00} transverse mode, meaning that the spatial distribution of each pulse has a Gaussian profile to a good approximation. The Q-switch delay of the system affects the pulse energy and duration; in the configuration where the energy output is optimised, each UV pulse has a temporal FWHM of 4 ns and an energy of 15 mJ. In all experiments described in this thesis, the laser was operated at a 10 Hz pulse rate.

The output of the Nd:YAG laser is split using a dichroic mirror, where only the 532 nm green light component is reflected and any radiation at the fundamental frequency is directed towards a beam dump. The green pulses are directed towards a Glan-Taylor prism, where only the vertically polarised component is transmitted; the green output from the Nd:YAG laser is

primarily of a single polarisation type, so only a small fraction of the energy is reflected into a beam dump located near the prism. Each pulse then arrives at a highly birefringent, potassium dideuterium phosphate (KD*P) crystal; this is a non-linear frequency doubling crystal. The crystal converts a fraction of the incident light into 266 nm UV radiation of an orthogonal polarisation. Higher energy UV pulses can create a thermal grating with a higher reflectivity and this consequently intensifies the LIGS signal; thus the UV output from the crystal is maximised by carefully rotating the crystal to identify the optimum angle for achieving this objective. Next, the pulses reach a second Glan-Taylor prism that reflects only the horizontally polarised UV component, depositing the remaining green light into a beam dump.

Each UV pulse is then split into two using a 50:50 beamsplitter and mirror pairing as illustrated in Figure 3.1. Following the splitting process, one pulse in the pair passes through a fused silica optical delay compensator prior to reaching the crossing lens, to account for the additional distance introduced into the optical path of the other beam during the splitting process. It is necessary to do this because the two pulses must arrive at the crossing point within one coherence length of each other in order to maximise the visibility or contrast in the laser intensity fringe pattern at the pump interaction region.

A 300 mW diode-pumped solid state laser (DPSSL) is the origin of the 671 nm continuous wave (CW) probe beam, and it is the Bragg-scattering of this beam from the thermal grating that generates the LIGS signal beam of the same wavelength. During the alignment procedure detailed in Section 3.3, a second CW beam of 633 nm originating from a helium-neon (HeNe) laser acts as a dummy LIGS signal and traces the LIGS signal path.

The two pump pulses and the two CW laser beams are then directed towards a plano-convex focussing lens, identified as the crossing lens in Figures 3.1 and 3.2. Consequently the two pump pulses cross and interfere at the position marked in red as the measurement point in Figure 3.2. In the experiments that follow, the pump pulses and the probe beam are focused or collimated as required using spherical lenses placed in the optical path; further information

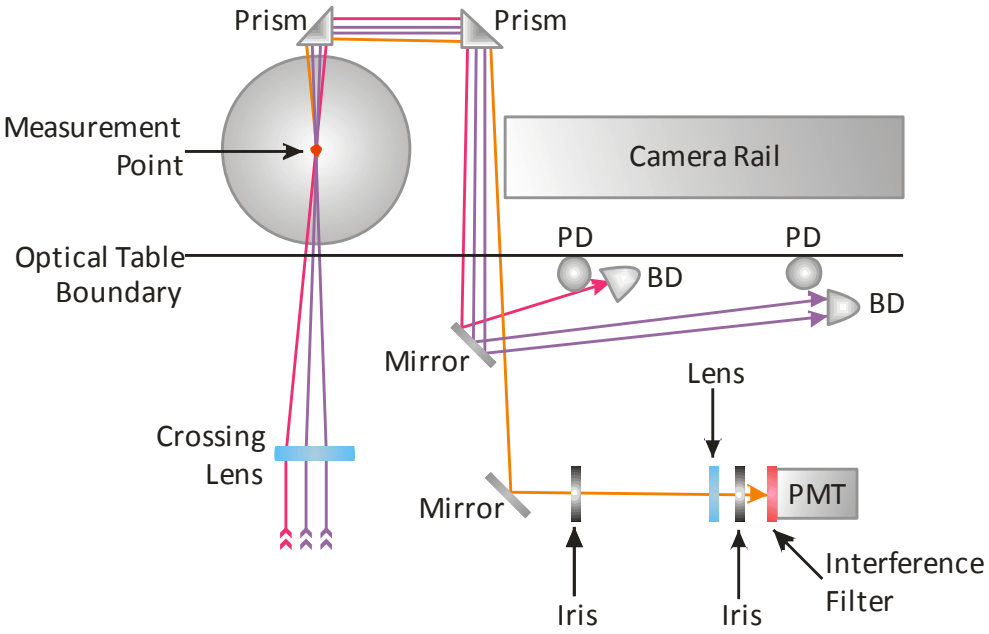


Figure 3.2: Schematic diagram of the experiment set-up illustrating the LIGS measurement point and instrumentation used in data collection. The paths of the pump pulses are indicated in purple, while the probe beam is illustrated in red. In this figure, the LIGS signal beam is indicated in orange for clarity, but is the same colour as the probe beam in reality. Silicon photodiodes are identified as PD and beam dumps are identified as BD. A fraction of the outgoing pump pulses and probe beam are monitored by the photodiodes. The LIGS signal is monitored with a photomultiplier tube module, which is identified as PMT in this figure.

about how this affects the diameter of the pump and probe is discussed where appropriate. The purpose of collimating or focussing the laser output is to allow for the size of the point-type interaction volume at the measurement point to be carefully controlled. Careful consideration was given to the selection of the focal length of the crossing lens and the spatial separation between each pair of pump pulses, since the geometry at the crossing point determines the LIGS grating spacing, Λ, as defined by Equation 2.1. It was explained in Section 2.1.2 that certain factors constrain the permissible size of the grating spacing; thus a suitable value for this parameter is calculated and imposed by regulating the geometry of the set-up at the crossing point. Purpose-built alignment masks are used to implement this geometry; the alignment procedure is detailed in Section 3.3.

LIGS signal measurements are made with a Hamamatsu H6780-20 photomultiplier tube (PMT) module, while the outgoing pump pulses and probe beam are monitored after the measurement point using silicon photodiodes; the latter is an attempt to identify any fluctuations in intensity of the pump and probe laser output. The two irises and 671 nm interference filter placed in the path of the LIGS signal beam, as shown in Figure 3.2, serve the purpose of minimising scattered light from the pump and probe sources reaching the PMT. A short focal length lens is placed in front of the last iris and is positioned such that it brings the signal beam to a focus at the central aperture of the iris, after which the beam diverges to occupy the entire detector surface of the PMT; this decreases the possibility of the photocathode saturation which may result if a high intensity signal with a small beam diameter illuminates only a small fraction of the active detector area. The PMT is optically shielded using housing made from black cardboard in order to further reduce stray light reaching the detector. The gain of the PMT is adjusted prior to recording data in order to optimise the LIGS signal-to-noise ratio.

A LeCroy WaveRunner 6100A oscilloscope is used to record all data from the PMT and photodiodes on three channels of the oscilloscope, where the instrument is externally triggered using the connection port that is synchronised with the Nd:YAG output. Next, the data is transferred onto a computer where MATLAB software is installed in order to analyse the data. The camera rail shown in Figure 3.2 is used to mount a camera for imaging the Gülder burner flame as detailed in Chapter 5.

3.2 Apparatus Set-Up at the Measurement Point

This section provides a detailed description of the apparatus arrangement at the location marked as the measurement point in Figure 3.2, for the four types of measurement environment detailed in this thesis.

3.2.1 Toluene Test Cylinder

A few drops of toluene placed inside a short length of plastic tube, 5 cm in length and of 1 cm diameter, is used to provide a reliable LIGS signal to aid in optimising the alignment of the measurement system. The liquid toluene evaporates to form a vapour that acts as the pump energy absorber and this test is discussed further in Section 3.3. The high density of absorbing species arising from such an arrangement generates a highly reflective thermal grating, and consequently provides a high intensity LIGS signal that is easily measurable for test purposes. The small cylinder is placed on an aluminium rail that is securely fixed to the optical table for the duration of each alignment test.

3.2.2 High Pressure Gas Cell

Section 3.6 outlines some preliminary work carried out in a high pressure gas environment. In this set-up, the measurement point is enclosed within a cylindrical stainless steel cell; the cell is 30 cm in length and approximately 4 cm in diameter. Fused-silica windows, 50 mm in diameter and 12.7 mm in thickness, are fitted on to the two ends of the cylinder to provide optical access to the cell interior. Toluene condenses and forms films on cell windows, so acetone is used instead as the absorbing species. The quantity of acetone used is one that is previously determined as producing an unsaturated vapour in the cell volume; thus the tests are conducted with a few drops of acetone, which are introduced into the cell through a valve, via a syringe.

The gas composition is controlled by a high pressure gas system connecting the cell to oxygen and nitrogen cylinders. Each gas cylinder is connected to a manifold constructed from stainless steel piping, via a valve and a regulator; the gas pressure is measured with a transducer upon entry into the cell and is displayed in bar gauge relative to the atmospheric pressure. During the preliminary work reported in Section 3.6, experiments are conducted at

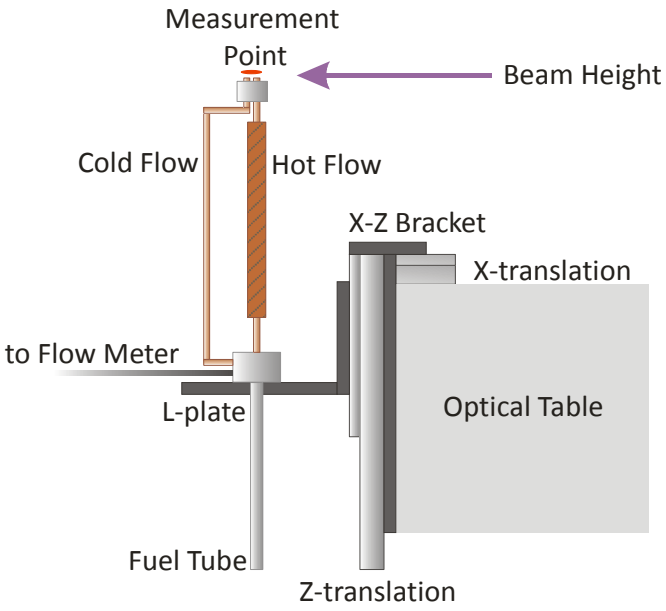


Figure 3.3: Simplified diagram of the dual ethylene flow set-up at the LIGS measurement point. The *hot flow* is connected to a heating element; the *cold flow* is at room temperature. The L-plate holds the two flows in place and attaches them to the translation stages, marked as Z- and X-translation in the diagram; this enables the user to adjust the position of the flow system relative to the optical table.

pressures of up to 8 bar, which is significantly lower than the maximum pressure that the cell is able to withstand according to its design specification.

3.2.3 Ethylene Flow

Chapter 4 of this thesis reports a series of tests carried out using an experiment set-up that includes a temperature-controlled ethylene flow system; this is illustrated in Figure 3.3. The apparatus arrangement consists of a fuel tube originating from a valve and regulator that is connected to an ethylene gas cylinder, which is securely attached to two copper pipes, as seen in the figure above. One pipe is connected to a heating element and thus provides a heated flow of ethylene, while the other provides a room temperature ethylene flow; these are labelled as *hot flow* and *cold flow* respectively.

The flow rates are controlled and monitored using a flow meter, which allows the user to control each flow separately and operate the system as single flow or dual flow. Adjusting the voltage applied to the heating element enables the user to control the temperature of the hot flow. However, ethylene auto-ignites at 763 K in an air environment [34]; accordingly, for safety reasons, it is essential to carefully monitor the temperature of the hot flow to ensure that it is kept well below this point. In the experiments described in Chapter 4, the temperature of each flow is initially measured using a thermocouple, prior to calculating it using LIGS data. Additionally, both copper pipes are enclosed within highly insulating material to minimise heat transfer between the two pipes (not shown in Figure 3.3). The separation of the two pipes corresponds to the size of the probe volume and this is discussed further in Chapter 4.

As shown in Figure 3.3, the ethylene flow system is attached to the L-plate, which is fixed to the Z-translation stage. This dual flow set-up is a basic system intended to demonstrate the effect of two temperature zones contributing to the LIGS probe volume. Hence it was necessary to improve the precision and accuracy of LIGS by minimising the risk of unknown temperature gradients being introduced into the probe volume through the mixing of gas flows. Therefore, the height of the flow output was adjusted relative to the height of the incoming pump pulses and probe beam to minimise flow mixing; the measurement point was set to less than 0.5 mm above the upper end of the two copper pipes. Consequently, this also generates higher intensity LIGS signals by maximising the density of absorbing species at the measurement point and improves the signal-to-noise ratio. The Z-translation stage itself is mounted onto an X-Z bracket that is attached to the X-translation stage, which allows the flow system to be translated in and out of the page, in the context of Figure 3.3. This allows the user to adjust the lateral position of the ethylene flow, such that the centre of the flow is aligned well with the centre of the LIGS probe volume.

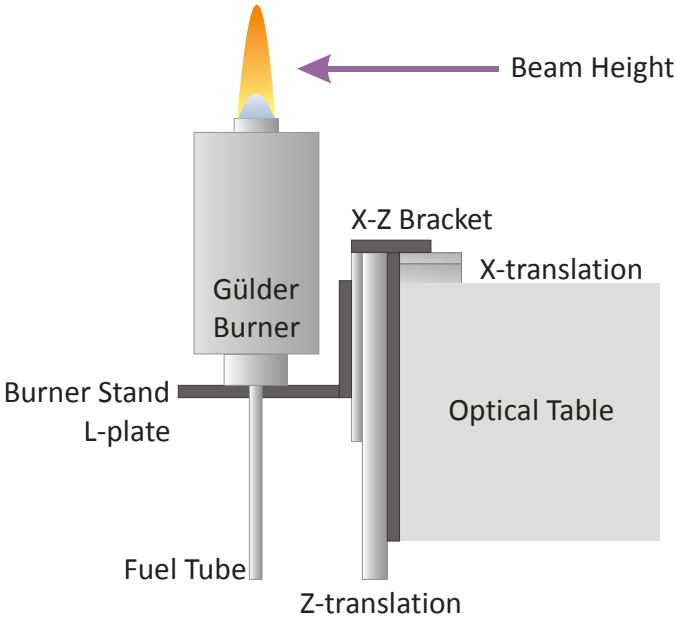


Figure 3.4: Simplified diagram of the Gülder burner set-up at the LIGS measurement point. The L-plate holds the two flows in place and attaches them to the translation stages, marked as Z- and X-translation in the diagram; this enables the user to adjust the position of the Gülder burner flame relative to the optical table.

3.2.4 Gülder Burner

In Chapter 5 of this thesis, a set of experiments carried out using a Gülder burner are reported; the experimental set-up for the burner is shown in Figure 3.4. A Gülder burner is a type of standardised laboratory burner that provides a co-flow laminar diffusion flame, with a central nozzle providing an ethylene flow and an outer annulus of the cylindrical burner providing an air flow. Mass flow controller units, connecting the ethylene and air systems to the burner, allow careful control over flow stoichiometry. A collaborating research group within the University of Oxford has conducted three colour pyrometry measurements in the flame of the burner used during this study [23]. Based on the results of this work, a fixed stoichiometry flow rate of 180 mL min^{-1} ethylene and 120 L min^{-1} air is selected to produce a tall, stable, non-turbulent flame. These conditions produce a flame that is approximately 7 cm in height as measured from the base at the burner nozzle, to the visible tip.

The lowest part of the flame contains unburned fuel under the flame front. Polycyclic aromatic hydrocarbon (PAH) molecules, which are precursors to soot formation, are found in the lower, more transparent region; the yellow part of the flame contains soot, with, broadly speaking, larger aggregates higher up in the flame [3] [4]. Consequently, in addition to ethylene, it is possible that the PAHs and soot particles may act as absorbing species when LIGS is applied to a flame environment. A detailed discussion on this topic can be found in Chapter 5.

Similarly to the ethylene flow system, the Gülder burner is also set up on a translation stage arrangement, identical to that described in Section 3.2.3. This allows the user to access any point in the flame for the purpose of making a LIGS measurement. A non-turbulent flame produced using a Gülder burner has cylindrical symmetry. Therefore it is unnecessary to incorporate a third translation stage into the set-up to allow for the motion of the flame in the Y-direction, perpendicular to the X- and Z-directions.

3.3 Alignment Procedure

As noted previously, all laser beams must be aligned to produce a pre-calculated geometry that is suitable for generating a LIGS signal from which temperatures, and other combustion-relevant parameters, can be measured. Based on the theory discussed in Chapter 2, for a LIGS signal to be useful for combustion parameter measurement, it requires the geometry at the measurement point to give rise to LIGS signals with several resolvable oscillations to allow for the calculation of a precise oscillation frequency from its Fourier transform. The alignment procedure illustrated in Figure 3.5 is used for this purpose.

A MATLAB program was developed by the author to calculate the Gaussian beam diameters and geometry required to produce suitable LIGS signals for a variety of experiment conditions by specifying the parameters corresponding to each experimental variable. Subsequently, the appropriate spatial positions of the incoming and outgoing beams, at specific

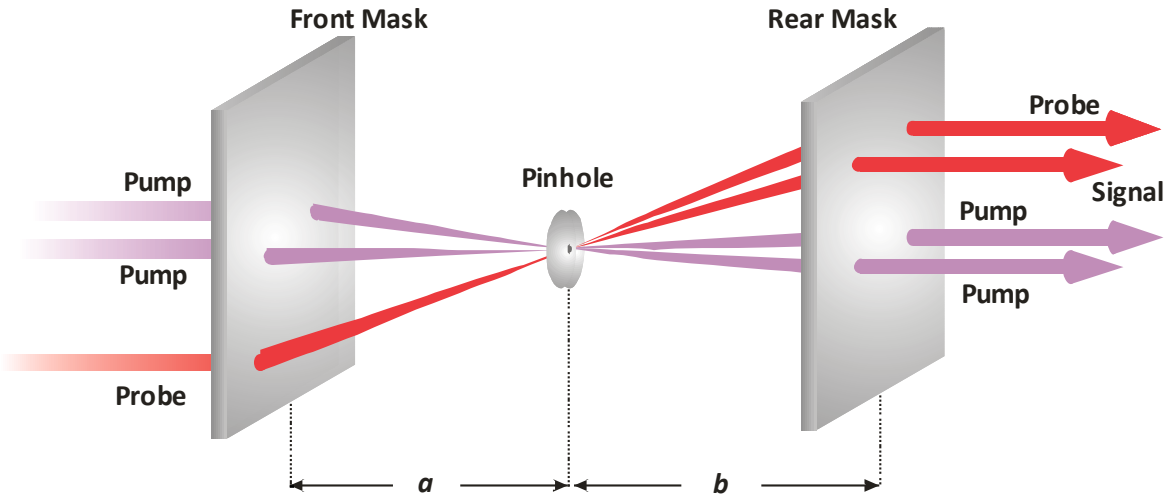


Figure 3.5: Alignment of the pump, probe and LIGS beams using an arrangement of two masks and a pinhole placed at the crossing point. The masks are positioned at distances *a* and *b* from the pinhole by securely attaching them to a rail that is fixed to the optical table. The distances between the three objects shown in the figure, along with the spatial separation of holes in the masks which the beams pass through, determine the beam geometry at the measurement point.

distances from the beam crossing point, were successfully determined. Two alignment masks were constructed from 5 mm thick aluminium plate, containing holes that are 1 mm in diameter; the holes were drilled in specific positions to allow the beams to pass through them to generate the desired geometry when the masks are positioned at distances *a* and *b* from the crossing point.

During the alignment procedure, the masks are secured in place with the use of a rigid aluminium rail fixed above the measurement point, containing screw holes in carefully calculated positions. A pinhole that is 500 µm in diameter, is mounted to an arrangement of translation stages to provide full X-, Y- and Z-translation capability. The pinhole is carefully centred such that the beams cross at the exact position where the first LIGS measurement in a set of measurements is to be made. In the case of the Gülder burner, this is the centre of the burner nozzle, at 0 mm height above burner. Next, the two pump pulses are aligned, after which the probe and HeNe (the dummy LIGS signal) beams are aligned; all beams are aligned by making adjustments to the optics placed between the laser source and the crossing lens. When

the system is successfully aligned in accordance with the desired geometry, all four beams pass through both masks and the pinhole. If the diameter of a beam exceeds that of the holes in either mask or pinhole, the beam is aligned such that its centre is positioned on the hole.

Next, the pinhole and masks are removed, and an alignment test is carried out using the set-up described in Section 3.2.1. The plastic tube is positioned such that it is centred at the initial measurement point as set by the pinhole. If the alignment is successful, when the Nd:YAG and probe laser are in operation, a LIGS signal should be displayed on the LIGS channel of the oscilloscope. LIGS signals can be optimised by making delicate adjustments to the optics, while monitoring the intensity of the signal with the oscilloscope, to achieve the best possible alignment. Once the signal has been optimised, the toluene test cylinder is removed and the high pressure gas cell, the ethylene flow or the Gülder burner, can be installed in its place. If the alignment test returns a negative result, it is necessary to examine possible sources of error in implementing the alignment procedure, make appropriate corrections and repeat the process until the alignment test produces a positive result: a LIGS signal with a high signal-to-noise ratio, where the term high in this context typically refers to a maximum signal intensity that is at least an order of magnitude larger than the baseline noise level.

3.4 Design, Selection and Construction of Apparatus

The design for the dual ethylene flow system illustrated in Figure 3.3 was developed following a series of preliminary tests carried out using a variety of single and dual flow set-ups to establish the best arrangement for successful LIGS measurement; this is discussed further in Chapter 4.

One difficulty faced in implementing the LIGS set-up illustrated in Figure 3.2 was that while the ethylene flow system and the Gülder burner could not be placed on the optical table due to the placement of the long, rigid fuel tube illustrated in Figures 3.3 and 3.4, there was no

apparatus readily available to mount either the flow system or the burner to the side of the optical table. Thus it was necessary to construct such a set-up from the beginning.

The translation stages were purchased from Thorlabs, Inc. after careful assessment of the variety of products available on the market, in order to select the type of stage that is best suited to the experiments detailed in Chapters 4 and 5. Factors considered in making the purchase included the maximum mass the stage is able to translate without difficulty, the associated precision of motion and the cost of the stage relative to its advantages. After developing a detailed layout plan for the optical components required for experiments detailed in Chapter 4 and 5 using CorelDRAW Graphics Suite X4 software, suitable components were selected and purchased from Thorlabs, Inc. The L-plate and the X-Z bracket seen in Figures 3.3 and 3.4 were designed by the author using CorelDRAW since suitable devices were not readily available on the market; both pieces of apparatus were constructed by the author at the Research Workshop facility at the Department of Physics, University of Oxford. The alignment masks and rigid aluminium rail used for the alignment procedure were also designed and constructed by the author.

Another difficulty faced in achieving the desired experiment set-up shown in Figure 3.2 was the lack of surfaces to which the two prisms positioned outside the boundary of the optical table could be mounted. Thus a small extension to the optical table was constructed by the author and securely attached to the main table at a suitable location.

3.5 Analysis of LIGS Signal Data

The oscilloscope data collected from each experiment is saved into a set of data folders. Each folder is labelled by the specific conditions under which the experiment was carried out, for example, temperature, pressure or gas composition. Therefore, if data is recorded at several different pressures in an environment where temperature and gas composition is kept constant,

the folders are labelled by the gas cell pressure. Each data folder contains multiple datasets: data from each oscilloscope channel, and a large number of repeat measurements recorded with a specific experimental condition for the purpose of calculating mean values and the associated standard deviation.

All data analysis is performed using MATLAB. The author has written a new data analysis program based on one that was originally developed by B. A. O. Williams at the University of Oxford in 2010, and updated in 2011 by M. Edwards [35]. An in depth discussion of the data analysis method is found in Chapter 4; the MATLAB scripts and functions that comprise the LIGS data analysis program are included in Appendices 1, 2, 3 and 4.

However, the preliminary work presented in Section 3.6 uses the earlier version of the data analysis program created by Edwards [35]. The program executes a primary MATLAB script, which employs three user-written functions to carry out separate tasks. The first function loads all raw oscilloscope data from the LIGS channel contained within a specified data folder into the MATLAB workspace; the signal and time vector information are extracted from each set of data and prepared for further analysis. The second function identifies and saves data shots where the signal intensity falls within a pre-defined range of intensities, where the minimum threshold value is set relative to the baseline noise level in the signal and the maximum permissible value is determined by the detector saturation limit. The selected data shots are passed through to the third function; this function calculates the mean oscillation frequency and standard deviation for a single experimental condition, by computing the power spectrum corresponding to each LIGS signal using the in-built Fourier transform function. The output from the data analysis program is consequently used to generate line plots of the mean LIGS signal and its corresponding power spectrum. The program also calculates the peak oscillation frequency, which is then used to determine a temperature value.

3.6 Preliminary Work

Prior to conducting experiments in non-uniform temperature fields and flames, some preliminary work was carried out in a high pressure, room temperature environment; a LIGS system has previously been tested under such conditions [32]. The objective of this preliminary work is to familiarise oneself with the use of a LIGS experiment set-up and the relevant alignment procedure, as well as the use of MATLAB for the analysis of LIGS signal data.

The apparatus was arranged on the optical table as illustrated in Figures 3.1 and 3.2. The set-up detailed in Section 3.2.2, with the high pressure gas cell, was implemented at the measurement point for this set of experiments. Spherical lenses were added to the path of the pump pulses and the probe beam such that the beams arriving at the measurement point are collimated; however, it should be noted that focussed beams were used in the experiments detailed in Chapters 4 and 5. Based on the diameter of the probe beam and the geometry of the set-up, the probe region was calculated to be 1.2 mm in diameter and 50.0 mm in length; the relatively large probe length here arises from the fact that the probe beam is incident on the thermal grating at a very small angle (less than 2°) in order to match the Bragg scattering condition. However, at this stage, the size of the probe region is irrelevant because this is a constant temperature test and thus no temperature gradient exists within the probe region.

A LIGS signal recorded with acetone as the pump absorbing species, at room temperature in a 6 bar pure oxygen environment, is shown in Figure 3.6. According to a thermocouple measurement, the temperature was 295.0 ± 0.5 K. The signal plotted in Figure 3.6 is the mean of individual signals from 50 oscilloscope data shots; calculating the mean from a large number of data shots serves the purpose of averaging over random noise present in each LIGS signal and thus improving the overall signal-to-noise ratio.

The form of the LIGS signal presented in Figure 3.6 is comparable to the 5 bar modelled LIGS signal in Figure 2.7, discussed in the previous chapter. Higher pressure retards the

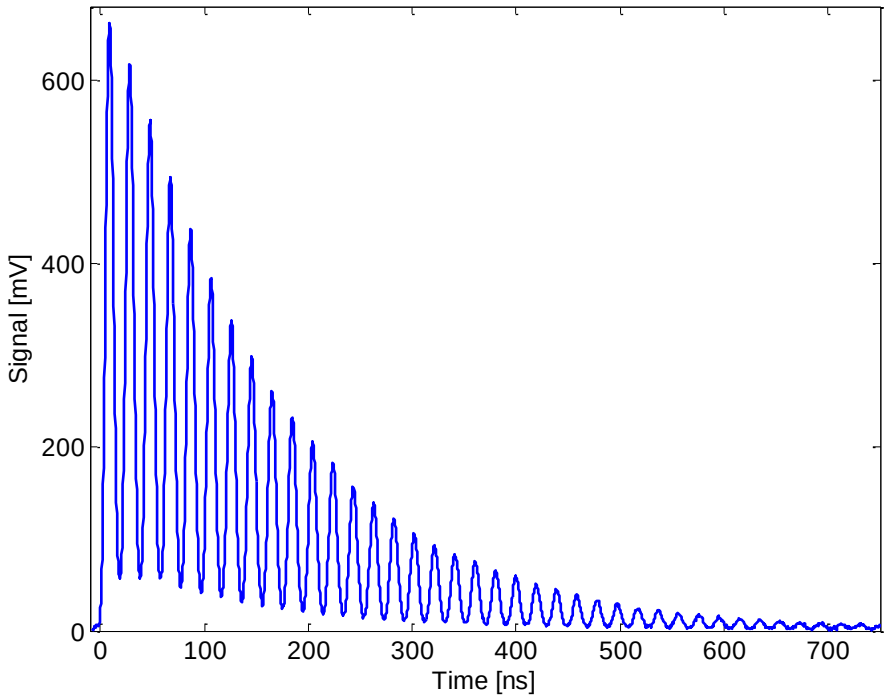


Figure 3.6: LIGS signal recorded with acetone as the pump absorbing species, in a 6 bar oxygen atmosphere, at 295 K.

diffusion rate of gas molecules, preventing the interaction region from quickly returning to equilibrium. This prolongs the lifetime of the density modulation, and this is apparent from the fact that the oscillations are resolvable for a longer time frame when compared with the expected duration of a signal recorded at atmospheric pressure.

Next, the frequency spectrum of the signal shown in Figure 3.6 was calculated using the Fourier transform function in MATLAB; this is presented in Figure 3.7. The peak frequency is identified by the red line in the figure. From the peak frequency value, a temperature of 295.0 ± 0.3 K was calculated as the temperature of the measurement point, where the uncertainty specified here is derived from the standard deviation of oscillation frequency over the 50 shots in the dataset, and is thus a measure of experimental precision. It can be seen that the precision of this temperature measurement is 0.1%, which is representative of the typical degree of precision LIGS can achieve [1]. The accuracy of the measurement is dependent on the accuracy

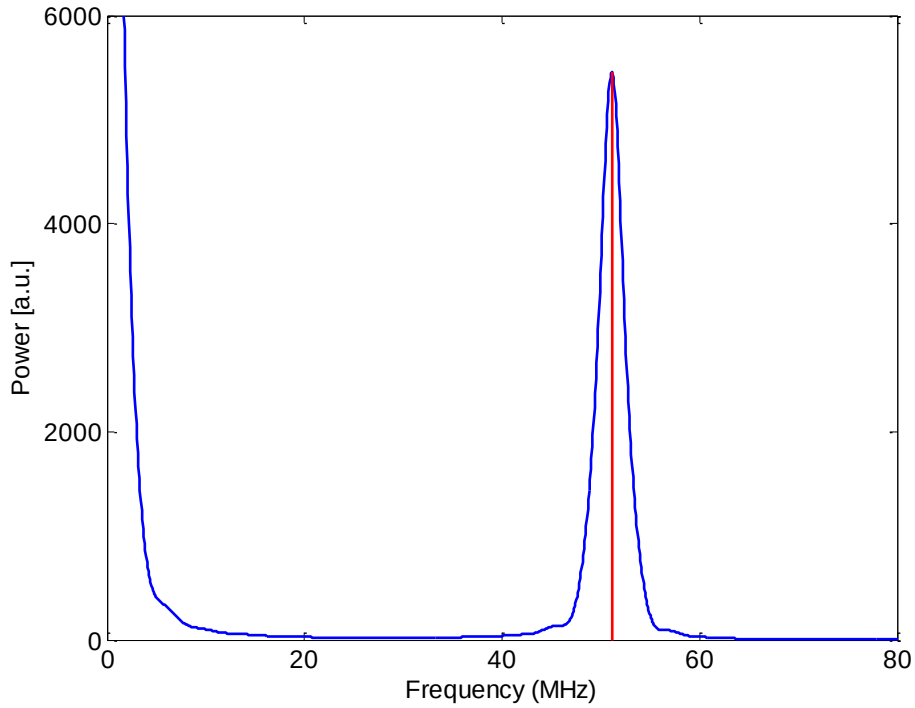


Figure 3.7: Frequency spectrum calculated from the Fourier transform of the LIGS signal data recorded with acetone, in a 6 bar oxygen atmosphere at 295 K, with acetone as the pump absorbing species, as displayed in Figure 3.6. The red line identifies the peak oscillation frequency from which the temperature is calculated.

to which $\sqrt{\frac{m}{\gamma}}$ is known, and in this experiment, a carefully controlled gas composition within the cell enables this parameter to be determined to a high degree of accuracy. Consequently, the temperature measurement made using LIGS is expected to be highly accurate; it is within the experimental uncertainty of the thermocouple measurement. Furthermore, the results from this preliminary test agree well with those from earlier studies of the same physical environment [32].

Finally, a series of LIGS measurements were made with oxygen and nitrogen gas mixtures at a room temperature of 295 K and a total pressure of 4 bar, with the partial pressure of oxygen (p.p. O_2) varied from 0 bar to 4 bar. The data was analysed with a MATLAB program used in the author's research group, which was appropriately edited to account for differences

in experimental set-up. Since this work simply repeats the results presented by Williams [32] for preliminary test purposes, the results have not been presented in this thesis. It was found that increasing p.p. O_2 led to a reduction in the oscillation frequency of the LIGS signal, which is in good agreement with the results presented by Williams. According to Equation 2.5, the oscillation frequency is inversely proportional to $\sqrt{\frac{m}{\gamma}}$. Since the ratio of specific heats, γ, is approximately equal for nitrogen and oxygen at room temperature [36], it is possible to conclude that this trend is a consequence of oxygen having a higher molecular mass.

Since the results from this preliminary work correlate well with those from previously published studies as noted above, this demonstrates that the author has been able to successfully design and implement an appropriate experimental set-up for LIGS. Therefore, a similar set-up can now be employed to test the application of LIGS in two new environments: a non-uniform temperature field produced using a dual ethylene flow, and a Gülder burner flame.

4 LIGS Thermometry in an Ethylene Flow

As outlined in Chapter 1, one of the two key objectives of this study is to investigate non-uniform temperature fields originating from temperature-controlled ethylene flows. In the first section of this chapter, a method of selecting an appropriate probe volume for the experiment is provided. Next, LIGS measurements from a dual ethylene flow set-up are presented. The first set of results is a test measurement, with the flow system operating as a single flow. The second set of results presented form the primary focus of this chapter, and originate from the simultaneous dual ethylene flow operation, which generates a controlled non-uniform temperature field within the probe volume. The purpose of these measurements is to determine how contributions to the probe volume from regions of different temperature affect the LIGS signal. A model is developed to simulate the effect of having two or more regions of different temperature within the probe volume; the modelled data is presented with the experimental data for comparison. Finally, the achievements and limitations of the model are discussed.

4.1 Calculation and Verification of Probe Volume

All LIGS measurements presented in this chapter were made using the experimental set-up described in Section 3.2.3 and illustrated in Figure 3.3. The first step in making a set of measurements using the dual ethylene flow and the Gülder burner flame is to identify an appropriate probe volume for the measurement.

In the case of the flame, it is desirable for the diameter of the probe volume to be small relative to the diameter of the burner nozzle to provide good spatial resolution along one axis of translation; this is necessary to investigate temperature differences that exist at different radial positions relative to the central vertical axis. For the length scales explored in the flame, the

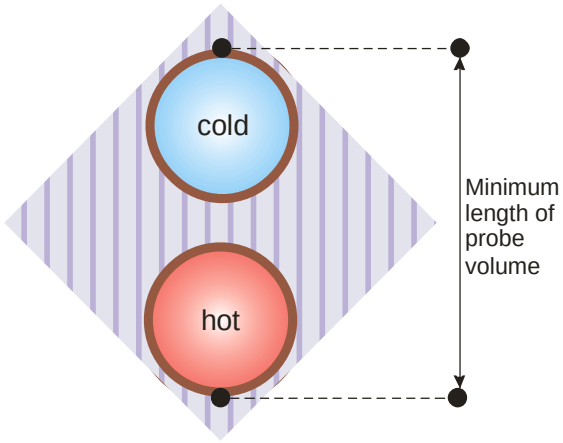


Figure 4.1: In the dual ethylene flow set-up, the output from both copper pipes must exist within the pump interaction region, as illustrated in this image. The probe diameter and beam geometry at the measurement point is set such that the length of the probe volume spans a distance greater than that defined by the upper edge of the cold flow pipe to the lower end of the hot flow pipe; this is necessary to ensure that both flows contribute fully to the LIGS signal when simultaneously operated.

minimum diameter of a focused probe beam, as determined by diffraction or optical aberrations, sets the limit of resolution achievable with the LIGS technique when constructing a temperature map.

In the case of the dual ethylene flow, the diameter of the probe volume must simply be equal to or smaller than the diameter of the gas flow pipes, as seen in Figure 4.1. The reasoning behind this is to use the energy of the incoming probe beam efficiently to generate a high intensity LIGS signal with a high signal-to-noise ratio. The diagram in Figure 4.1 shows two ethylene flow pipes in contact with air at atmospheric pressure, lying within the pump interaction region where intensity fringes form. In the regions where the ethylene flows exist, ethylene molecules absorb the pump energy and transfer it to the bulk gas through collisional quenching. Thus the thermal grating which scatters the probe beam forms only where the ethylene flow is present and consequently, there is no contribution to the LIGS signal from the surrounding region. Therefore, restricting the diameter of the probe volume as noted above maximises the proportion of the probe scattered by the thermal grating. In the experimental set-up used in this study, the diameter of the probe volume is equal to the diameter of the probe

beam at the crossing point, where the two values are in agreement to ±1 μm; this was verified using a basic spatial resolution calculation program developed by the author in MATLAB. The similarity between the two diameters arises from the fact that the probe beam is incident on the thermal grating at a very small angle (less than 2°) in order to satisfy the Bragg scattering condition corresponding to the spacing of the thermal grating planes.

However, in both the dual ethylene flow set up and the Gülder burner set-up, the length of the probe volume is of critical importance. In LIGS measurements where the probe volume is assumed to be of a single temperature, the beam geometry is set to implement the minimum possible probe length, as this minimises the risk of sampling a probe volume with a non-uniform temperature field where regions of multiple temperature contribute to the LIGS signal. Since the aim of this thesis is to explore the effect of multiple temperature contributions to a probe volume, it is desirable to select a probe length that is sufficiently long to sample the entire non-uniform temperature region of interest. In the case of the Gülder burner flame, this is a line segment that exceeds the diameter of the burner nozzle, so a single LIGS measurement at any radial position within the flame samples a chord of known length passing through its circular cross section. In the dual ethylene flow set-up, this must be a length that spans a distance greater than that defined by the upper edge of the cold flow pipe to the lower end of the hot flow pipe, as defined in Figure 4.1. This ensures that both ethylene flows contribute fully to the LIGS signal when simultaneously operated.

Based on the limits discussed above, the length of the probe volume must exceed 11.6 mm. The probe length is dependent on both the probe beam diameter at the crossing point, which is controlled by the optics placed between the probe laser and this position, as well as the angle at which the probe is incident. The latter is fixed relative to the angle at which the pump pulses are crossed, in accordance with Equations 2.1 and 2.2. Thus a suitable beam geometry must be calculated and implemented, such that the angle at which the pump pulses cross

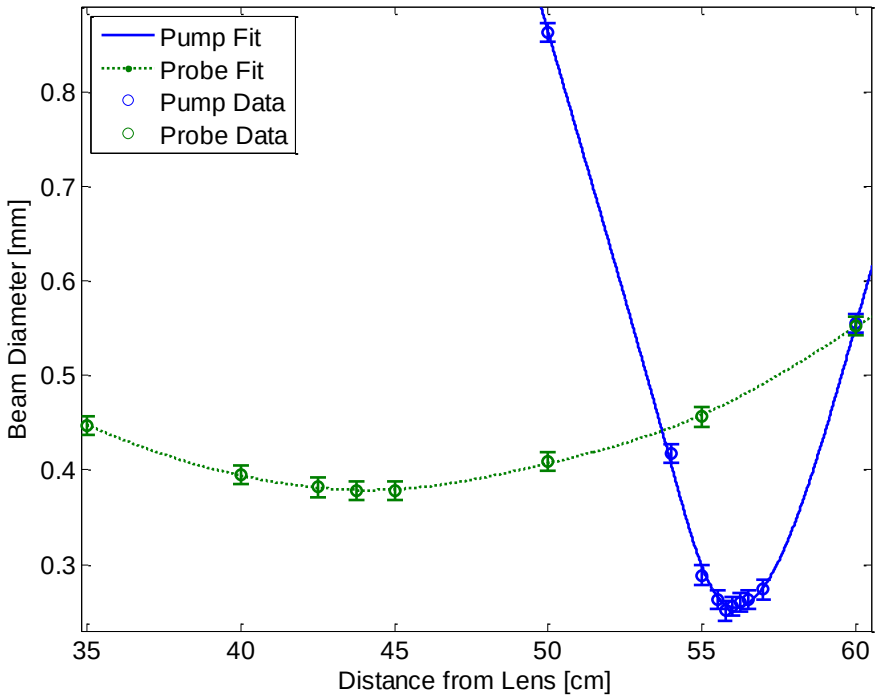


Figure 4.2: Variation of probe beam and pump pulse diameter with distance from the crossing lens, as calculated from the $1/e^2$ definition of Gaussian width, for the case where the probe and pump are brought to a focus without any telescope systems placed in the optical paths. The error bars represent the uncertainty in the power measurement recorded by the power meter, as observed by fluctuations in the value about the mean.

generates a grating spacing which would result in a probe beam incident at the Bragg angle to produce a probe length that exceeds the minimum value specified above. Consequently, a probe diameter of approximately 300 μm, achievable with the use of a focused probe beam, and a probe length of 13.3 mm, were deemed to be suitable for the LIGS measurements discussed in this chapter and the next. The precise value of the probe length is unimportant because it has been chosen for practical reasons relevant to the alignment procedure.

Figure 4.2 shows a set of measurements that were made to determine how the diameter of the pump and probe beams vary as a function of distance when they are focused by the crossing lens, when no other lenses are present in the optical path. The diameter of the beam was measured using a knife edge set-up on a high precision translation stage, which was

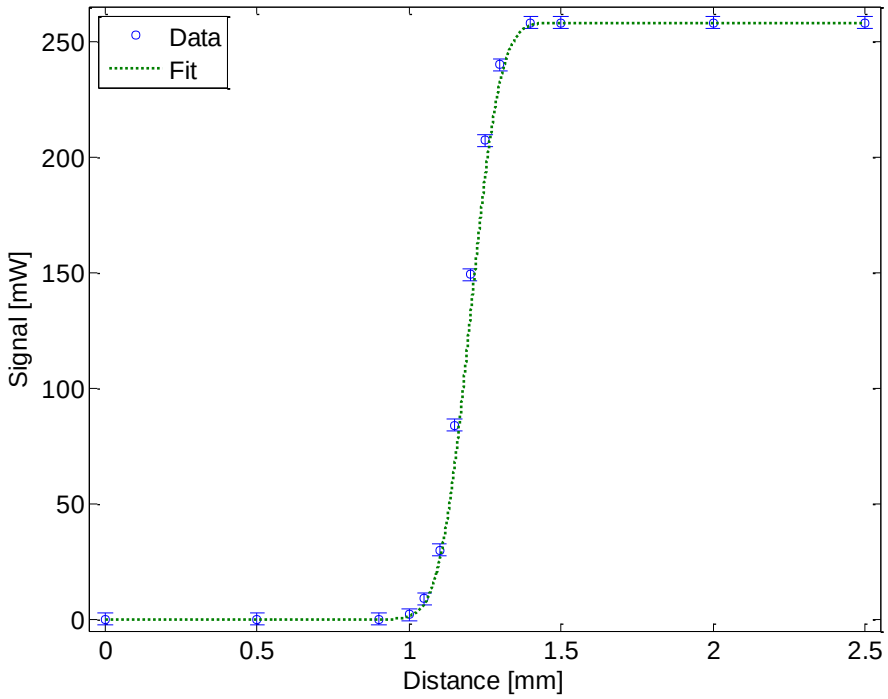


Figure 4.3: Experimental data from a single beam diameter measurement for the probe laser beam, recorded at the crossing point, with a cumulative Gaussian fit. The beam diameter was found to be 300 μm in this case from the Gaussian calculated from this fit, using the $1/e^2$ definition of Gaussian width. The error bars represent the uncertainty in the power measurement recorded by the power meter, as observed by fluctuations in the value about the mean.

translated transversely through cross sections of the beam, while a power meter was used to record a cumulative Gaussian intensity profile; similar to that shown in Figure 4.3. A suitable fitting routine was implemented with MATLAB in order to determine the beam diameter at each spatial position, defined in this case as the $1/e^2$ definition of Gaussian width.

If the probe beam is focused, it is also necessary to focus the pump pulses in order for the probe volume to be of a similar size to the pump interaction region; this allows for the efficient use of pump and probe energy, which should consequently give rise to higher intensity LIGS signals with a high signal-to-noise ratio. From Figure 4.2, it is apparent that a pump pulse diameter of approximately 300 μm could easily be achieved by setting the crossing point at a distance close to the 55 cm location. Note that the pumps cross at a smaller angle than the angle

at which the probe is incident and thus the pump interaction length for a given diameter will always exceed the probe length for the same beam diameter. It can be seen from the Figure 4.2 that it is necessary to place an appropriate combination of spherical lenses in the path of the probe beam in order to reduce its beam waist to a value approaching 300 μm. Consequently a probe beam diameter of 300 ± 10 μm was achieved using a suitable lens telescope system, where the beam diameter near its focus was reduced by increasing the spot size at the crossing lens; the uncertainty represents the standard deviation of a set of measurements. The diameter of the pump pulses at the selected crossing point was measured to be 320 ± 20 μm, and so is similar in magnitude to the probe diameter as desired.

4.2 Uniform Temperature Field: Results and Discussion

Before experimenting with the ethylene flow set-up described in Section 3.2.3 in its simultaneous dual flow operation mode, tests were carried out under single flow operation, the results of which are detailed in this section. It was possible to conveniently switch between operating each of the two flows illustrated in Figure 4.1 by adjusting settings in the flow meter which regulates the entry of ethylene from the mass flow controller unit to the dual flow system. The ethylene flow originates from a single high pressure ethylene cylinder, which is connected to the mass flow controller unit via a valve and a regulator. The controller unit is linked to a computer, which contains a LabVIEW program developed by the research group to control the stoichiometry of the Gülder burner flame. It was possible to modify appropriate settings within this program to set the ethylene flow rate into the dual flow system to a value of 180 mL min^{-1}, which is the same flow rate that the burner is operated under for reasons discussed in Section 3.2.4.

There were three key motives for conducting the single ethylene flow experiments in a uniform temperature field prior to working with the dual flow in a non-uniform temperature

field. One reason is that it was first necessary to familiarise oneself with the use of LIGS in an ethylene flow set-up to identify potential difficulties and limitations that may arise when working with the dual flow. Secondly, as discussed in Chapter 3, ethylene auto-ignites at 763 K in an air environment [34]; thus it was necessary make a number of measurements with the heating system in operation to determine how the temperature of the heated flow depends on the voltage applied to the heating element, and thus identify a maximum voltage limit for safe operation of the dual flow system to prevent the ethylene auto-igniting during the study. Finally, fitting the existing single temperature probe volume model to the single flow data would provide useful information on how parameters critical to the multiple temperature LIGS model vary with temperature. Hence this data could be fed into the multiple temperature model once that is developed to improve the correspondence between theoretical and experimental LIGS signals for specific conditions.

4.2.1 Room Temperature Single Ethylene Flow

As a first test, LIGS measurements were made on a single flow of ethylene operated at room temperature, and measured as 293 ± 1 K using a thermocouple. The results are presented in Figure 4.4. A simulated signal for the same conditions, generated using the basic signal generator model currently used within the research group, is also plotted for comparison.

The LIGS signal data plotted in Figure 4.4 is the mean signal intensity calculated from 482 data shots; the seemingly arbitrary choice for the number of data shots over which the signal is averaged originates from the data sampling criterion applied to a 1000 data shot measurement set. Minimum and maximum limits are defined such that the LIGS intensity falls within a specific range of values; the 1000 shot measurement set is then processed using a MATLAB script written by the author to automatically select the data shots that fit the pre-defined intensity criterion. The intensity limits are specified to exclude signals with a very low

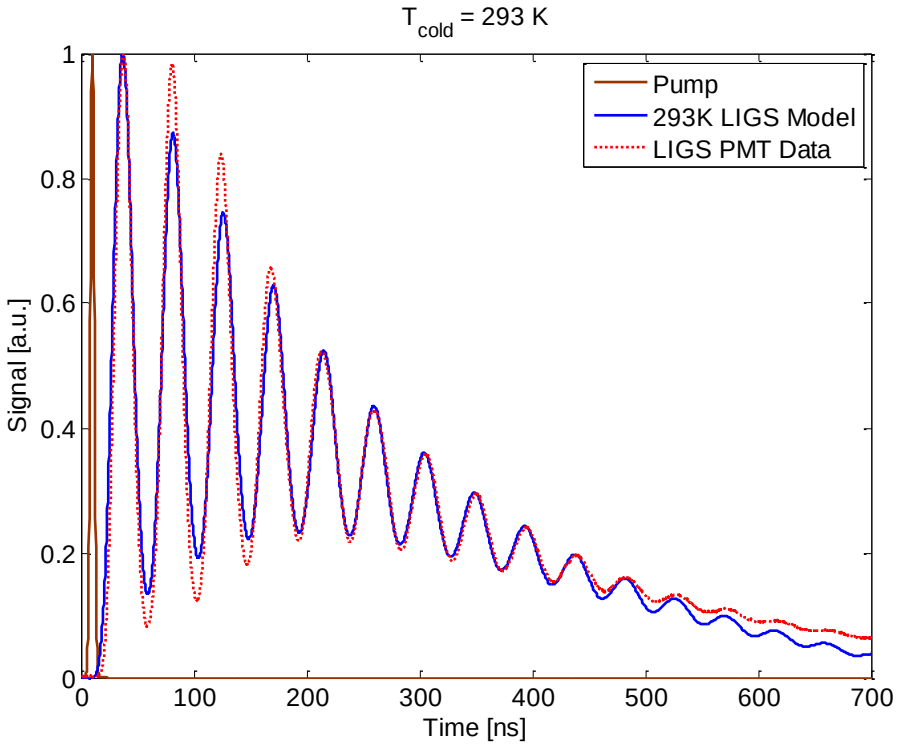


Figure 4.4: Single cold flow LIGS measurement (cold flow on, hot flow heater off) in ethylene at atmospheric pressure showing the correspondence between averaged experimental data from the photomultiplier tube (PMT) module and the 293 K (room temperature) modelled signal.

signal-to-noise ratio and very high intensity signals demonstrating characteristics of detector saturation. In all figures presented in this chapter, an identical data shot selection procedure has been implemented for reasons explained above.

The temperature corresponding to the oscillation frequency of the LIGS signal in Figure 4.4 was calculated to be 293 ± 2 K, where this temperature value is the mean of temperatures extracted from each of the 482 data shots, and the uncertainty represents the associated standard deviation. This value is in agreement with the thermocouple reading and has a precision of 0.7%, a value which correlates well the precisions typically achieved using the LIGS technique and is significantly superior to the typical precisions achievable through intensity dependent FWM techniques [1].

The results in Figure 4.4 also demonstrate good agreement between the MATLAB modelled signal for a 293 K environment, generated as detailed in Section 2.2, and the experimental data collected with the photomultiplier tube (PMT) module. However, it is important to note that this fit was achieved through manual manipulation of parameters that alter the model. Hence the most probable cause of the deviation of simulated data from the experimentally measured signal is the difficulty in determining the exact temperature dependent quenching rates, as well as the difficulty in identifying the branching ratio that defines the relative significance of the slow and fast quench times. Consequently, without this knowledge it is challenging to precisely determine the temporal evolution of the thermal grating and thus the form of the LIGS signal, which is a representation of the time-dependent reflectivity of the grating. While developing an appropriate fitting routine to improve the fit of the model to the experimental data is beyond the scope of this thesis, it provides a basis for future work in further developing the multiple temperature model which is presented in Section 4.3.2.

4.2.2 High Temperature Single Ethylene Flow

Thermocouple readings of the heated flow temperature were recorded at a spatial position less than 0.5 mm above the upper end of the copper pipe, at the centre of its cross section, within the probe volume. It was found that the temperature of the heated ethylene flow had a strongly non-linear dependence on the voltage applied to the heating element. Consequently, it was necessary to take extreme caution when increasing the applied voltage to prevent the system from approaching the auto-ignition temperature. 50 V was thus identified as the highest voltage that could safely be applied and this corresponded to a thermocouple measurement of 386 ± 9 K, where the quoted uncertainty represents fluctuations in the displayed reading about a mean value. All results presented in the rest of this chapter which use the temperature-controlled heated flow were recorded under this condition; the maximum possible hot flow temperature was selected for study because it is expected that a larger difference in temperature between

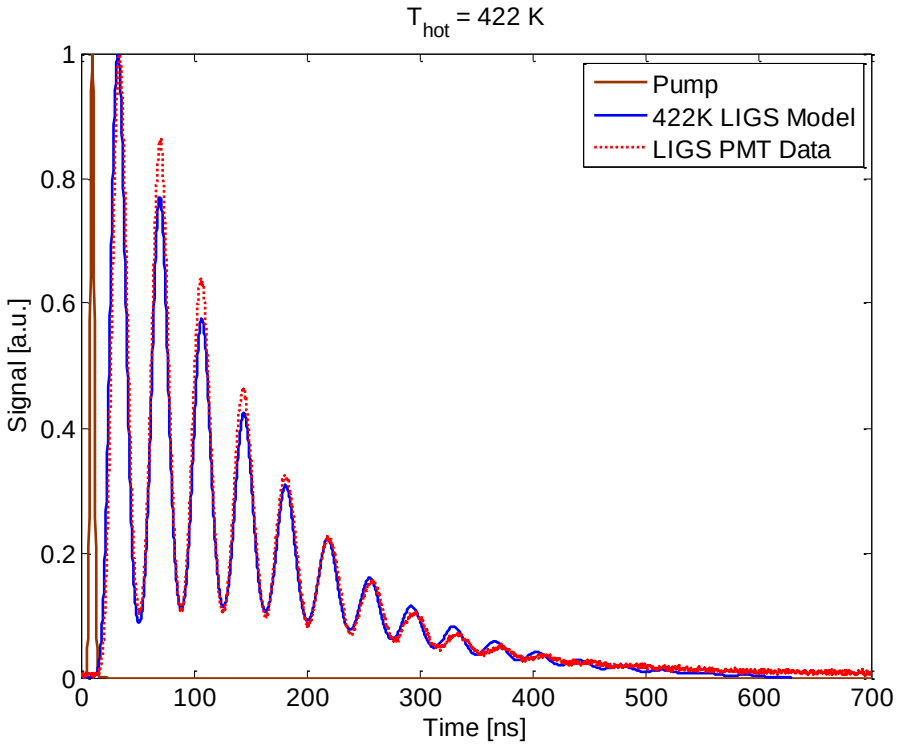


Figure 4.5: Single hot flow LIGS measurement (hot flow on, hot flow heater on) in ethylene at atmospheric pressure showing the correspondence between averaged experimental data from the photomultiplier tube (PMT) module and the 422 K modelled signal.

the two regions contributing to the probe volume of a dual flow would have a more pronounced effect on the frequency spectrum of the LIGS signal.

It was also found that the temperature of the flow was higher towards the edge of the copper tube, which could be explained by the fact that the ethylene flowing through the centre of the tube has not been in direct contact with the heated walls of the flow pipe. This could potentially cause complications when analysing and modelling the data because the initial expectation was that each of the two flows would make a single temperature contribution to the probe volume. However, since the temperature gradients that exist within the heated flow are small relative to the temperature difference between the two flows, where the unheated flow is operated at room temperature, it is anticipated that the hot flow could still be approximated as a single temperature flow for the purpose of developing the model. It is predicted that the effect

this small temperature gradient would have on the hot flow LIGS frequency spectrum is a broadening of the LIGS oscillation frequency peak in the frequency domain, due to the addition of a range of frequency components.

Figure 4.5 shows the result of the LIGS measurement from the heated flow. Again, the modelled signal is displayed on the same axes for comparison. The temperature calculated from the oscillation frequency of the LIGS signal was found to be 422 ± 3 K. Similarly to the room temperature measurement, this measurement has a precision of 0.7%, which corresponds well with typical values stated in the literature [1].

However, there is a clear discrepancy between the temperature measured using LIGS and that measured by the thermocouple. Real temperature differences between the location of the thermocouple measurement and LIGS interaction region can cause such discrepancies, as reported by Stevens and Ewart [15]. For reasons discussed previously, the thermocouple reading was found to be dependent on its position relative to the centre of the ethylene flow. Therefore it can be assumed that the LIGS measurement is likely to be a more accurate representation of the mean temperature of the complete flow cross-section. When fitting the model to the experimental data, it was found that a signal simulated for a temperature of 422 K provided a much better fit in comparison to one simulated at 386 K. It can be noted from the room temperature measurement in Figure 4.4 that the model is capable of reproducing the temperature dependence of an experimental signal to an excellent degree of accuracy; this provides further evidence to suggest that the LIGS measurement is more accurate. Furthermore, it is usually the case that physical probes such as thermocouples perturb the measurement environment and conduct heat away from the measurement point, which is a key reason for developing non-invasive techniques like LIGS. In addition to the centre of the flow being cooler than its circumference, heat conduction through the thermocouple could explain why the temperature recorded by the thermocouple is lower than that measured using LIGS. All plots

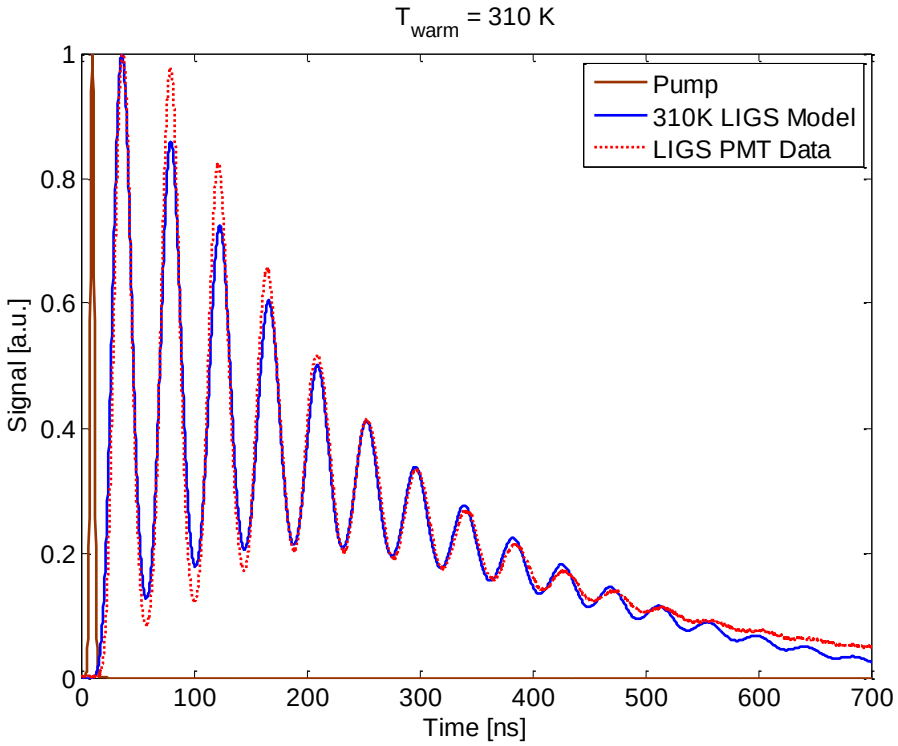


Figure 4.6: Single warm flow LIGS measurement (cold flow on, hot flow heater on) in ethylene at atmospheric pressure showing the correspondence between averaged experimental data from the photomultiplier tube (PMT) module and the 310 K modelled signal.

presented in this chapter have been labelled by the temperature of the modelled LIGS signal for consistency.

It should also be noted that the heated flow signal in Figure 4.5 has been averaged over far fewer data shots than the room temperature flow signal in Figure 4.4 (48 shots for the former as opposed to 482 shots for the latter). The difference in the number of shots falling into a specific intensity band is likely to be due to the temperature dependence of gas flow density, because as discussed in Section 2.1.4, the LIGS signal intensity is a measure of the species concentration within the probe volume.

Figure 4.6 shows a single flow measurement from the unheated flow recorded while the hot flow pipe was heated with an applied voltage of 50 V; the heated flow itself was not in operation. While careful efforts were made to insulate the flow system to prevent the hot flow

from warming the cold flow, this demonstrates that there has been limited success. A significant temperature difference has been maintained between the two adjacent flows, but the cold flow has experienced a small amount of heating. The new temperature of the previously cold flow in this situation was measured to be 313 ± 5 K as measured by the thermocouple and 310 ± 2 K (0.6% precision) as measured by LIGS, where the two values are in agreement. This is again likely to add another level of complexity when modelling the dual flow signal. Heat transfer between flows has given rise to the possibility of a temperature gradient also existing in the unheated flow, due to some or all of the room temperature ethylene in the cold flow pipe being warmed by the presence of the adjacent hot flow pipe. For ease of analysis in the rest of the chapter, the three flow temperatures discussed in this section are labelled:

T_{cold} = 293 K,

T_{warm} = 310 K, and

T_{hot} = 422 K

The results shown in Figures 4.5 and 4.6 also demonstrate good agreement between the MATLAB modelled signals and the experimental data. However, similarly to the room temperature data, these fits were achieved through manual manipulation of model parameters. Therefore the deviation of the simulated data from the experimentally measured signal could again be explained by the difficulty in determining the exact quenching rates and branching ratios, and could potentially be improved once an appropriate fitting routine is employed.

4.3 Non-Uniform Temperature Field: Results and Discussion

The non-uniform temperature field measurements use the dual ethylene flow set-up detailed in Section 3.2.3 and build on the uniform temperature field measurements from Section 4.2. This

section presents the results from the dual flow measurements, as well as an overview of the new multiple temperature signal model developed during the course of this study. Comparisons are made between modelled and experimental data, where a discussion of the model's validity is provided where relevant.

4.3.1 Dual Ethylene Flow LIGS Measurements

In the dual flow set-up where both flows are simultaneously operated, the pump interaction region was positioned as illustrated by the square in Figure 4.1, while the 13.3 mm probe length was centred on the two flows and aligned along the length shown in the figure by adjusting the position of the flow system using the translation stages.

The flow meter was used to split the incoming ethylene flow rate of 180 mL min^{-1} in half such that the output from each copper pipe is approximately 90 mL min^{-1}. Initially, a room temperature LIGS measurement was made with both ethylene flows in operation. This test was conducted as a check to ensure that LIGS signals from each pipe and the combined signal from both pipes were the same. Since all three measurements originate from identical, uniform temperature test environments, the signals are expected to have a similar form (decay rate, for instance) with equal oscillation frequency. Analysis of the signal data confirmed that this was the case. The simultaneous dual flow measurement from the uniform room temperature probe volume produced a LIGS signal with a frequency spectrum containing a single primary peak, where the oscillation frequency corresponded to a temperature of 293 ± 5 K, and demonstrated the existence of only a single temperature contribution to the signal. Thus it was verified that the system is ready to be tested in a more challenging situation where there is more than one temperature contribution to the probe volume.

During the room temperature test, care was taken to ensure that the LIGS signal intensities originating from each flow, as measured using the oscilloscope, were approximately

equal. Following on from the signal intensity discussion in Section 2.1.4, it can be noted that the integral of the LIGS signal is a measure of ethylene concentration in the probe volume, because heat deposition during the formation and evolution of the thermal grating is proportional to species number density. Consequently, if the intensities of the LIGS signals originating from the two flows are set to be approximately equal, it can be assumed that the composition of the two flows is similar. Thus the molecular mass and ratio of specific heats, which are both gas composition dependent, can be treated as fixed quantities during the initial development of the multiple temperature model; the temperature dependence of these quantities can be incorporated in to the model at a later stage once a basic working model has been established. Furthermore, if the contribution from one flow to the LIGS signal is several orders of magnitude smaller than the contribution from the other, the smaller flow is unlikely to have any resolvable impact on the form of the combined LIGS signal from the dual flow.

4.3.2 Overview of the Multiple Temperature Model

A copy of the multiple temperature LIGS model developed in MATLAB during the course of this study, with detailed annotations explaining the operations carried out at each step of the simulated data calculation, can be found in Appendices 1, 2, 3 and 4. It should be noted that unlike the single temperature model previously used by the research group, this model allows the user to simultaneously analyse experimental LIGS data and plot the results together with the model for easy comparison. However, in a situation where it is preferable to work with the data simulation alone, the primary MATLAB script presented in Appendix 1 can very easily be edited to ignore commands relevant to the analysis of experimental data, as these sections are clearly identified with the green comment label ‘EXPT’. Likewise, the program can be used as a data analysis script, following a simple modification to ignore sections that are labelled as ‘MODEL’.

The primary script that launches the model is titled 'LIGSmodel_multi_temp.m' and is found in Appendix 1. The version of the program included in Appendix 1 is that which accepts an input vector of three temperatures and associated weighting factors, corresponding to a probe volume where three distinct temperature regions contribute to the signal; this is discussed in Section 4.3.4. However, the model in the form presented in Appendix 1 can also be used to model a LIGS signal with two temperature zones, or alternatively operated as a single temperature LIGS model. The commands contained within this M-file are separated into 18 parts with descriptive titles, where the set of commands within each portion of the script carries out a specific task.

Parts 1 and 2 allow the user to specify the values of parameters that affect the shape of the modelled LIGS signal. Note that the relative weightings specified for each input temperature is intended to represent the relative contribution each temperature region makes to the probe volume. In Part 3, the single temperature model titled 'LIGSmodel_single_temp.m' simulates a signal for each temperature, plots the modelled signals and saves the simulated data into a matrix; a copy of this function M-file is included in Appendix 2. 'LIGSmodel_single_temp.m' is a significantly modified version of the existing single temperature model (see Section 2.2) currently used by the research group. It has been altered by the author to enable it to be incorporated into the multiple temperature model because it did not previously have this functionality. The functions which are employed within it are similar to those detailed in Section 2.2 as functions used in the original model and thus have not been presented in this thesis. Single temperature experimental signals can be extracted from oscilloscope data sets and plotted for comparison with the modelled signals in Part 4 of the script, where two functions titled 'LIGSxpt_read_files.m' and 'LIGSxpt_analyse_data.m' are used for this purpose; these functions can be found in Appendix 3 and 4 respectively.

The rest of the parts that are identified as 'MODEL' are used to compute the simulated multiple temperature LIGS signal and calculate its frequency spectrum, from which the primary

peaks are identified as LIGS oscillation frequencies and used to calculate corresponding temperature values. It is expected that a dual ethylene flow with two significantly different temperature components would produce LIGS signals where the corresponding power spectrum has two primary peaks as determined by the two temperatures. The multiple temperature signal is computed as a weighted sum of single temperature signals that were calculated and saved in Part 3 of the script.

The rest of the parts that are identified as 'EXPT' are used to analyse experimental data from a non-uniform temperature field, where the probe volume contains multiple temperature zones. After the frequency spectrum of the LIGS signal is calculated and the primary peaks are identified as LIGS oscillation frequencies, the corresponding mean temperature values and their associated standard deviations are determined. Finally, the experimental signal data and its frequency spectrum are plotted onto the same MATLAB figures as the simulated data for ease of comparison.

4.3.3 Two Temperature Model for the Dual Ethylene Flow

Figure 4.7 presents data from the ethylene dual flow set-up, with both flows operating simultaneously, where the voltage applied to the heating element connected to the hot flow pipe was 50 V. The experimental data, averaged over 142 data shots, is plotted as the dotted red line; the simulated data is plotted as the solid blue line.

The experimentally measured LIGS signal shows a feature that was not seen in any of the single temperature data presented in this chapter. There is evidence of an envelope function modulating the intensity of the LIGS oscillations, with a local intensity minimum resulting in a signal feature that is similar in appearance to frequency beating, observed at the 100-200 ns location. In acoustics, this phenomenon is characteristic of the temporal interference between signals of two different frequencies, and arises as a consequence of the wave superposition

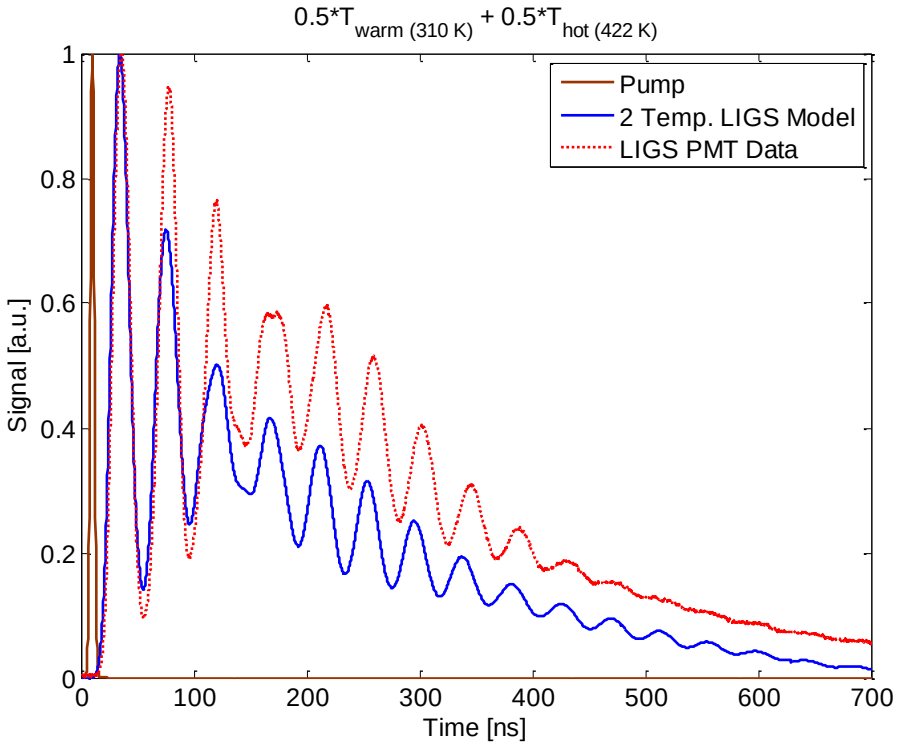


Figure 4.7: Dual flow LIGS measurement in ethylene at atmospheric pressure, with modelled signal for 0.5*T_{warm} + 0.5*T_{hot}, where T_{warm} is 310 K and T_{hot} is 422 K.

principle [37]. Such a phenomenon is observed in cases where the two signals have a frequency difference that is small relative to the frequencies themselves. Based on the single flow measurements reported in Section 4.2, this would be true for LIGS signals originating from the dual ethylene flow; the oscillation frequency of each LIGS signal is of the order of 30 MHz, while the frequency difference corresponding to the controlled temperature difference established between the two flows is of the order of 5 MHz. When the oscillations of the two signals are in phase, the resultant oscillations are of high intensity. The composite signal in such a situation is the sum of variations in intensity, and not variations in amplitude. Hence the observed phenomenon is not a result of signal interference in the conventional sense; what is observed here is a change in the visibility of temporal intensity maxima and minima in the LIGS signal. Over some period of time, the two signals eventually become out of phase and thus the intensity of the signal sum decreases. This process repeats itself, giving rise to a periodic modulation of the intensity of the combined LIGS signal. In such a situation, the frequency difference between

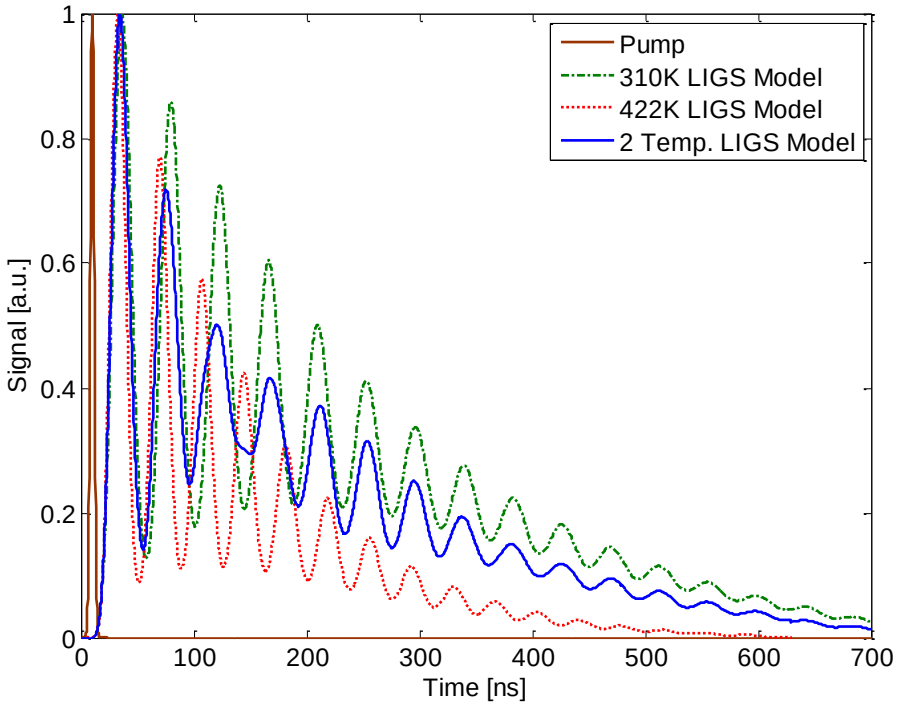


Figure 4.8: Illustration of how an equally weighted sum of two single frequency signals affects the form of the composite signal. The modelled signal for 0.5*T_{warm} + 0.5*T_{hot} (shown in blue) is compared with the models for T_{warm} = 310 K (shown in green) and T_{hot} = 422 K (shown in red).

the original signals that interfered to form the composite signal can be determined from this beat frequency. Consequently, it is expected that the frequency spectrum of the LIGS signal in Figure 4.7 would identify two oscillation frequencies separated by a frequency difference corresponding to the temperature difference of the regions they originate from.

It can be noted from Figure 4.7 that the simulated signal, which is an equally weighted sum of T_{warm} and T_{hot}, also shows similar frequency beating characteristics, with the local minimum of the intensity modulation located at the same temporal position as that observed in the experimental data. However there is a discrepancy between the decay rates of the two signals, which is likely to have arisen due to a mismatch in the predicted quench times input into the model and would consequently be improved through the implementation of a rigorous fitting routine in the future.

Figure 4.8 demonstrates how two equally weighted, single temperature modelled signals, corresponding to T_{warm} and T_{hot} in this example, combine to form the composite dual temperature signal. Since the frequency difference between the T_{warm} and T_{hot} signals is relatively small, the oscillations are initially in phase and thus add to produce high intensity oscillations in the signal sum. The two constituent signals eventually move out of phase due their frequency difference; Figure 4.8 clearly demonstrates how addition of intensities gives rise to a local minimum in the intensity modulation in the 100-200 ns time window. The oscillations of the T_{warm} and T_{hot} signals then move back into phase with each other and start to add constructively. It can be seen that the T_{hot} signal decays much faster than the T_{warm} signal due to the increase in the rate of particle diffusion at higher temperatures. At lower temperatures, the slower diffusion rate produces a thermal grating that exists for a longer time period prior to the system returning to equilibrium. Consequently, the latter part of the composite signal is dominated by the contribution from the cooler temperature signal as a result of its much larger amplitude relative to the T_{hot} signal.

As seen in Figure 4.7, the basic form of the experimentally measured LIGS signal from the dual ethylene flow is in good agreement with that predicted using the two temperature model. Therefore, much of what has been observed from the experimental results can be explained theoretically; this is a successful and encouraging result.

However, despite attempts to modify temperatures, weightings and other parameters input into the model, it was not possible to use the model in its existing form to reproduce the double-peak feature positioned at the fourth oscillatory peak in the experimentally measured signal (see Figure 4.7). When the frequency separation between the two peaks in this feature was measured, it was found to correspond exactly to the temperature difference between T_{warm} and T_{cold}. This suggests that a third temperature component contributes to the probe volume: room temperature ethylene present in the unheated flow. The double-peak feature is expected to be the result of T_{warm} and T_{cold} signals from the unheated flow interfering with the T_{hot} signal.

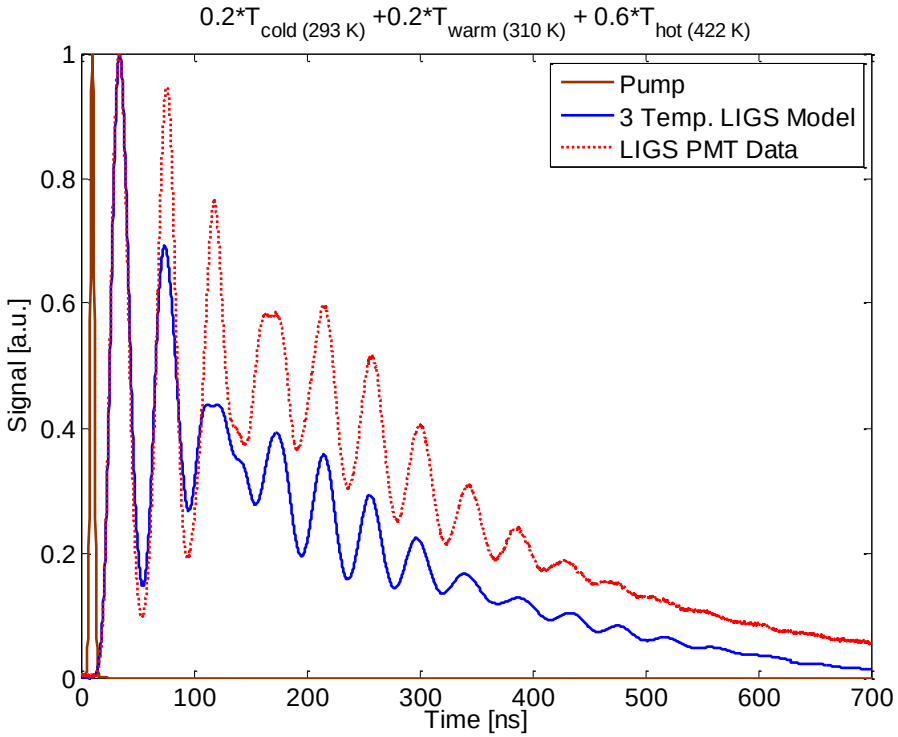


Figure 4.9: Dual flow LIGS measurement in ethylene at atmospheric pressure, with modelled signal for $0.2*T_{cold} + 0.2*T_{warm} + 0.6*T_{hot}$, where T_{cold} is 293 K (room temperature), T_{warm} is 310 K and T_{hot} is 422 K.

Therefore, a three temperature model was devised to test this hypothesis and its results are discussed in Section 4.3.4.

Furthermore, it can be noted that the intensity of the two peaks contributing to the double-peak feature are equal. This implies that the contributions T_{warm} and T_{cold} make to the probe volume are equal. Consequently, these two temperatures must be equally weighted when modelling the signal.

4.3.4 Three Temperature Model for the Dual Ethylene Flow

The two temperature model was thus modified to incorporate an additional temperature component, as seen in the MATLAB script presented in Appendix 1. Figure 4.9 shows the first attempt at fitting the three temperature model to the experimentally measured LIGS signal from

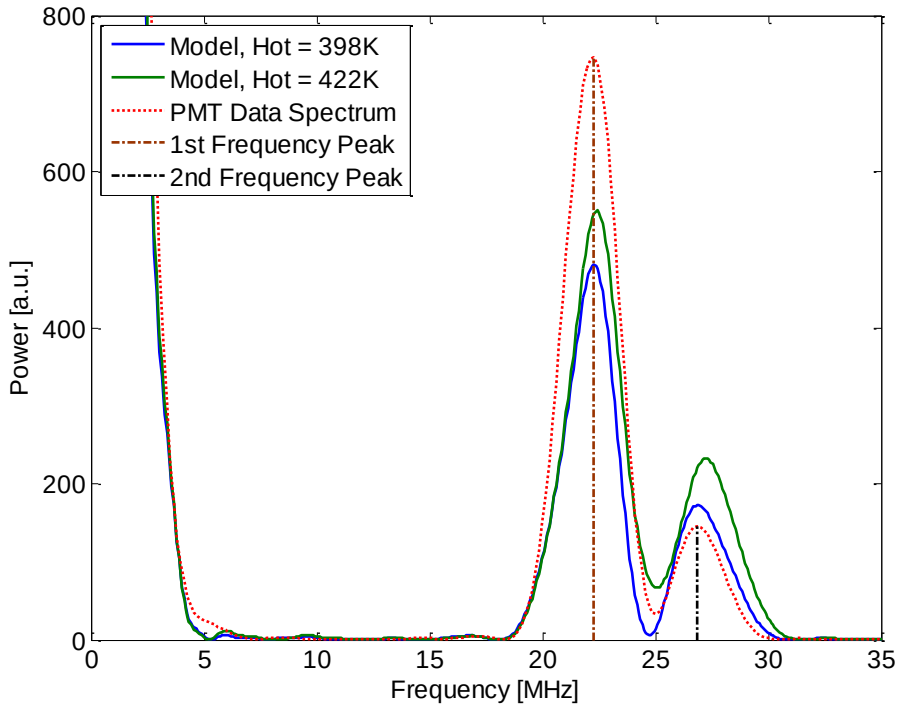


Figure 4.10: Frequency spectrum calculated from the Fourier transform of the ethylene dual flow LIGS signal data, compared with the spectra corresponding to the T_{hot} = 422 K and T_{hot} = 398 K cases from the three temperature model.

the dual ethylene flow. The resulting simulated signal was successful in reproducing a double-peak feature with a frequency separation that corresponds exactly to the temperature difference between T_{warm} and T_{cold}. However, manipulation of the temperature and weighting factor input vectors demonstrated that the position of the double-peak feature was highly sensitive to variations in both. Therefore, without the capability to implement a rigorous fitting routine, it would be extremely challenging to identify a combination of input parameters able to simulate the exact form the experimentally measured signal.

Next, the frequency spectra of both the experimental and simulated signals shown in Figure 4.9 were computed; the resulting plot is presented in Figure 4.10. Note that unlike the frequency spectrum of a LIGS signal originating from a uniform temperature probe volume, an example being the one presented in Figure 3.7, these spectra contain two primary peaks as opposed to a single peak. From the power spectrum computed for the ethylene dual flow

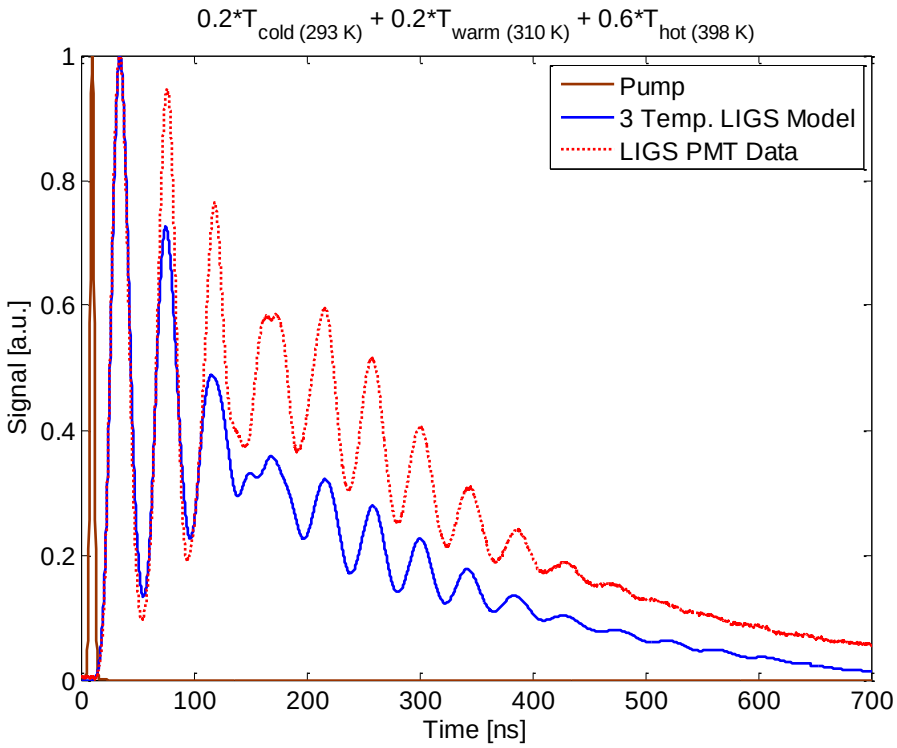


Figure 4.11: Dual flow LIGS measurement in ethylene at atmospheric pressure, with modelled signal for $0.2*T_{cold} + 0.2*T_{warm} + 0.6*T_{hot}$, where T_{cold} is 293 K (room temperature), T_{warm} is 310 K and T_{hot} is 398 K.

experimental data, the temperatures corresponding to the spectral peaks were identified as: T_1 = 297 ± 21 K (7% precision) and T_2 = 432 ± 25 K (6% precision).

Thus the temperature measurement from the first spectral peak from the dual flow is in agreement with both T_{cold} and T_{warm} from the single flow measurements, while the temperature measured from the second spectral peak from the dual flow correlates with T_{hot} measured using the single flow. This is a highly successful result which demonstrates that a single power spectrum from a LIGS measurement originating from a multiple temperature probe volume can be used to identify individual temperature regions present within that volume, by fitting the data to simulated signals generated using the multiple temperature model developed. The lower precision of these temperature measurements, as given by the standard deviation on the mean, is the result of the broadening of spectral peaks due to the presence of multiple frequency components, as hypothesised in Section 4.2.

Figure 4.11 illustrates a second attempt at modelling a three temperature LIGS signal. T_{hot} was set to a lower value of 398 K to investigate the possibility of a reduction in the temperature of the heated ethylene flow due to heat from the hot flow being convected away from the probe volume due to the mixing of flows, when both flows are simultaneously operated. Consequently, the double-peak feature in the modelled LIGS signal has shifted to a location that corresponds better with the experimental signal (see Figure 4.11), but the modelled signal is still not an exact match to the experimental data. Therefore, it is still necessary to develop a rigorous fitting routine in the future to improve the agreement between experiment and model.

However, the frequency spectra plots presented earlier in this chapter in Figure 4.10 show that when compared with the T_{hot} = 422 K modelled spectrum, the frequency peaks in the modelled spectrum for T_{hot} = 398 K correlate better with the one computed using the experimental data. The derived frequency data is tabulated in Table 4.1; peaks 1 and 2 refer to the pair of primary frequency peaks identified in Figure 4.10. The tabulated experimental value is the mean and standard deviation calculated from 142 measurements.

Origin of LIGS Signal	f_{osc} from peak 1 [MHz]	f_{osc} from peak 2 [MHz]
Ethylene dual flow experiment	22.3 ± 0.8	26.9 ± 0.8
Three temp. model, T_{hot} = 398 K	22.4	27.2
Three temp. model, T_{hot} = 422 K	22.8	27.6

Table 4.1: LIGS oscillation frequencies derived from the frequency spectra (see Figure 4.10) of LIGS signals originating from different sources, one being an experimentally measured signal and the other two being modelled signals. Peaks 1 and 2 refer to the pair of primary frequency peaks observed in the spectra in Figure 4.10.

This suggests that the lower value of T_{hot} more accurately represents the mean temperature of the heated flow in the dual flow system, when compared with the value derived

from the single heated flow measurement. It is also expected that a model based on a continuous gradient of temperatures, as opposed to one based on a few discrete temperature values as presented in this chapter, would better represent the physical systems under investigation and further improve the fit of simulated data to the experimentally measured signals.

Nevertheless, a key objective of this study was to simulate the temperature distribution of a probe volume by comparing a LIGS signal measured in a non-uniform temperature field with modelled data, and this has successfully been demonstrated. Following the encouraging results obtained in this chapter, attempts will now be made to incorporate temperature gradients into the existing model in order to examine its validity in a more complicated environment. Section 5.3.3 of the next chapter presents a comparison of such a model with LIGS measurements made in a flame.

5 LIGS Thermometry in a Gülder Burner Flame

The second key objective of this study was to investigate the suitability of LIGS as a thermometry tool in an ethylene-air standard laboratory flame, as a precursor to work in more complicated combustion systems. As discussed in Chapter 1, it is important to improve current understanding of physical combustion processes, in order identify ways in which the production of harmful substances can be reduced. Reaction rates are critically temperature dependent [7], and thus it is necessary to develop accurate and precise thermometry techniques; it is preferable for these methods to be non-invasive measurements in order to avoid perturbing the combustion environment. Results from such experiments can then be used to validate computer-based models capable of simulating combustion processes that are difficult to investigate experimentally.

This chapter starts with a description of the Gülder burner, which provides a stable, co-flow, laminar diffusion flame. Next, results from an OH* chemiluminescence experiment are presented, the purpose of which was to identify the location of the flame front as this information would be useful for the analysis and modelling of LIGS data for a flame environment. LIGS thermometry results are then presented, demonstrating how the relative spatial position of the measurement affects the LIGS signal. Following comparisons with measurements made in a non-ignited ethylene flow, a modified version of the multiple temperature model discussed in Chapter 4 is provided, along with some preliminary results.

5.1 Gülder Burner

A Gülder burner is a standard laboratory burner that provides an ethylene-air co-flow, laminar diffusion flame. The central nozzle provides the ethylene flow and an outer annulus provides

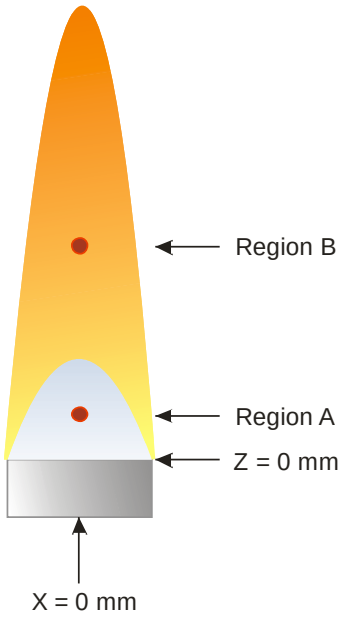


Figure 5.1: Gülder burner flame. The red points in the image identify two regions of interest: Regions A and B. Region A is the more transparent lower part of the flame, which contains a significant proportion of unburned fuel molecules and PAHs. Region B is the more opaque upper part of flame, which contains a significant amount of soot particles and larger soot aggregates. Positions are measured relative to the X = 0 mm (radial position) and Z = 0 mm (vertical position) locations identified in the figure.

the air flow. Gülder burners provide well characterised, reproducible, flame environments in which novel measurement techniques can be tested. An illustration of the flame is shown in Figure 5.1. Based on the results of work carried out by a collaborating research group [23], a flow with a fixed stoichiometry of 180 mL min^{-1} ethylene and 120 L min^{-1} air was selected to produce a tall, stable, non-turbulent flame. These conditions produce a flame that is approximately 7 cm in height relative to the Z = 0 position in Figure 5.1. The flame has cylindrical symmetry about the central vertical axis (X = 0).

In Figure 5.1, two key regions that are separated by the flame front have been identified: Region A and Region B. The lower part of the flame, Region A, is the more transparent region where soot is yet to form; it is expected to primarily consist of unburned ethylene molecules and polycyclic aromatic hydrocarbons (PAHs) [3] [4]. Higher up in the flame, in Region B, soot particles form and grow into larger aggregates with increasing height above burner (HAB,

equivalent to Z-position). It is the large concentration of soot present in Region B which causes it to appear largely opaque, while the yellow radiation originates from the incandescence of heated soot. Following on from the ethylene flow experiments in Chapter 4, the experiments detailed in this chapter have been conducted in Region A, where heated ethylene can act as an absorber. However, PAHs are also a potential absorber in this region and a discussion is later provided on how to identify what the absorbing species is. In Region B, soot particles can potentially act as the absorbing species and this is briefly discussed in Chapter 6. This work builds on the research of Zhao *et al.* [23], who were able to construct a temperature map of Region B for a flame of this type using alternative techniques that rely on the presence of soot, but were unable to do the same for Region A due to the absence of soot in this region.

The Gülder burner was set-up as detailed in Section 3.2.4, according to the diagram in Figure 3.4. Mass flow controller units connected the ethylene and air sources to the burner via a series of regulators and valves. Both flow systems are operated using a LabVIEW program developed by the research group. The program allows the user to operate the ethylene and air flows individually or simultaneously, and monitor the rate of both flows using on-screen displays. The air flow originates from a connection to the central laboratory air supply and is controlled using a regulator; the ethylene flow originates from a high pressure gas cylinder and is carefully regulated using the LabVIEW program. The burner can be manually ignited when both the air and fuel flows are in operation.

The flame can be translated vertically and horizontally using the two high precision (±5 μm) translation stages on which the burner is set-up. In Figure 5.1, the zero HAB position is identified as Z = 0, while the location of the central vertical axis is identified as X = 0. In the results presented in this chapter, all locations are measured relative to these positions. First, chemiluminescence measurements were made in order to identify the location of the flame front by monitoring the intensity of 310 nm radiation originating from OH* radicals present within the reaction zone. The results from this measurement are presented in the next section.

5.2 OH* Chemiluminescence Measurement

Recent studies have demonstrated that tomographic reconstruction of OH* chemiluminescence in a flame is a suitable technique for probing the flame front in order to gain an insight into combustion properties in a range of flame types [38] [39] [40]. In cooler parts of the flame, OH exists primarily in its ground state. In hotter parts of the flame, a high concentration of OH* is formed in the reaction zone within the flame front where combustion occurs; it can then decay back to the ground state over a short timescale following the emission of a photon, which can be recorded with the use of an appropriate imaging system as a chemiluminescence measurement. In the case of a typical Gülder burner flame, the reaction zone in Region A is significantly hotter than any part of Region B [23]. Consequently, the 310 nm chemiluminescence originating from OH* provides an instantaneous snapshot of the flame front reaction zone in Region A at any given time. This information is useful to the LIGS study in identifying the areas in which unburned ethylene exists, as opposed to PAHs and other combustion products.

The next two sub-sections outline how a two-dimensional (2D), line-of-sight integrated image of the OH* distribution was first recorded, after which the three-dimensional (3D) distribution of OH* was determined through a tomographic reconstruction procedure.

5.2.1 2D Flame Image

An intensified CCD camera (Princeton Instruments, ICCD 512T) was positioned facing the measurement point on a camera rail, as illustrated in the overview of the LIGS experiment set-up shown in Figure 3.2. An appropriate lens (105 mm, F4.5) with integrated UV optics was used, and to this a 310 nm filter (10 nm FWHM) was attached to ensure that only radiation of this wavelength reached the detector. Figure 5.2 shows a 2D image of the Gülder burner flame that was captured by this camera set-up; it has been processed using MATLAB in order to subtract

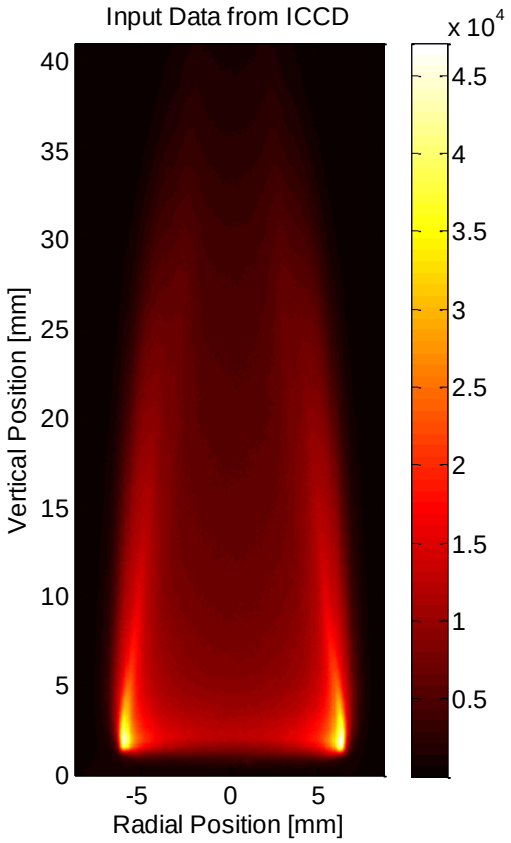


Figure 5.2: Two dimensional output image of Gülder burner flame from the ICCD, after background subtraction and detector non-uniformity correction. This is a line-of-sight integrated measurement of the OH* chemiluminescence. The intensity of the chemiluminescence as indicated by the colour map is in arbitrary units, with black indicating low intensity and white indicating high intensity.

scattered background light and correct for non-uniformities in the detector surface. The image does not show the complete height of the flame because the region of interest is the lower part of the flame; the tip of the flame extends beyond the upper end of the image.

A spectrometer was used to monitor the emission spectrum of the flame, where the flame was shielded by a plastic screen with a sharp transmission cut-off at 400 nm. Consequently, it was possible to confirm that the 310 nm radiation detected by the ICCD originates from OH* chemiluminescence as opposed to broadband soot emission. However, with a simple 2D image, it is not possible to identify the exact location in the flame from which the chemiluminescence originates. The intensity at any given point in the image represents the total

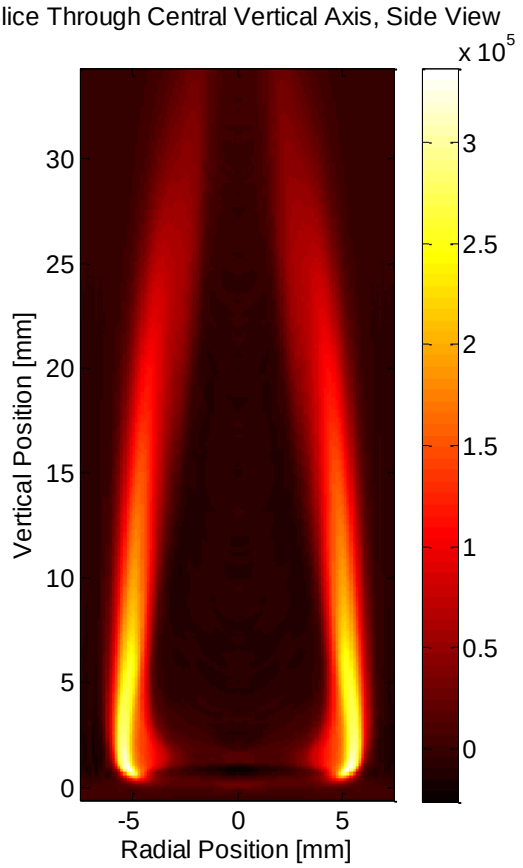


Figure 5.3: A single 2D slice through the central vertical axis of a 3D tomographic reconstruction of the Gülder burner flame, after background subtraction and detector non-uniformity correction. This shows the spatial distribution of the OH* chemiluminescence. The intensity of the chemiluminescence as indicated by the colour map is in arbitrary units, with black indicating low intensity and white indicating high intensity.

OH* distribution along a line through a cross section of the flame. The image in Figure 5.2 is thus a line-of-sight integrated measurement of the OH* distribution in the flame. Therefore it is necessary to use a computational technique to reconstruct the 3D distribution of OH* in order to identify the location of the flame front in region A.

5.2.2 3D Tomographic Reconstruction of the Flame

Figure 5.3 shows a result from the 3D tomographic reconstruction; it is a single 2D slice through the central vertical axis in the 3D reconstruction of the flame. Unlike the original 2D image from

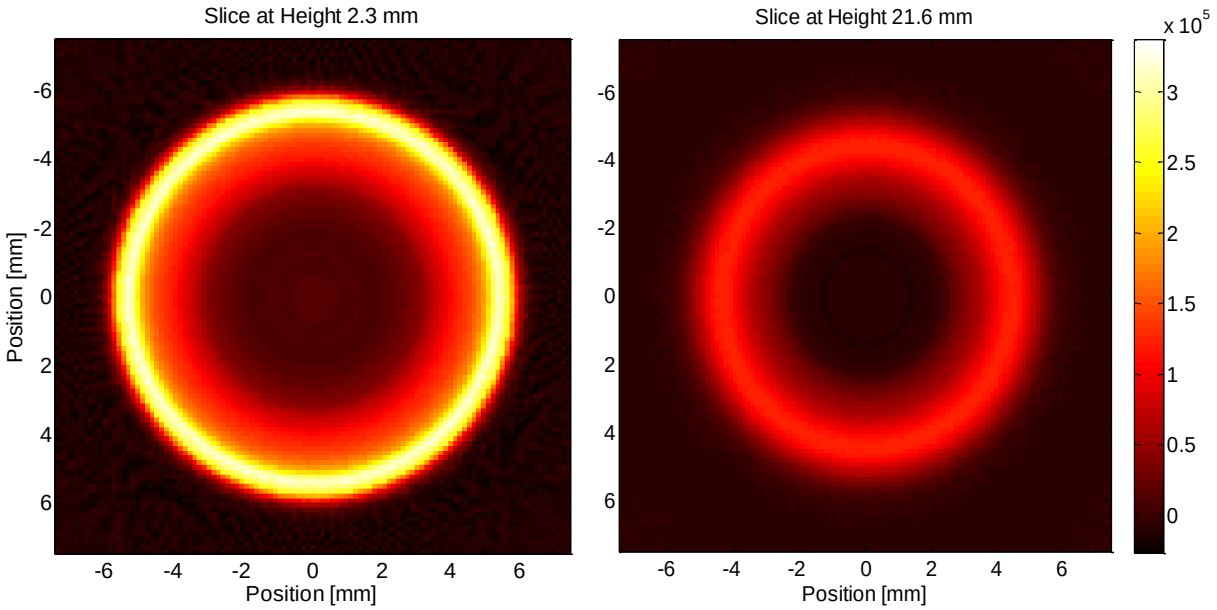


Figure 5.4: Slices through heights 2.3 mm (Region A) and 21.6 mm (Region B) of the 3D Gülder burner flame reconstruction, where vertical position is measured relative to the Z = 0 position as indicated on Figure 5.1. This shows the spatial distribution of the OH* chemiluminescence. The intensity of the chemiluminescence as indicated by the colour map is in arbitrary units, with black indicating low intensity and white indicating high intensity.

the ICCD camera, the 3D reconstruction demonstrates that the chemiluminescence detected primarily originates from the outer edge of the lower part of the flame. The horizontal cross-sectional 2D slices taken at heights of 2.3 mm and 21.6 mm, as shown in Figure 5.4, also confirms this. As expected, there is a high intensity of chemiluminescence originating from Region A, while very little is detected in Region B; the intense yellow ring in the 2.3 mm slice in Figure 5.4 shows the location of the flame front near the base of the flame.

The images in Figures 5.3 and 5.4 were produced using open source cone beam reconstruction software called OSCaR. A collaborating research group adapted the software for flame measurements made using the three colour pyrometry technique [23]. The program was further modified by B. A. O. Williams at the University of Oxford in 2013, who adapted the software to process images from the ICCD camera. The software first adjusts the 2D image by carrying out a background subtraction and applying a median filter to improve the signal-to-noise ratio. Next, the Feldkamp-Davis-Kress algorithm is employed to conduct the

reconstruction. Typically, the 3D reconstruction requires a collection of 2D images from a range of angles. However, since the Gülder burner flame has cylindrical symmetry, a single 2D image representing identical views from 180 different angles was processed multiple times. From this, the 3D spatial distribution of the OH* chemiluminescence was calculated and returned as a 109 x 109 x 254 element matrix, where each element is representative of the OH* concentration in a specific location of the flame.

From the reconstruction data, it was also found that:

Z = 0 mm corresponds to the 1.1 mm vertical position in the 3D image, and

X = 0 mm corresponds to the 0 mm radial position in the 3D image.

This calibration information is used later in this chapter during the analysis and modelling of LIGS signals from the flame.

5.3 LIGS Thermometry: Results and Discussion

A set of LIGS measurements were made in the Gülder burner flame with the experimental set-up illustrated in Figures 3.1, 3.2 and 3.4. The probe volume used for the measurements presented here is the same as that used in the ethylene dual flow experiment. This section first examines how the form of the LIGS signal and the temperature data extracted from its frequency spectrum varies as a function of spatial position within Region A of the flame. Next, comparisons are made between LIGS signals originating from the ethylene-air flame and those recorded in a non-ignited ethylene flow. Finally, an improved version of the multiple temperature model used in the last chapter is presented; some preliminary data from the simulation is provided, along with a discussion on the model's suitability for use in flame environments.

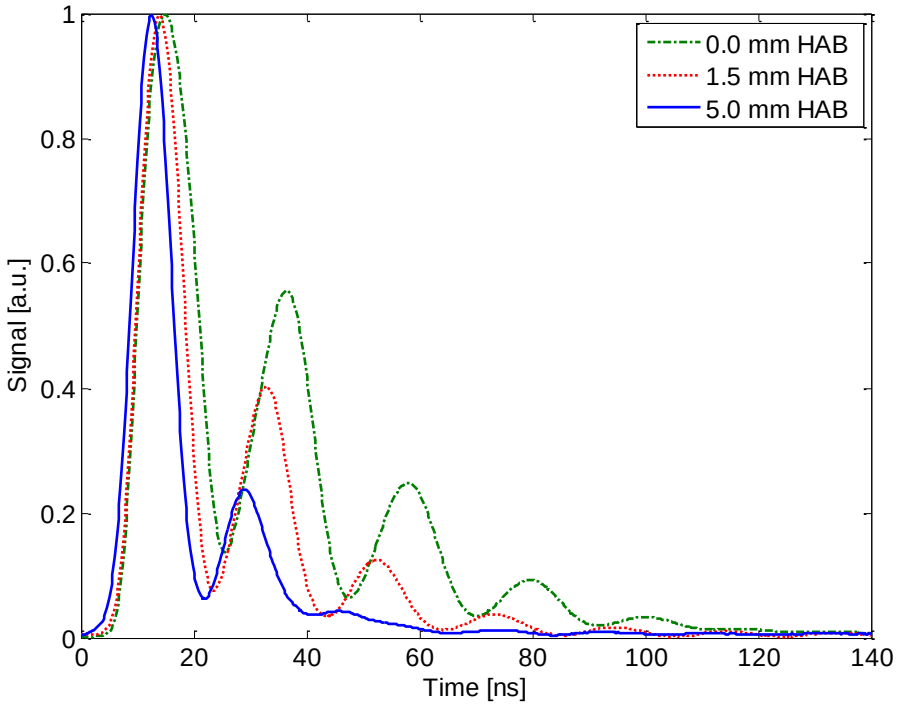


Figure 5.5: LIGS signals measured in Region A of the flame at atmospheric pressure at three different HAB positions (0.0 mm, 1.5 mm and 5.0 mm), on the central vertical axis. All signals have been averaged over 200 data shots.

5.3.1 Effects of Spatial Position

Figure 5.5 shows LIGS signals recorded at three different HAB locations within Region A, at the X = 0.0 mm position on the central vertical axis, at a fixed stoichiometry flow rate of 180 mL min^{-1} ethylene and 120 L min^{-1} air. LIGS measurements were made at 0.5 mm intervals in the range 0.0 mm HAB to 5.0 mm HAB, and at 2.0 mm intervals in the range 5.0 mm HAB to 15.0 mm HAB. Only three such measurements are selectively presented in Figure 5.5 for ease of comparison. The same data analysis procedure used in Chapter 4 was employed here to analyse LIGS signals and extract temperature information from the frequency spectra. These spectra did not feature a pair of distinct primary peaks, as that seen in the controlled dual ethylene flow case. Instead, a single broad primary peak was observed, suggesting that multiple temperature contributions to the probe volume were likely to be in the form of a continuous range of

HAB [mm]	Temperature [K]	Uncertainty [K]	Precision [%]
0.0	747	± 7	0.9
0.5	815	± 10	1.2
1.0	889	± 9	1.0
1.5	920	± 7	0.8
5.0	954	± 10	1.0

Table 5.1: Dependence of derived temperature on HAB, for LIGS signals experimentally measured at the X = 0.0 mm position on the central vertical axis, at a fixed stoichiometry flow rate of 180 mL min^{-1} ethylene and 120 L min^{-1} air.

temperatures; this would result in a continuous range of frequencies contributing to the primary peak in the frequency spectrum, causing it to broaden in the frequency domain. The spatially averaged temperature values tabulated in Table 5.1 were derived from the primary frequency peak, where each mean value was calculated from a sample of 200 data shots, and the associated uncertainty indicates the standard deviation of the sample. Note that some of the LIGS data relating to the derived temperatures tabulated in Table 5.1 were not featured in Figure 5.5. It is evident that the temperatures tabulated in Table 5.1 are significantly lower than standard Gülder burner flame temperatures, which typically range from 1500 – 2000 K [23]; further discussion is provided later in this section. It was also observed that even at very small differences in Z-position, temperature differences were detected.

LIGS signals were also recorded at the base of the flame (0.0 mm HAB), radially outward from the central vertical axis, again at a fixed stoichiometry flow rate of 180 mL min^{-1} ethylene and 120 L min^{-1} air. Measurements were made at 0.5 mm intervals from X = 0.0 mm to X = 6.0 mm; three are selectively presented in Figure 5.6 for ease of comparison. It was observed that at the 5.0 mm and 5.5 mm radial positions, the intensity of the LIGS signal was an order of

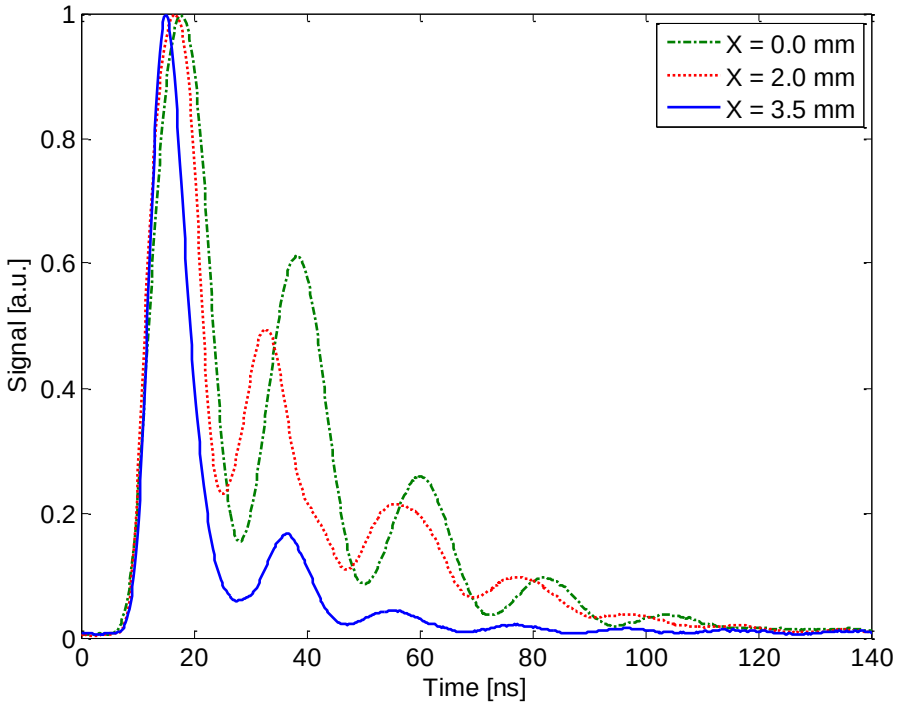


Figure 5.6: LIGS signals measured in Region A of the flame at atmospheric pressure at three different radial positions (0.0 mm, 2.0 mm and 3.5 mm), at a vertical position of 0.0 mm HAB. All signals have been averaged over 200 data shots.

magnitude smaller than that at the centre of the flame; no oscillations could be resolved either. Based on the OH* chemiluminescence distribution measurements, this is expected to be the approximate location of the reaction zone at this HAB position and was thus expected to be the radial location with the highest concentration of combustion products such as PAHs, as opposed to unburned ethylene molecules. This suggests that the primary absorber contributing to the LIGS signals in Region A is heated ethylene. However, there is no conclusive proof at this stage, and so further controlled tests would need to be conducted and compared with an appropriate data simulation to gather further evidence.

The spatially averaged temperature values tabulated in Table 5.2 were derived from the primary frequency peaks of the data presented in Figure 5.6, which was a single broad peak indicative of a continuous range of temperature contributions to the probe volume.

X [mm]	Temperature [K]	Uncertainty [K]	Precision [%]
0.0	747	± 7	0.9
2.0	872	± 29	3.3
3.5	895	± 39	4.4

Table 5.2: Dependence of derived temperature on radial distance from the central vertical axis, for LIGS signals experimentally measured at the 0.0 mm HAB position, at a fixed stoichiometry flow rate of 180 mL min^{-1} ethylene and 120 L min^{-1} air.

The values tabulated in Table 5.2 are also significantly lower than standard Gülder burner flame temperatures, which typically range from 1500 – 2000 K [23]. Therefore, it is necessary to use simulated data from the multiple temperature LIGS model to understand exactly what range of temperatures are contributing to the probe volume to produce these results. This is discussed in Section 5.3.3. However, before performing further calculations with the MATLAB model, some trends can be noted from the temperature data presented in Tables 5.1 and 5.2; thus some information about the flame environment can be deduced.

The first observation is that within Region A, the derived LIGS temperature increases with increasing HAB. In Region A, the reaction zone in the flame front from which the OH* chemiluminescence originates is clearly observed as a bright yellow high intensity annulus in the image slices taken at each HAB position; an example is seen in Figure 5.4. Thus a simple edge finding function was written using MATLAB by the author to identify the points where the intensity of the image dropped below a specified limit; this is expected to correspond to the approximate location of the flame front. Consequently, the radial thickness of the annulus-type reaction zone was determined to be 0.80 ± 0.05 mm at both 0.0 mm and 5.0 mm HAB. Similarly the approximate location of the inner edge of the reaction zone was found to be at X = 5.0 ± 0.05 mm for 0.0 mm HAB, but at X = 4.8 ± 0.05 mm for 5.0 mm HAB. It can thus be understood that the diameter of the cooler central region containing unburned ethylene decreases in diameter

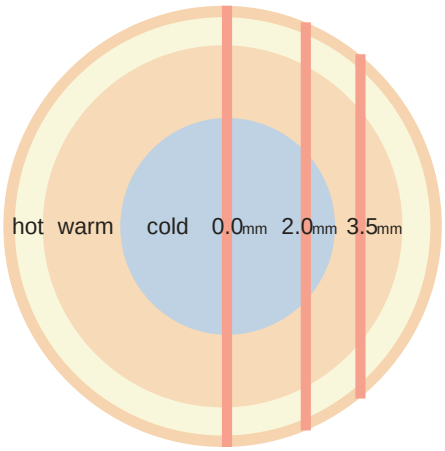


Figure 5.7: Cross section of Region A in the Gülder burner flame at 0.0 mm HAB. Probe volumes at three different radial positions relative to the central vertical axis (X = 0.0 mm, 2.0 mm and 3.5 mm) are identified in red in the diagram. Different temperature bands have been marked as hot, warm and cold regions; *hot* refers to the 1800 - 2000 K typical flame temperatures found near the reaction zone [23], and *cold* refers to room temperature unburned ethylene heated only by the surrounding hot material. The *warm* region is expected to contain unburned ethylene and combustion products heavily heated by the heat release at the reaction zone. The relative size of each region is based on OH* chemiluminescence data.

from 0.0 mm to 5.0 mm HAB, but the hotter annulus-type reaction zone where combustion reactions occur and release heat, remains a constant thickness. This means that at 5.0 mm HAB, the mean temperature of the probe volume is higher because there is a proportionally larger contribution from the hotter region. However it is yet unclear whether the absorbing species in this situation is heated ethylene alone, or if there is an additional contribution from PAHs, which are also present in this region.

The second key observation is that within Region A, the derived LIGS temperature increases with increasing radial distance from the central vertical axis. Based on the OH* chemiluminescence data, Figure 5.7 was drawn to illustrate this phenomenon; a higher derived temperature corresponds to a larger proportion of hotter material being sampled by the LIGS probe volume. It is also interesting to note that the LIGS signal originating from the X = 2.0 mm position has a feature that resembles the phenomenon analogous to frequency beating observed in the signals from the dual ethylene flow (see Figure 5.6). At this position it could be the case that there are contributions from at least two distinct regions of significantly different

temperature: the inner unburned ethylene at a temperature closer to room temperature, plus hot ethylene on the inner surface of the reaction zone. The effect of the geometry here is that the probe volume is a chord of the circle where the contributions or weightings from the different temperature regions approximate to a two-temperature or three-temperature spatial average (see Chapter 4). The position of the peak of the fast decaying signal at 3.5 mm is determined by the weighting of the various contributions of different temperatures.

Furthermore, the plots in Figures 5.5 and 5.6 show that the LIGS signals with a higher derived mean temperature decays faster. This is because at higher temperatures, the rate of diffusion is higher; faster diffusion rates lead to a reduction in the lifetime of the thermal grating. Since the LIGS signal is a measure of the reflectivity of the thermal grating, at higher temperatures, faster decaying LIGS signals with fewer resolvable oscillations are observed. However, there could be a second contribution to the apparent increase in the signal decay rate. If the LIGS signals originating from certain locations in the flame originate from probe volumes containing a broader range of temperature zones, the composite LIGS signal would appear to decay faster due to oscillations from many signals of varying frequencies quickly moving out of phase. The faster decaying signal at X = 3.5 mm may be the result of a continuous gradient of temperatures present in the probe volume, rather than being dominated by a few distinct temperature zones as in the X = 2.0 mm case (see Figure 5.6). The position of the oscillatory maxima in each case would be determined by the relative contributions from each temperature zone. This is explored further in Section 5.3.3.

5.3.2 Comparison of Ethylene-Air Flame with Ethylene Flow

Figure 5.8 shows a comparison between LIGS signals recorded in two environments at atmospheric pressure: an ethylene-air flame and a room temperature single ethylene flow. In order to keep other variables constant for a direct comparison between the two environments,

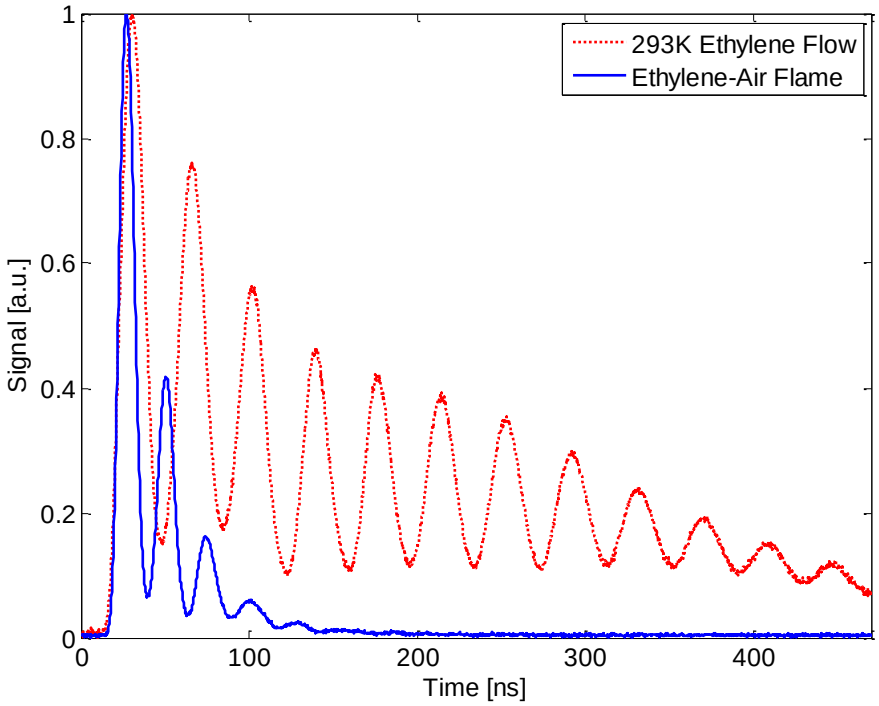


Figure 5.8: Comparison of LIGS signals from the Gülder burner; one signal is from a single non-ignited ethylene flow from the burner nozzle, and the other is from the ethylene-air flame. Both are atmospheric pressure signals averaged over 500 data shots, recorded at 2.0 mm HAB, on the central vertical axis. The derived temperature of the flame signal was 934 ± 10 K.

the non-ignited ethylene flow used was the output from the Gülder burner nozzle, not the dual flow system. However it can be seen from Figure 5.8 that the LIGS signal from the ethylene flow from the Gülder burner nozzle has the same basic form as the 293 K measurement from the dual flow system presented in Figure 4.4 in Chapter 4. LIGS measurements were made at exactly the same spatial position in both the flame and the non-ignited flow.

The primary difference between the two signals featured in Figure 5.8 is the decay rate. The LIGS signal recorded at flame temperature decays over a much shorter timescale in comparison to that recorded at room temperature in the ethylene flow. As temperature increases, the rate of diffusion also increases; as noted previously, this gives rise to a fast decaying LIGS signal due to the reduction in the lifetime of the thermal grating from which the probe beam is scattered. However, as discussed in Section 5.3.1, when the probe volume

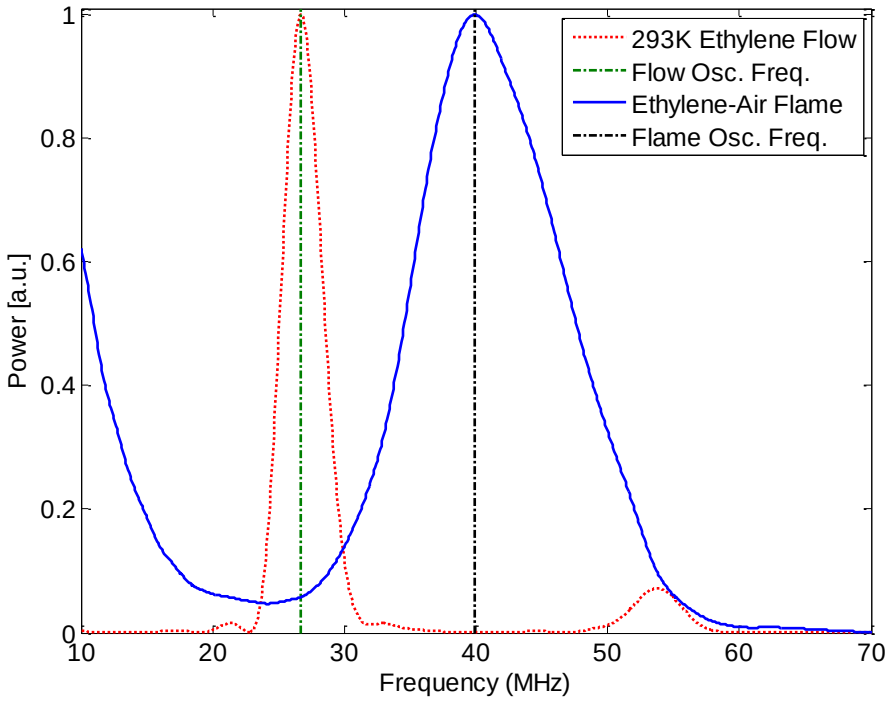


Figure 5.9: Comparison of frequency spectra calculated for the LIGS data from the Gülder burner; one signal is from a single non-ignited ethylene flow from the burner nozzle, and the other is from the ethylene-air flame. Both were atmospheric pressure signals averaged over 500 data shots, recorded at 2.0 mm HAB, on the central vertical axis.

contains a broad range of temperature zones as is the case for the flame, as opposed to the room temperature ethylene flow originating from a uniform temperature probe volume, the composite LIGS signal would decay faster due to oscillations from many signals of varying frequencies moving out of phase over time. The consequence of LIGS signals from the flame having fast decay rates is that it could limit the precision of atmospheric pressure flame measurements. This is because if a greater number of oscillatory peaks are resolvable, the Fourier transform produces a primary frequency peak with a smaller FWHM (see Figure 5.9). Thus for single shot measurements, the oscillation frequency can then be determined to a greater degree of precision. However it was found that when mean values were calculated over a large number of data shots, 500 in this case, there was little difference in precision between temperature values derived from the two different environments when standard deviation is used as an appropriate measure of uncertainty. The temperatures derived from the frequency

spectra in Figure 5.9 were calculated to have precisions of 0.8% for the room temperature ethylene flow data and 1.0% for the flame data.

When comparisons are made between the frequency spectra from the flame and the spectra from the multiple temperature dual ethylene flow, it can be seen that the distinct double peak features seen in Figure 4.10 are absent here. It was discussed in Chapter 4 that due to heat transfer between gas flows, temperature gradients do exist in the dual flow system, as opposed to two discrete temperature zones. However due to careful efforts being taken to minimise this heat transfer with an appropriate experiment set-up, it was still possible to maintain two distinct temperature regions within the probe volume, where the temperature difference between the two flows were measured to be of the order of 100 K. As a result, two primary peaks were present in the frequency spectra. The absence of multiple frequency peaks in the flame spectra indicate that the probe volumes in the flame consist of continuous temperature gradients. Therefore in order to simulate the LIGS data from the flame, the existing multiple temperature model was modified and the preliminary results are presented in Section 5.3.3.

5.3.3 Advanced Multiple Temperature Model for the Flame

The 'LIGSmodel_multi_temp.m' program discussed in Section 4.3.2 and included in Appendix 1, was modified to simulate LIGS signals originating from a probe volume containing smooth temperature gradients. The part of the data simulation program that specifies the temperature components in the probe volume was edited such that a vector containing a very large number of temperature elements could be used to model a signal. Each element has an associated weighting factor that defines the relative contribution of a temperature element to the LIGS signal; this represents the fraction of the gas within the probe volume which is at that temperature. As the number of elements in the temperature vector tends to infinity, the relative contribution of each element tends to zero and thus this discrete set of values becomes a good

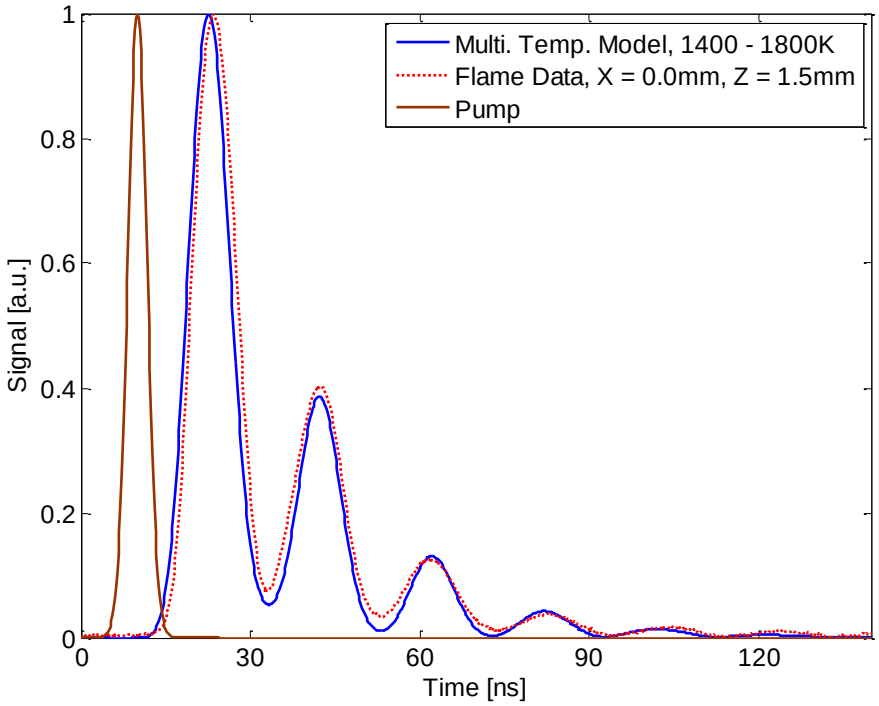


Figure 5.10: Preliminary result from the multiple temperature model being developed for the Gülder burner flame. The modelled signal uses a 401 element temperature input vector with equally weighted temperatures at 1 K intervals, in the 1400 K to 1800 K range (typical flame temperatures [23]). All other parameters in the model were fixed at typical values for an atmospheric pressure Gülder burner flame environment. Experimental data from the X = 0.0 mm and Z = 1.5 mm position is shown for comparison; the LIGS signal is averaged over 200 data shots.

approximation for a continuous temperature gradient. Considering the version of MATLAB and type of operating system installed on computers at the Department of Physics, University of Oxford, a vector created in MATLAB can contain a maximum of 2.8×10^{14} elements, which is more than sufficient for this type of simulation.

Figure 5.10 shows results from a first attempt at simulating LIGS signals in a flame using the modified version of the 'LIGSmodel_multi_temp.m' program. All parameters in the model, with the exception of temperature and weighting factor, were fixed at typical values for an atmospheric pressure Gülder burner flame environment. The signal was simulated using a 401 element temperature input vector with equally weighted temperatures at 1 K intervals, ranging

from 1400 K to 1800 K. 1800 K represents a typical flame temperature near the reaction zone in Region A [23], while 1400 K was arbitrarily selected to represent the mean temperature of a region containing unburned ethylene in addition to flame temperature material. At this stage, no effort was made to account for differences in variables such as quench times and branching ratios. However, it can be seen from Figure 5.10 that the model is already a good fit to the experimental data. This is a successful result which indicates that the modified version of the model is already capable of simulating LIGS signals originating from a probe volume with a continuous temperature gradient. Adjusting other parameters in the model and using a rigorous fitting routine could improve the correspondence between experiment and model even further.

Next, a second signal corresponding to a different location within the flame was modelled using a 1708 element temperature input vector with equally weighted temperatures at 1 K intervals, ranging from 293 K to 2000 K. This is shown in Figure 5.11. In this case, 293 K represents typical room temperature. It was found that to simulate a very fast decaying LIGS signal where no oscillations are resolvable, a broad range of closely spaced temperatures needed to be input into the model. Again, no effort was made at this stage to account for differences in variables such as quench times, so while the modelled and experimental signal are of the same basic form, attempts must be made to match the other variables in order to improve the fit. The temperature and weighting factors themselves could also be adjusted in accordance with the OH* chemiluminescence data. Considering the fact that the simulated signal in Figures 5.10 and 5.11 were generated without utilising the full capabilities of the model, the results are certainly encouraging. Therefore, based on the results in this chapter and the former one, it is evident that LIGS signals originating from multiple temperature probe volumes can be simulated using the modelling program developed during this study in order to derive useful temperature data from the signal. Hence it can be concluded that the LIGS technique is suitable for thermometry in non-uniform temperature fields and flames.

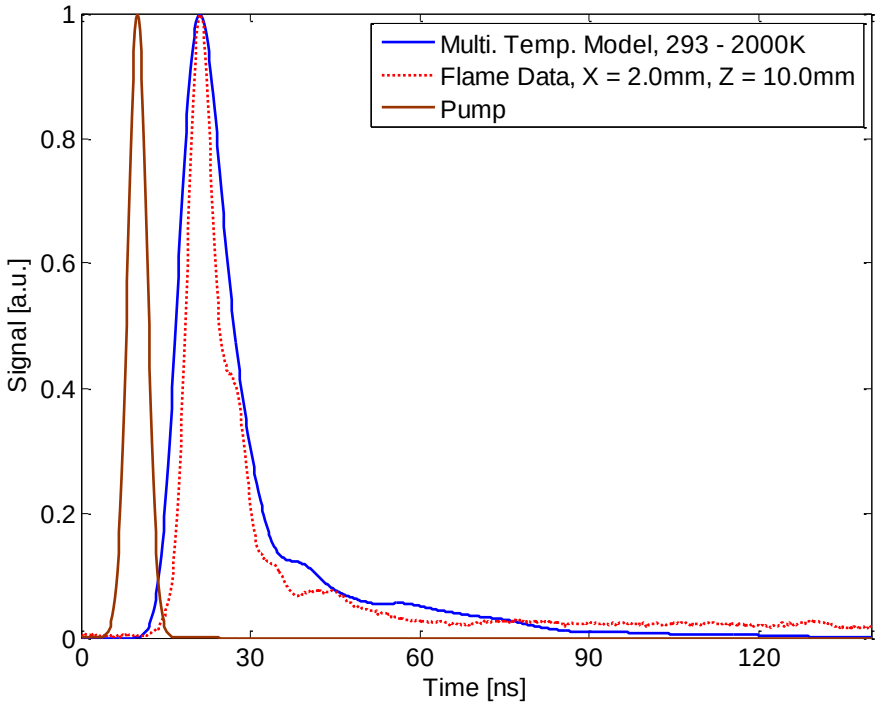


Figure 5.11: Preliminary result from the multiple temperature model being developed for the Gülder burner flame. The modelled signal uses a 1708 element temperature input vector with equally weighted temperatures at 1 K intervals, in the 293 K (typical room temperature) to 2000 K range (typical maximum flame temperature in Gülder burner [23]). All other parameters in the model were fixed at typical values for an atmospheric pressure Gülder burner flame environment. Experimental data from the X = 2.0 mm and Z = 10.0 mm position is shown for comparison; the LIGS signal is averaged over 200 data shots.

6 Conclusions and Future Work

6.1 Conclusions

During this investigation, the application of LIGS in thermometry of non-uniform temperature fields and flames has been successfully demonstrated. Major achievements were developing a model to simulate LIGS signals originating from probe volumes containing temperature non-uniformities, and verifying the validity of the model with experimental data from two environments: an ethylene flow and a Gülder burner flame. The main objective of the study was to identify how contributions from different temperature regions present within the LIGS probe volume altered the form of the LIGS signal and to examine what effect this had on the derived temperatures.

Controlled, multiple temperature ethylene flows were first investigated as a precursor to making LIGS measurements in an ethylene-air laminar diffusion flame. The purpose of this was to understand how best to extract temperature data from LIGS signals originating from multiple temperature probe volumes, by first studying an environment where the non-uniformities are known quantities, prior to applying the technique to flames where unknown temperature gradients are present. Thus a suitable LIGS experiment set-up was designed and assembled; some apparatus were custom-built by the author. An appropriate length and diameter for the LIGS probe volume were carefully calculated as 13.3 mm and 300 μm respectively; this allowed the entire region of interest in the environments intended for study (temperature-controlled ethylene flow and ethylene-air laminar diffusion flame) to be sampled in a single LIGS measurement. The effects of varying pressure and composition in a high pressure cell containing oxygen and nitrogen were initially measured as a test to verify the capabilities of the new measurement system. Once the experiment set-up was shown to operate as expected, the ethylene dual flow system was installed at the measurement point.

The probe volume in the dual flow contained two distinct temperature regions: one contribution from an unheated flow and a second contribution from a heated flow, where the temperature was controlled by regulating the voltage applied to the heating element. LIGS measurements were made with the flow system operating in both single and dual flow modes. Meanwhile, a MATLAB model was also developed to simulate how the LIGS signal from a probe volume in a particular environment is affected by contributions from regions of different temperature. Initially, the total intensity of the spatially averaged composite signal was modelled as the weighted sum of LIGS signal intensities from individual temperature zones. The data analysis was conducted using MATLAB commands incorporated into the multiple temperature LIGS model, which enabled comparisons between experimental and modelled data to be easily made. The MATLAB model was found to correspond very well with the experimental data from the ethylene flow system. It was also possible to successfully identify two discrete contributions to the signal from temperature regions at 293 ± 2 K and 310 ± 3K. These features were recognised as LIGS signals originating from the cooler ethylene flow, where two temperature components were present due to part of the room temperature ethylene flow experiencing secondary heating due to the placement of the heated flow nearby.

Since both the experimental technique and the data simulation model were shown to be successful in achieving the initial objective of the investigation, the same study was carried out with a Gülder burner installed in place of the dual ethylene flow. The burner was operated with a fixed stoichiometry such that it provided a stable, laminar diffusion flame suitable for laboratory tests. LIGS measurements were made at several spatial positions in the lower region of the flame, where unburned ethylene and PAHs were suspected to be the laser absorbing species. Signals were recorded and analysed in the HAB range of 0.0 – 5.0 mm; radially, the X = 0.0 – 3.5 mm region was carefully studied. Temperatures were derived from the frequency spectra of LIGS signals with precisions of 0.9 – 4.4%. Furthermore, the OH* chemiluminescence from the flame was measured to determine the location of the reaction zone. The experimental data from both the LIGS experiment and the OH* chemiluminescence experiment, combined

with comparisons made between the flame measurements and ethylene flow data, were used to improve the existing LIGS model and modify it such that it was able to simulate the effects of continuous temperature gradients, as opposed to distinct temperature regions. The model was used to demonstrate that the derived temperatures from the flame measurements were the spatial average of a continuous temperature gradient, indicating that the probe volume contained colder unburned ethylene in addition to hotter flame material; thus the derived temperatures were significantly lower than the typical 1500 – 2000 K flame temperatures expected from a Gülder burner [23].

In summary, LIGS has been demonstrated as a highly effective technique for thermometry in environments where the probe volume contains multiple temperature regions, where each region is a distinct temperature. Results from the flame study strongly suggest that LIGS is also suitable for studying environments that contain continuous temperature gradients. A limitation of the existing LIGS model is that it requires the user to accurately estimate the quench times and branching ratios for the environment under study. Therefore, while the results reported in this thesis are certainly encouraging, further improvements could be made to the model by incorporating a rigorous multiple parameter fitting routine, such that the simulated LIGS data would be a closer match to the experimentally measured signals.

6.2 Future Work

The primary focus of future work which follows on from this thesis should be to improve the multiple temperature LIGS model so that it is better suited to simulating flame environments. It is necessary to incorporate a rigorous multiple parameter fitting routine into the model to improve the quality of the data fits that it is able to achieve. Once this has been accomplished, the model could be used to analyse the data collected from a range of spatial positions within the flame, which were presented in Section 5.3.1. The aim is to successfully simulate the LIGS

signals experimentally measured at each spatial position; this would make it possible to precisely and accurately determine the temperature zones present within the probe volume at each location, along with the values of other parameters such as quench times and branching ratio. The derived temperature from the LIGS signal is a spatially averaged result; thus it is not possible to determine relative positions of the different temperature zones within the probe volume using a single set of LIGS data. However, it may be possible to combine such measurements with tomographic analysis to build a 2D map in order to determine the spatial distribution of the different temperature regions. The ultimate objective of such work would be to use LIGS to produce a precise and accurate temperature distribution map of the Gülder burner flame, in order to better understand combustion processes that lead to the production of soot and other combustion products. It is thus desirable to identify methods to improve the spatial resolution of the LIGS technique.

However, during the course of this study, two relevant experiments, not directly related to the focus of this thesis, were also conducted. The experiments yielded some interesting and encouraging results, which could potentially form the focus of additional future work. The following two sections of this chapter provide a brief overview of each experiment and the level of progress made in achieving the experiment objectives.

6.2.1 Effects of Soot

Some preliminary LIGS measurements were made in the yellow sooty part of the flame, which was identified in Figure 5.1 as Region B. As with previous measurements, flow rates of 180 mL min^{-1} ethylene and 120 L min^{-1} air were used. Signals were recorded at 5.0 mm intervals in the 20.0 - 70.0 mm HAB range using the experiment set-up illustrated in Figures 3.1, 3.2 and 3.4. However, no LIGS signals were detected from HAB 55.0 mm upwards. A possible explanation for this observation is that the high concentration of soot present in this region elastically scatters

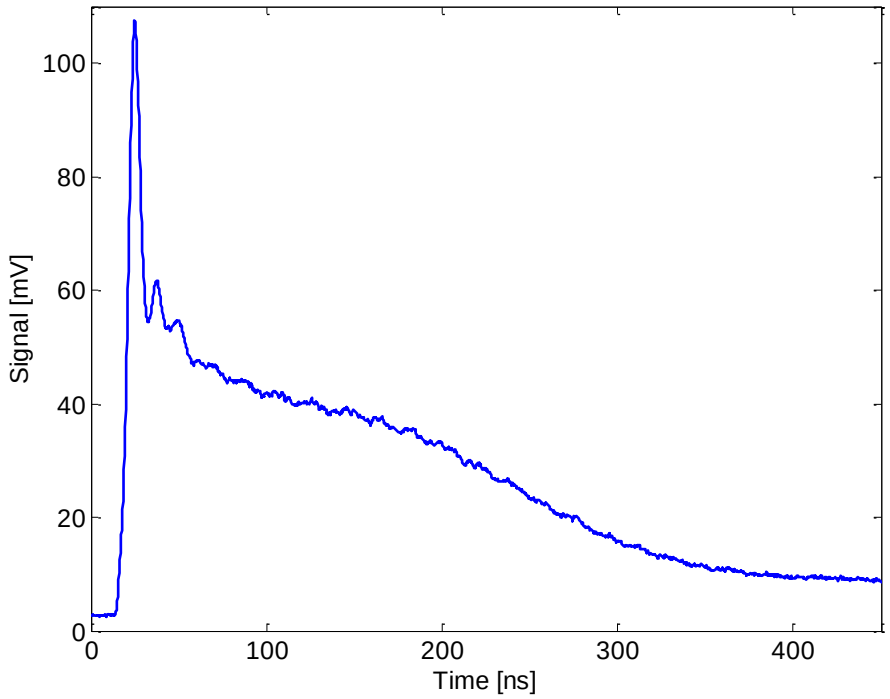


Figure 6.1: LIGS signal recorded in Region B at atmospheric pressure and averaged over 100 data shots, at 25.0 mm HAB, on the central vertical axis. Three oscillatory peaks, separated by a time period typical of τ, are visible at the start of the signal, after which a non-oscillatory feature decays over time. The signal is an order of magnitude smaller in intensity than signals recorded in Region A; thus the signal-to-noise ratio is lower. The temperature derived from the oscillatory peak separation is T = 1880 ± 60 K.

the probe beam, in addition to absorbing both the pump and the probe; thus the probe transmission is too low to generate a LIGS signal. This could be investigated further in future studies. Furthermore, while it was possible to make LIGS measurements from HAB 20.0 – 50.0 mm, the intensity of signals from Region B was typically found to be an order of magnitude smaller than those from Region A.

Measurements made at HAB 25.0 mm and 30.0 mm are shown in Figures 6.1 and 6.2 respectively. The LIGS signals in both figures have been averaged over 100 data shots. However, due to the lower intensity of the LIGS signals measured in this region, the signal-to-noise ratio is significantly smaller when compared with measurements from Region A, which were presented in the previous chapter; Since LIGS thermometry is not intensity dependent, the low intensities

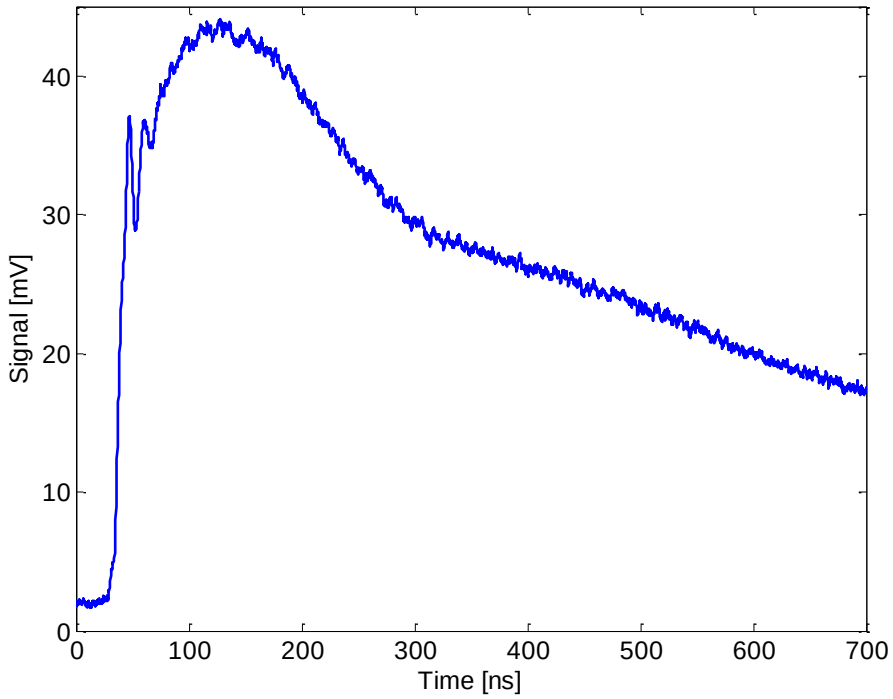


Figure 6.2: LIGS signal recorded in Region B at atmospheric pressure and averaged over 100 data shots, at 30.0 mm HAB, on the central vertical axis. Two oscillatory peaks, separated by a time period typical of τ, are visible at the start of the signal, after which a non-oscillatory feature grows in intensity and decays over time. The signal is an order of magnitude smaller in intensity than signals recorded in Region A; thus the signal-to-noise ratio is lower. The temperature derived from the oscillatory peak separation is T = 1690 ± 60 K.

do not affect the precision of the derived temperatures. The signal intensity can potentially provide additional information about the flame in such a situation, for instance, by providing a measure of the soot volume fraction at each point.

The LIGS signals recorded in Region B are significantly different in shape to those recorded in Region A of the flame. These measurements show oscillations at the start, which appear to then be superimposed with a decaying, non-oscillatory background from another stationary grating. Figures 6.1 and 6.2 both show evidence of multiple decay rates affecting the non-oscillatory component. The oscillations were found to have a period that is consistent with typical flame temperature LIGS signals; the derived temperatures were 1880 ± 60 K at 25.0 mm HAB and 1690 ± 60 K at 30.0 mm HAB. The uncertainties quoted are standard deviations

associated with mean values calculated using MATLAB. Moreover, these two signals significantly differ in shape and decay over different time scales; this is indicative of multiple heat transfer and decay mechanisms occurring in this region. Non-oscillatory decay signals indicate the absence of an acoustic grating, signifying heat deposition rates too slow to create one. Heated soot can transfer heat slowly to its surroundings, over time scales much larger than LIGS grating lifetimes [41]. The initial rise seen in the intensity of the non-oscillatory feature might be caused by continuing heat deposition into the stationary grating component. It would be necessary to conduct further experiments to confirm the identity of the laser absorbing species and determine the heat transfer mechanisms which give rise to these features.

6.2.2 One-Dimensional Measurement of LIGS Signals

LIGS signals were recorded as time varying images, with an experimental set-up where the PMT in Figure 3.2 was replaced with a streak camera and an electron multiplying charge-coupled device (EMCCD). The objective was to develop a one-dimensional imaging system, which could be used to make temporally and spatially resolved LIGS measurements in a line-type interaction volume. One-dimensional LIGS measurements have previously been performed in gas mixtures [15] and the present study builds on this research.

Spherical lenses were replaced with cylindrical lenses and arranged such that sheets of laser light which crossed to form a line, 4 mm in height and 1 mm in thickness, were produced. A toluene test cylinder was used as described in Section 3.2.1. However, a metal tube was used instead of a plastic tube; this was attached to a heater and the temperature was monitored using a thermocouple. LIGS measurements were made at two temperatures, measured as 293.0 ± 0.5 K (room temperature) and 366.0 ± 0.5 K using the thermocouple; the data are presented in Figure 6.3. Temporal behaviour of the signal is shown on the horizontal axis, while the vertical

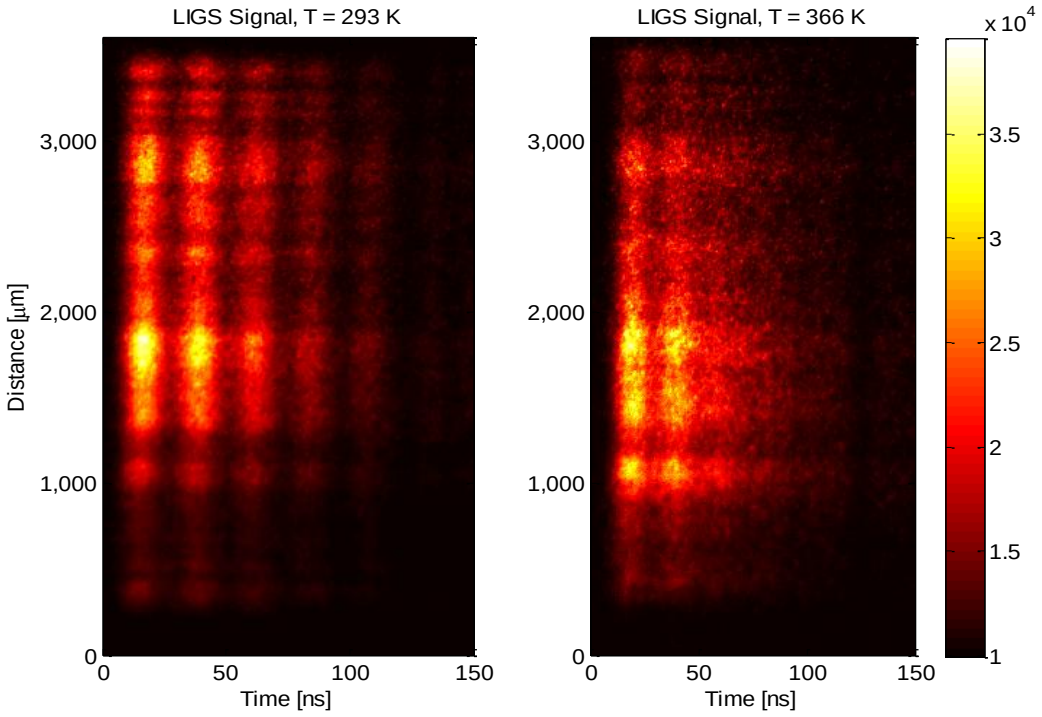


Figure 6.3: One-dimensional LIGS signals recorded at temporally stable, spatially uniform temperatures and atmospheric pressure using a streak camera. Each image is labelled with a temperature measured using a thermocouple. The intensity of the LIGS signal as indicated by the colour map is in arbitrary units, with black indicating low intensity and white indicating high intensity.

axis displays the spatial distribution. The LIGS images were temporally calibrated by imaging two laser pulses of known temporal separation. The spatial calibration was performed by imaging scattered background light through a copper mask with precise 1.0 mm slit separation; a MATLAB script was employed to identify the correspondence between pixel number in the image and real spatial distance.

The lower signal-to-noise ratio of the 366 K measurement was caused by the rapid evaporation of toluene at higher temperatures. The images were processed using MATLAB to extract the oscillation frequency, from which the temperatures were calculated as 293 ± 2K (0.7% precision) for the room temperature measurement and 364 ± 4K (1.0% precision) for the heated toluene measurement. The uncertainty indicates the standard deviation of temperature

values extracted at twenty vertical positions in the one-dimensional signal. The thermocouple reading and the LIGS derived temperature were in agreement for both measurements. These results demonstrate that a one-dimensional imaging system has been successfully set-up, and is capable of making highly precise and accurate temperature measurements. Another member of the research group then recorded a temperature gradient along a vertical line-segment in heated toluene using the same LIGS imaging system. The next step would be to use such a set-up to simultaneously image points at a range of HAB positions in a Gülder burner flame.

7 Appendices

7.1 Appendix 1

MATLAB script: 'LIGSmodel_multi_temp.m'

```
%% NILUSHI WIJEYASINGHE, 31 AUGUST 2013, THREE TEMPERATURE INPUT VERSION.
% Accepts temperature and weighting input data for multi temp probe volume.
% Generates a modelled LIGS signal and power spectrum.
% Plots model and experimental data for specified conditions.

% Start by clearing workspace and command window.
clear
clc


%% (1) MODEL - INPUT TEMPERATURE and WEIGHTING.

% Specify temperatures and their respective weightings to feed into model:
    Temperature=[293 310 422];
    Weighting=[0.2 0.2 0.6];


%% (2) MODEL - GENERATE AND PLOT LIGS SIGNALS FOR EACH TEMPERATURE.

    figure(1)
    SD=[];

for k=1:1:3;

    % Extract each temperature from input vector:
        T=Temperature(k);

    % Specify variables that are fixed for all values of k:
        gamma = 1.247; %Ratio of specific heats
        Na = 6.022e23; %Avagadro constant
        m = 28.05e-3/Na; %Molecular mass
        Lambda = 14.875e-6; %Grating spacing
        pumpfwhm = 4e-9; %Pump pulse width (FWHM)
        kb = 1.38e-23; %Boltzmann constant
        pressure = 1; %Pressure
        Pr = 0.7; %Prandtl number

    % Specify parameters that alter the model:

        if k==1;
           Re = 128*pressure; %Reynold's number
           Q1 = 4.75e-9; %Fast quench time
           Q2 = 650e-9; %Slow quench time
           Br = 0.38; %Branching ratio
           Params = [Re Q1 Br Q2]; %Set up parameters for the fit
           NotParams = [pressure pumpfwhm Pr gamma];
        end
```

```
    if k==2;
       Re = 128*pressure; %Reynold's number
       Q1 = 4.75e-9; %Fast quench time
       Q2 = 600e-9; %Slow quench time
       Br = 0.37; %Branching ratio
       Params = [Re Q1 Br Q2]; %Set up parameters for the fit
       NotParams = [pressure pumpfwhm Pr gamma];
    end

    if k==3;
       Re = 117.5*pressure; %Reynold's number
       Q1 = 4.75e-9; %Fast quench time
       Q2 = 250e-9; %Slow quench time
       Br = 0.35; %Branching ratio
       Params = [Re Q1 Br Q2]; %Set up parameters for the fit
       NotParams = [pressure pumpfwhm Pr gamma];
    end


%% (3) MODEL - RUN SINGLE TEMP LIGS MODEL FOR EACH INPUT TEMPERATURE.

% Generate a set of modelled LIGS signals for each value of k:
    [tp, PumpPulse, Sim_data] = LIGSmodel_single_temp(T, Params,...
                                NotParams, Lambda, gamma, m);

% Convert the output electric field vector from
% LIGSmodel_single_temp.m to a LIGS signal intensity vector:
    intensity=Sim_data.*conj(Sim_data);

% Normalise modelled LIGS signal:
    y_offset=intensity(find(tp==0));
    sim_signal = (intensity-y_offset)./max(intensity-y_offset);

% Plot modelled LIGS signals for each temperature as subplots within a
% single figure:
    subplot(2,2,k)
    plot(tp*1E9,PumpPulse(:,2),tp*1E9,sim_signal)
    xlabel 'Time [ns]'
    ylabel 'Signal [a.u.]'
    plot_name1=['T = ' num2str(T,'%2.0f') ' K'];
    title(plot_name1)
    box on
    hold on

% Find rising edge of each modelled LIGS signal in order to later
% realign modelled data with experimental data:
    limit1=0.8;
    sig_idx1 = find(sim_signal==limit1,1);
    edge_time1 = tp(sig_idx1);

% Save electric field vectors from each run of LIGSmodel_single_temp.m
% into a matrix to be summed later to generate multi temp signal:
    SD=[SD Sim_data];


%% (4) EXPT - EXTRACT LIGS SIGNAL INFO FROM DATA FOR EACH TEMPERATURE:

    desc = 'signalG';
    date = '31-08-2013';
```

```
    % Specify all oscilloscope data folders selected for analysis:
        types = [{'0V 293K'},{'50V 313K'},{'50V 386K'}];

    % Open all oscilloscope data files in each folder and save into array:
        dirold=cd;
        display(['Opening ' dirold, '\', types{k}]);
        LIGSxpt_read_files(types{k},date,desc);

    % Run the experimental data analysis function:
        if exist(['output\dataset_' types{k} '.mat'],'file')
           [norm_time,norm_signal] = LIGSxpt_analyse_data(types{k},...
                                     edge_time1,time_corr);
        end

    % Plot experimentally measured LIGS signals for each temperature as
    % subplots within a single figure:
        plot(norm_time*1E9,norm_signal,'red')
        xlim([0 700])
        ylim([0 1])
        legend('Pump','LIGS Model','LIGS PMT Data')
end


%% (5) MODEL - MULTI TEMP LIGS SIGNAL IS WEIGHTED SUM OF SINGLE TEMP
       SIGNALS.

% Calculate sum of single temperature signals:
    sig_sum=zeros(size(tp));

    for j=1:1:length(Weighting);
        W=Weighting(j);
        sig_sum=sig_sum+W*(SD(:,j).*conj(SD(:,j)));
    end

% Normalise modelled LIGS signal:
    y_offset2=sig_sum(find(tp==0));
    norm_sim=(sig_sum-y_offset2)./(max(sig_sum)-y_offset2);

% Plot the multiple temperature modelled signal:
    subplot(2,2,4)
    plot(tp*1E9,PumpPulse(:,2),tp*1E9,norm_sim)
    xlabel 'Time [ns]'
    ylabel 'Signal [a.u.]'
    plot_name2='Multi Temperature LIGS';
    title(plot_name2)
    box on
    hold on


%% (6) EXPT - PLOT MULTIPLE TEMP OSCILLOSCOPE DATA.

        desc = 'signalG';
        date = '31-08-2013';

    % Specify all data folders selected for analysis:
        types = {'50V 313K 386K'};
        n=1;
```

```
    % Open all oscilloscope data files in each folder and save into array:
        dirold=cd;
        display(['Opening ' dirold, '\', types{k}]);
        LIGSxpt_read_files(types{k},date,desc);

    % Run the experimental data analysis function:
        if exist(['output\dataset_' types{k} '.mat'],'file')
           [norm_time,norm_signal] = LIGSxpt_analyse_data(types{k},...
                                     edge_time1,time_corr);
        end

    % Plot experimentally measured LIGS signals for each temperature onto
    % the same subplot as the modelled data for that temperature:
        plot(norm_time*1E9,norm_signal,'red')
        xlim([0 700])
        ylim([0 1])
        legend('Pump','LIGS Model','LIGS PMT Data')


%% (7) MODEL - CALCULATE MULTI TEMP FREQENCY SPECTRUM AND FIND PEAK VALUES.

% Calculate Fourier transform of modelled multi temp LIGS signal:
    time=tp;
    signal=norm_sim;

    newlength=2^16;
    newtime=(1:newlength)*(time(2)-time(1));
    newsig=zeros(newlength,1);

    % Smooth out the padding at edges using windowing function:
        win=hann(length(time));
    % Remove noise on signal with non-linear filtering:
        newsig(1:length(time))=wiener2(signal).*win;
    % Calculate FFT of time series data:
        tfm = fft(newsig);
    % Generate frequency vector:
        freq = (time(2)-time(1))^-1/2 * linspace(0,1,newlength/2+1);
    % Compute power spectrum:
        pow = real(tfm.*conj(tfm));
    % Power spectrum is symmetrical about zero.
    % Negative and positive frequencies are identical.
    % Keep positive half of power spectrum vector:
        pow=pow(1:newlength/2+1);


%% (8) MODEL - FIND FIRST OSCILLATION PEAK IN FREQUENCY SPECTRUM:

    % Search for the elements in the 20MHz and 50MHz window:
        low_lim=20E6;
        high_lim=50E6;
        [val low_idx] = min(abs(freq-low_lim));
        [val high_idx] = min(abs(freq-high_lim));

    % Identify LIGS oscillation frequency:
        [val idx] = max(pow(low_idx:high_idx));
        oscfrq=freq(idx+low_idx-1);
        display(['Model, first peak frq: ' ...
        num2str(((oscfrq)*1E-6),'%2.1f') 'MHz'])
```

```
    % Frequency limits maybe badly defined or script maybe unable to
    % identify a frequency peak. In these cases, issue a warning:
        if oscfrq-low_lim < 1E6
           display('!!WARNING!! Peak at lowest value of frequency window.')
        end


%% (9) MODEL - CALCULATE TEMP CORRESPONDING TO FIRST LIGS OSCILLATION FREQ:
    Sum_Temp1=(1/kb)*(Lambda^2)*(oscfrq^2)*(m/gamma);
    display(['Model, first peak temp:' num2str(Sum_Temp1,'%2.0f') 'K'])


%% (10) MODEL - FIND SECOND OSCILLATION PEAK IN FREQUENCY SPECTRUM.

% Use the same method as the first peak, but search for the elements in a
% different frequency window:
    low_lim=26E6;
    high_lim=50E6;
    [val_two low_idx] = min(abs(freq-low_lim));
    [val_two high_idx] = min(abs(freq-high_lim));
    [val_two idx] = max(pow(low_idx:high_idx));
    oscfrq2=freq(idx+low_idx-1);
    display(['Model, second peak frq: ' ...
    num2str(((oscfrq2)*1E-6),'%2.1f') 'MHz'])
    if oscfrq2-low_lim < 1E6
       display('!!WARNING!! Peak at lowest value of frequency window.')
    end

%% (11) MODEL - CALCULATE TEMP CORRESPONDING TO SECOND LIGS OSCILLATION
        FREQ:
    Sum_Temp2=(1/kb)*(Lambda^2)*(oscfrq2^2)*(m/gamma);
    display(['Model, first peak temp:' num2str(Sum_Temp2,'%2.0f') 'K'])


%% (12) MODEL - PLOT FREQUENCY SPECTRUM FOR THE MULTI TEMP LIGS SIGNAL.

    figure(2)
    plot(freq*1E-6,pow,'blue')
    xlabel 'Frequency (MHz)'
    ylabel 'Power'
    out = get(gca,'YLim');
    line([oscfrq oscfrq]*1E-6,[out(1) val],'Color','blue')
    line([oscfrq2 oscfrq2]*1E-6,[out(1) val_two],'Color','blue')
    pause(0.2)
    hold on


%% (13) EXPT - CALCULATE MULTI TEMP FREQENCY SPECTRUM AND FIND PEAK VALUES.

% This follows exactly the same steps as the calculation for the modelled
% LIGS data as detailed above:
    time=norm_time;
    signal=norm_signal;
    newlength=2^16;
    newtime=(1:newlength)*(time(2)-time(1));
    newsig=zeros(newlength,1);
    win=hann(length(time));
    newsig(1:length(time))=wiener2(signal).*win;
```

```
    tfm = fft(newsig);
    freq = (time(2)-time(1))^-1/2 * linspace(0,1,newlength/2+1);
    pow2 = real(tfm.*conj(tfm));
    pow2=pow2(1:newlength/2+1);


%% (14) EXPT - FIND FIRST OSCILLATION PEAK IN FREQUENCY SPECTRUM.

    low_lim=20E6;
    high_lim=50E6;
    [val_three low_idx] = min(abs(freq-low_lim));
    [val_three high_idx] = min(abs(freq-high_lim));
    [val_three idx] = max(pow2(low_idx:high_idx));
    oscfrq3=freq(idx+low_idx-1);
    display(['Expt, first peak frq: ' ...
    num2str(((oscfrq3)*1E-6),'%2.1f') 'MHz'])
    if oscfrq3-low_lim < 1E6
       display('!!WARNING!! Peak at lowest value of frequency window.')
    end


%% (15) EXPT - CALCULATE TEMP CORRESPONDING TO FIRST LIGS OSCILLATION FREQ:
    Sum_Temp3=(1/kb)*(Lambda^2)*(oscfrq3^2)*(m/gamma);
    display(['Expt, first peak temp: ' num2str(Sum_Temp3,'%2.0f') 'K'])


%% (16) EXPT - FIND SECOND OSCILLATION PEAK IN FREQUENCY SPECTRUM.

    low_lim=26E6;
    high_lim=50E6;
    [val_four low_idx] = min(abs(freq-low_lim));
    [val_four high_idx] = min(abs(freq-high_lim));
    [val_four idx] = max(pow2(low_idx:high_idx));
    oscfrq4=freq(idx+low_idx-1);
    display(['Expt, second peak frq: ' ...
    num2str(((oscfrq4)*1E-6),'%2.1f') 'MHz'])
    if oscfrq4-low_lim < 1E6
       display('!!WARNING!! Peak at lowest value of frequency window.')
    end


%% (17) EXPT - CALCULATE TEMP CORRESPONDING TO SECOND LIGS OSCILLATION
        FREQ:
    Sum_Temp4=(1/kb)*(Lambda^2)*(oscfrq4^2)*(m/gamma);
    display(['Expt, second peak temp: ' num2str(Sum_Temp4,'%2.0f') 'K'])


%% (18) EXPT - PLOT FREQUENCY SPECTRUM FOR THE MULTI TEMP LIGS SIGNAL.

% Plot expt data onto the same figure as modelled data for easy comparison:
        figure(2)
        ratio=max(pow2)/max(pow);
        plot(freq*1E-6,pow2/ratio,'red')
        xlabel 'Frequency (MHz)'
        ylabel 'Power'
        xlim([0 50]); ylim([0 1000])
        out = get(gca,'YLim');
        line([oscfrq3 oscfrq3]*1E-6,[out(1) val_two/ratio],'Color','red')
        line([oscfrq4 oscfrq4]*1E-6,[out(1) val_four/ratio],'Color','red')
        title('Power Spectrum')
```

7.2 Appendix 2

MATLAB function: 'LIGSmodel_single_temp.m'

```
function [tp, PumpPulse, Sim_data] = LIGSmodel_single_temp(T, Params,...
                                     NotParams, Lambda, gamma, m)

% NILUSHI WIJEYASINGHE, 31 AUGUST 2013.
% Generates a modelled LIGS signal for a single input temperature.
% Based on the 'LIGS_signal_generator.m' function developed by
% B. A. O. Williams, University of Oxford (August 2011).

%% GENERATE MODEL LIGS SIGNAL.

% Calculate the time period tau that should result from the fringe spacing
% specified in the 'LIGSmodel_single_temp.m' script:
    kb=1.38e-23;
    tau = Lambda * sqrt(m/(gamma*kb*T));

% Generate a suitable pump pulse:
    tp = (-200:5000)'*2e-10;
    PumpPulse = [tp GaussFitFunc([10e-9 NotParams(2)/(2*sqrt(2*log(2)))...
                1],tp)];

% Calculate the model LIGS signal:
    [Signal] = multi_temp_TEMPORAL(Params, NotParams, T, tau, PumpPulse);
% The 'multi_temp_TEMPORAL.m' function and all functions employed within
% it are slightly modified versions of functions developed by B. A. O.
% Williams,University of Oxford (August 2011).

% Realign the pump pulse with the model LIGS signal:
    [Sim_data] = interp1(Signal(:,1),Signal(:,2),tp, '*cubic', 0);

end
```

7.3 Appendix 3

MATLAB function: 'LIGSxpt_read_files.m'

```
function LIGSxpt_read_files(condition,date,desc)

% NILUSHI WIJEYASINGHE, 31 AUGUST 2013.
% Function to convert oscilloscope data files into a large .mat
% Based on the 'ReadFiles_f' function developed by B. A. O. Williams,
% University of Oxford (August 2011).


% Data folders selected for analysis were specified in the script
% LIGSmodel_multi_temp.m
% The LIGS data originate from oscilloscope Channel 1.
% Search for all the C1*.dat files in the specified data folder:
    dirold=cd;
    folder = [condition, '\'];
    cd([dirold, '\', folder]);
    list=dir('C1*.dat');
    cd(dirold);
    display('Loading folder contents to structure..')

% Identify starting index:
    startidx = str2double(regexp(list(1).name,['(?<=', desc, ')(\d+)'], ...
               'match','once'));

% Open each file in the data folder and save the required information into
% a data structure:
    for i=1:1:length(list)
        j=startidx+i-1;
        % Form the filestring:
            filestring=[desc, num2str(j,'%0.5d'), '.dat'];
            T1=load([folder, 'C1', filestring]);
        % Save the raw data into a cell array:
            data.traces{i} = [T1(:,1) T1(:,2)];
    end

    pause(0.1)

% Save the data structure:
    data.desc = [date, ' ' condition];
    display('Saving data structure...')
    save(['output\dataset_', condition,'.mat'],'data');

    clear data filestring datalen

end
```

7.4 Appendix 4

MATLAB function: 'LIGSxpt_analyse_data.m'

```
function [norm_time,norm_signal] = LIGSxpt_analyse_data(condition, ...
                                   edge_time,time_corr)

% NILUSHI WIJEYASINGHE, 31 AUGUST 2013.
% Function that analyses experimental LIGS data.
% Employs the LIGSxpt_mean_std.m function to calculate mean and standard
% deviation of oscillation frequency and temperature.

% Process all the data shots in each data folder read by
% LIGSxpt_read_files.m
    load(['output\dataset_', condition, '.mat'])

for j=1
    start=1;
    last=numel(data.traces);
    clear time_signal

% Step through the list of indices and save LIGS signal vectors into a
% matrix if the intensity falls within a specified range:
    time_signal(:,1)=data.traces{1}(:,1);
    bigsum=[];

    for k=start:last
        % Specify baseline noise level, noting that signal intensity is -ve
        limit=-0.3;
        % Specify detector saturation limit
        saturation_limit=-0.75;
        % Save signals only if the intensity falls within this range:
        if min(data.traces{k}(:,2)) < limit && ...
           min(data.traces{k}(:,2))>saturation_limit;
           bigsum=[bigsum data.traces{k}(:,2)];
        end
    end

% Average over the saved data shots to construct a mean LIGS signal vector:
    avgwin=size(bigsum, 2);
    display([num2str(avgwin) ...
    ' shots with LIGS intensity above ' num2str(-limit) ' V'])
    mean_sig=mean(bigsum,2);
    time_signal(:,2)=mean_sig;

% Identify the time vector and signal vector:
    time = time_signal(:,1);
    signal=(-time_signal(:,2));

% Calculate the mean and standard deviation of the oscillation frequencies
% and corresponding temperatures:
    [mean_frq std_frq mean_temp std_temp] = LIGSxpt_mean_std(bigsum, ...
                                            mean_sig,time);
% The 'LIGSxpt_mean_std.m' function calculates the mean and std of
oscillation frequency and temperature using an identical method to the
procedure employed in 'LIGSmodel_multi_temp.m', which is the primary script
within which this function is executed.
```

```
% Display the calculated mean and std values in the command window:
    display([num2str(condition) 'Expt, Peak frq: ' ...
        num2str(((mean_frq)*1E-6),'%2.1f') 'MHz'])
    display([num2str(condition) 'Expt, Std frq: ' ...
        num2str(((std_frq)*1E-6),'%2.1f') 'MHz'])
    display([num2str(condition) 'Expt, Mean temp: ' ...
        num2str(mean_temp,'%2.0f') 'K'])
    display([num2str(condition) 'Expt, Std temp: ' ...
        num2str(std_temp,'%2.0f') 'K'])

% Identify appropriate X and Y limits to align the plot with the modelled
% data and shift time vector as required:
    y_min=min(signal); %Y-offset of expt data
    norm_signal=(signal-y_min)/max(signal-y_min);
    limit2=0.8;
    sig_idx2 = find(norm_signal==limit2,1);
    edge_time2 = time(sig_idx2);
    delay=edge_time2-edge_time;
    norm_time=time-delay+time_corr;
end

end
```

Bibliography

[1] J. Kiefer and P. Ewart, "Laser diagnostics and minor species detection in combustion using resonant four-wave mixing," *Progress in Energy and Combustion Science,* vol. 37, no. 5, pp. 525-564, 2011.

[2] S. Shafiee and E. Topal, "When will fossil fuel reserves be diminished?," *Energy Policy,* vol. 37, no. 1, pp. 181-189, 2009.

[3] R. Vander Wal, "Soot Precursor Material: Spatial Localisation via Simultaneous LIF-LII Imaging and Characterisation via TEM," NASA Contractor Report 198469, 1996.

[4] H. Richter and J. Howard, "Formation of polycyclic aromatic hydrocarbons and their growth to soot – A review of chemical reaction pathways," *Progress in Energy and Combustion Science,* vol. 26, no. 4-6, pp. 568-608, 2000.

[5] U.S. Environmental Protection Agency, "Air Quality Criteria for Particulate Matter," EPA 600/ P-99/ 002aF-bF, 2004.

[6] S. Solomon, D. Qin, M. Manning, Z. Chen, M. Marquis, K. B. Averyt, M. Tignor and H. Miller, Climate Change 2007: The Physical Science Basis, Cambridge University Press, 2007.

[7] P. Miller, M. Pilling and J. Troe, "Unravelling combustion mechanisms through a quantitative understanding of elementary reactions," *Proceedings of the Combustion Institute,* vol. 30, pp. 43-88, 2005.

[8] T. Seeger, M. Weikl, F. Beyrau and A. Leipertz, "Identification of spatial averaging effects in vibrational CARS spectra," *Journal of Raman Spectroscopy,* vol. 37, pp. 641-646, 2006.

[9] H. Kogelnik, "Holographic image projection through inhomogeneous media," *Bell Systems Technical Journal,* vol. 44, p. 2451–2455, 1965.

[10] D. Auth, "New high-power source of coherent microwave phonons," *Applied Physics Letters,* vol. 512, p. 16, 1970.

[11] D. Bloom and G. Bjorklund, "Conjugate wave-front generation and image reconstruction by four-wave mixing," *Applied Physics Letters,* vol. 31, no. 9, pp. 592-594, 1970.

[12] B. Cummings, "Laser - induced thermal acoustics: simple accurate gas measurements," *Optics Letters,* vol. 19, pp. 1361-1363, 1994.

[13] P. Paul, R. Farrow and P. Danehy, "Gas-phase thermal-grating contributions to four-wave mixing," *Journal of the Optical Society of America B,* vol. 12, pp. 384-392, 1995.

[14] H. Latzel, A. Dreizler, T. Dreier, J. Heinze, M. Dillman, W. Stricker, G. Lloyd and P. Ewart, "Thermal grating and broadband degenerate four-wave mixing spectroscopy of OH in high-pressure flames," *Applied Physics B,* vol. 67, pp. 667-673, 1998.

[15] R. Stevens and P. Ewart, "Single-shot measurement of temperature and pressure using laser-induced thermal gratings with a long probe pulse," *Applied Physics B,* vol. 78, pp. 111-117, 2004.

[16] D. R. Richardson, R. P. Lucht, W. D. Kulatilaka, S. Roy and J. R. Gord, "Theoretical modeling of single-laser-shot, chirped-probe-pulse femto second coherent anti-Stokes Raman scattering thermometry," *Applied Physics B,* vol. 104, pp. 699-714, 2011.

[17] D. Walker, R. Williams and P. Ewart, "Thermal grating velocimetry," *Optics Letters,* vol. 23, no. 16, pp. 1316-1318, 1998.

[18] A. Dreizler, T. Dreier and J. Wolfrum, "Thermal grating effects in infrared degenerate four-wave mixing for trace gas detection," *Chemical Physics Letters,* vol. 233, p. 525–532, 1995.

[19] M. Brown and W. Roberts, "Single-point thermometry in high-pressure, sooting, premixed combustion environments," *Journal of Propulsion and Power,* vol. 15, pp. 119-127, 1999.

[20] R. Hart, G. Herring and R. Balla, "Pressure measurement in supersonic air flow by differential absorptive laser-induced thermal acoustics," *Optics Letters,* vol. 2007, pp. 1689-1691, 2007.

[21] B. Williams, M. Edwards, R. Stone, J. Williams and P. Ewart, "High precision in-cylinder gas thermometry using Laser Induced Gratings: Quantitative measurement of evaporative cooling with gasoline/alcohol blends in a GDI optical engine," *Combustion and Flame,* vol. 161, pp. 270-279, 2013.

[22] D. Snelling, K. Thomson, G. Smallwood and Ö. Gülder, "Two-dimensional imaging of soot volume fraction in laminar diffusion flames," *Applied Optics,* vol. 38, no. 12, pp. 2478-2485, 1999.

[23] H. Zhao, B. Williams and R. Stone, "Measurement of the spatially distributed temperature and soot loadings in a laminar diffusion flame using a Cone-Beam Tomography technique," *Journal of Quantitative Spectroscopy and Radiative Transfer,* [In Press: Online] 2013. Available from: doi:10.1016/j.jqsrt.2013.07.024 [Accessed: 01 September 2013].

[24] R. Stevens and P. Ewart, "Simultaneous single-shot measurement of temperature and pressure along a one-dimensional line by use of laser-induced thermal grating spectroscopy," *Optics Letters,* vol. 31, no. 8, pp. 1055-1057, 2006.

[25] J. Daily, "Detectability limit and uncertainty considerations for laser induced fluorescence spectroscopy in flames," *Applied Optics,* vol. 17, no. 10, pp. 1610-1615, 1978.

[26] A. Eckbreth, Laser diagnostics for combustion temperature and species, Gordon and Breach, 1996.

[27] R. Miles and W. Lempert, "Two-dimensional measurement of density, velocity, and temperature in turbulent high-speed air flows by UV Rayleigh scattering," *Applied Physics B,* vol. 51, pp. 1-7, 1990.

[28] D. Hoffman, K. Münch and A. Leipertz, "Two-dimensional temperature determination in sooting flames by filtered Rayleigh scattering," *Optics Letters,* vol. 21, no. 7, pp. 525-527, 1996.

[29] J. -P. Taran, J. Boquillon, M. Pealat, P. Bouchardy, G. Collin and P. Magre, "Spatial averaging and multiplex coherent anti-Stokes Raman scattering temperature-measurement error," *Optics Letters,* vol. 13, no. 9, pp. 722-724, 1998.

[30] T. Parameswaran and D. Snelling, "Estimation of spatial averaging of temperatures from coherent anti-Stokes Raman spectroscopy," *Applied Optics,* vol. 35, no. 27, pp. 5461-5464, 1996.

[31] A. Thumann, T. Seeger and A. Leipertz, "Evaluation of two different gas temperatures and their volumetric fraction from broadband N2 coherent anti-Stokes Raman spectroscopy spectra," *Applied Optics,* vol. 34, no. 18, pp. 3313-3317, 1995.

[32] B. Williams, "Quantitative Laser Diagnotics for Combustion," DPhil Thesis, University of Oxford, 2009.

[33] R. E. Stevens, "Laser-Induced Grating Techniques for Combustion Diagnostics," DPhil Thesis, University of Oxford, 2004.

[34] B. C. Choi and S. C. Chung, "Autoignited laminar lifted flames of methane, ethylene, ethane, and n-butane jets in coflow air with elevated temperature," *Combustion and Flame,* vol. 157, no. 12, p. 2348–2356, 210.

[35] M. Edwards, "The effect of uncertainty in composition on Laser-Induced Grating thermometry," MSc Thesis, University of Oxford, 2011.

[36] D. Young, B. Munson, T. Okiishi and W. Huebs, A Brief Introduction To Fluid Mechanics, John Wiley & Sons, 2011.

[37] T. D. Rossing, Springer Handbook of Acoustics, Springer Science + Business Media, 2007.

[38] R. Suntz, H. Bockhorn and N. Anikin, "Tomographic reconstruction of 2D-OH* chemiluminescence distributions in turbulent diffusion flames," *Applied Physics B,* vol. 107, pp. 591-602, 2012.

[39] N. A. Worth and J. R. Dawson, “Tomographic reconstruction of OH* chemiluminescence in two interacting turbulent flames,” *Measurement Science and Technology,* vol. 24, no. 2, 024013, 2013.

[40] N. Anikin, R. Suntz and Bockhorn H., “Tomographic reconstruction of the OH* chemiluminescence distribution in premixed and diffusion flames,” *Applied Phys B,* vol. 100, pp. 675-694, 2010.

[41] K. A. Thomson, D. R. Snelling, G. J. Smallwood and F. Liu, “Laser induced incandescence measurements of soot volume fraction and effective particle size in a laminar co-annular non-premixed methane/air flame at pressures between 0.5 - 4.0 MPa,” *Applied Physics B,* vol. 83, pp. 469 - 475, 2006.